ACTA UNIVERSITATIS SZEGEDIENSIS

ACTA PHYSICA ET CHEMICA

NOVA SERIES

TOMUS XXX FASCICULI 3—4

AUSHAF 30 (3—4) (113—192) (1984)

HU ISSN 0324—6523 Acta Univ. Szeged
HU ISSN 0001—6721 Acta Phys. et Chem.

SZEGED, HUNGARIA
1984

ACTA UNIVERSITATIS SZEGEDIENSIS

ACTA PHYSICA ET CHEMICA

NOVA SERIES

TOMUS XXX FASCICULI 3—4

AUSHAF 30 (3—4) (1984)
HU ISSN 0324—6523 Acta Univ. Szeged
HU ISSN 0001—6721 Acta Phys. et. Chem.

SZEGED, HUNGARIA
1984

Kiadja
a József Attila Tudományegyetem Természettudományi Kara
(Szeged, Aradi vértanúk tere 1.)

Kiadványunk rövidítése:
Acta Phys. et. Chem. Szeged

ON THE INTERACTION OF AN ULTRASHORT LIGHT PULSE WITH A THIN RESONANT MEDIUM

By

M. G. BENEDICT and I. GYÉMÁNT

Institute of Theoretical Physics, Attila József University, Szeged

(Received May 20, 1984)

An optically thin, two level atomic system interacts with a pulse of resonant electromagnetic field. The transmitted and reflected waves are investigated for the case of exact resonance. The amplitudes and the phases of the secondary fields strongly depend on the area and on the width of the exciting pulse.

The resonant interaction of an ultrashort light pulse with a two level atomic system gives rise to several interesting pheomena [1]. Among them, however, only little attention has been paid to the reflected wave.

If the pulse is ultrashort and relaxation effects can be ignored, then the interaction of the two level system with the light field can be described by the optical Bloch equations. Using the rotating wave approximation one has [1]

$$\dot{u} = -\Delta v, \quad \dot{v} = \Delta u + \frac{p}{\hbar} E w, \quad \dot{w} = -\frac{p}{\hbar} E v. \tag{1}$$

Here u, v and w are the components of the Bloch vector, E is the slowly varying amplitude of the field acting on the atoms, p is the transition dipole moment beeing parallel to the linearly polarized field, and Δ is the detuning of the resonance frequency from the carrier frequency of the field.

If the medium is optically thin, then system (1) is usually solved for u, v and w regarding E as a given function of time, namely the incoming field. The effective field strength however consists of two parts. One is the external exciting field and the other is the field originating from the radiating dipoles themselves. The effects of this second field has been investigated in [2] and [3] for the case of superradiation when there is no external excitation but the system is in the upper unstable state.

We restrict our considerations to the case of exact resonance $\Delta = 0$. In this case the effective field is:

$$E = E_{ex} + \frac{2\pi n \omega_0 p}{c} v \tag{2}$$

where E_{ex} is the external excitation and the second term is the secondary field originating from the thin medium with a surface dipole density n. Substituting this expres-

sion into (1) with $\Delta=0$, and going over to a time scale $\tau_R=\hbar c/2\pi\omega_0 p^2 n$ we have

$$\dot{v} = (\mathscr{E}+v)w, \quad \dot{w} = -(\mathscr{E}+v)v \tag{3}$$

where $\mathscr{E}=\frac{p}{h}E_{ex}\tau_R$ is the dimensionless amplitude of the external field.

Introducing the Bloch angle with $v=-\sin\theta$, $w=-\cos\theta$ we get the single equation

$$\dot{\theta}+\sin\theta = \mathscr{E} \tag{4}$$

which has been obtained in [4] in another way. We note that τ_R is the superfluorescence time [3] and in the case of a solid material it falls into the nanosecond range.

The reflected wave is proportional to $v=-\sin\theta$ while the transmitted wave is the sum of the incoming and the forward scattered wave $\mathscr{E}+v=\dot{\theta}$, which is identical with the effective field. Eq. (4) has been solved analytically in [4] for a square pulse, and approximate considerations were made for exciting pulses of smooth envelope.

Here we shall present the results of numerical solutions of eq. (4) for smooth pulses of the form

$$\mathscr{E} = \mathscr{E}_0 \operatorname{sech}\frac{t-t_0}{\tau}, \quad \mathscr{E}_0 = \frac{A}{\tau\pi},$$

where A is the pulse area. We have performed calculations for Gaussian and Lorentzian pulses as well but except for one special case, which will be discussed below, there are no qualitative differences in the evolution of the process.

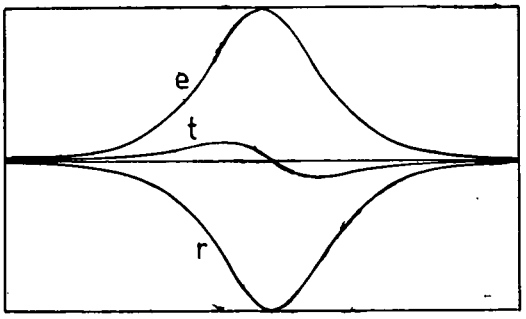

Fig. 1. $A=\pi/2$, $\tau=4$

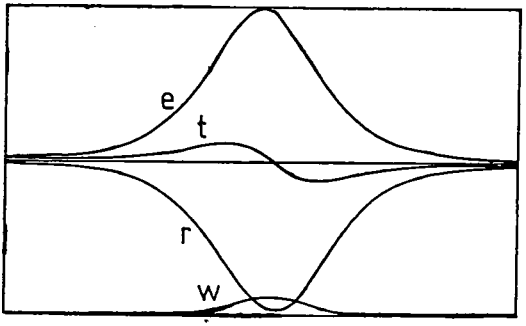

Fig. 2. $A=2\pi$, $\tau=4$

In Figs. 1-8 are shown the time dependence of the inversion (w) and of the exciting (e), transmitted (t) and reflected (r) waves.

The scales are fixed by the maximum of the exciting pulse, namely its position is at $t_0=5.5\tau$, its height is $\mathscr{E}_0$, while for the inversion the vertical scale goes from -1 to $+1$. Initially the two level system is in its ground state, $\theta=0$, $w=-1$. It is seen in all cases, that at the beginning of the excitation θ is increasing in time, the transmitted wave is positive, which means that it is in same phase as the incoming field. At the same time $-\sin\theta$ is negative, *i.e.* the reflected wave is in the opposite phase. The subsequent evolution of the process however depends on both the area of the incoming pulse and its steepness.

When the area is small, *e.g.* for a $\pi/2$ pulse, and the pulse width

is large, *e.g.* $\tau=4$, θ increases only slowly, $\dot{\theta}$ remains small, so that $\sin\theta=\mathscr{E}$, and the reflected wave will be nearly equal to the exciting wave (Fig. 1). The transmission of the medium turns to be small, the reflexion will dominate. The weak transmitted wave exhibits two small peaks at symmetric positions to the maximum of the exciting pulse. Between these peaks the transmitted wave changes its phase though the system remains close to its ground state, $w\approx -1$ during the whole process. Figs. 2 and 3 show the effects of 2π and 4π secant hyperbolic pulses with $\tau=4$, respectively. In these cases the evolving of the fields is similar to that of $\pi/2$ pulses but with a more pronounced increase in the inversion. Note however that the behaviour of the Bloch angle is far from what is expected when neglecting the self field.

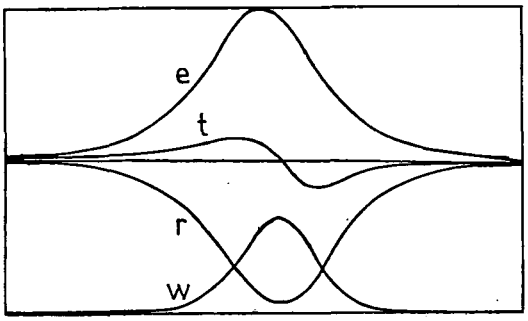

Fig. 3. $A=4\pi$, $\tau=4$

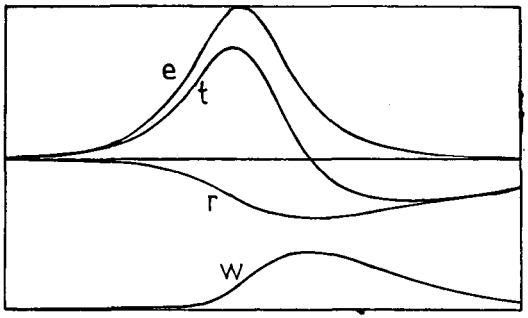

Fig. 4. $A=\pi/2$, $\tau=0.25$

A $\pi/2$ pulse of a much smaller width, $\tau=0.25$ shows a somewhat different character: the solution becomes asymmetric. The first peak of the transmitted amplitude is stronger and gets closer to the maximum of the exciting pulse, while the second peak in the opposite phase becomes smaller. The reflected wave is getting weaker too and its maximum is delayed (Fig. 4).

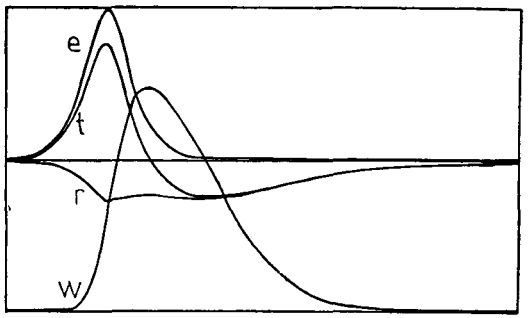

Fig. 5. $A=\pi$, $\tau=0.25$

Now if we have a short pulse of area π the picture is changing further (Fig. 5). The maximum of the amplitude of the transmitted wave takes place at the centre of the excitation, the reflected wave has a long smooth tail of small amplitude and after the decay of the incoming pulse the transmitted wave goes over into the same form as the reflected wave. This part of the transmission can be regarded as a forward scattered wave, which has to be the same as the backward wave. The inversion grows over zero, and the pulse evolving after the excitation can be regarded as superradiation from a not fully inverted state. This process is strengthened by the tail of the excitation.

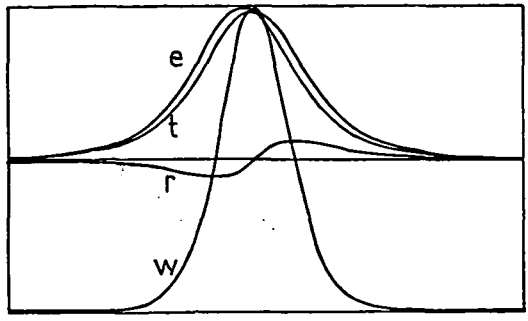

Fig. 6. $A=2\pi$, $\tau=0.25$

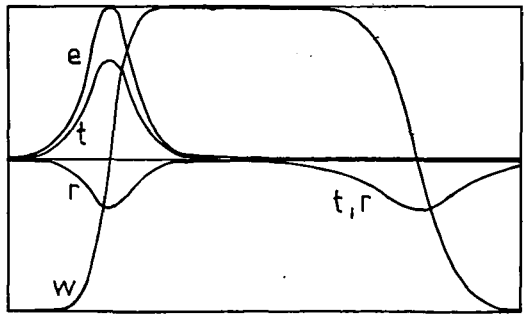

Fig. 7. $A=1.5\pi$ $\tau=0.5$

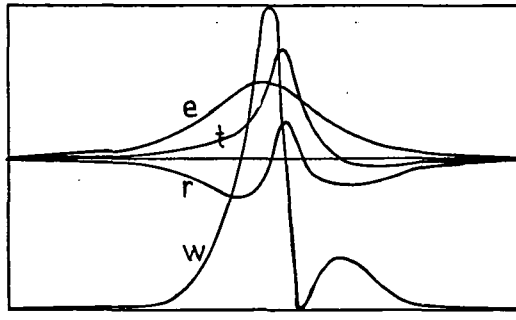

Fig. 8. $A=4\pi$ $\tau=2$

For short 2π pulses the situation will be the opposite to the weak and long excitation case. Now the transmitted wave will be in the same phase during the whole process, and its single maximum will somewhat delayed. The weak reflected wave is double peaked and changes its phase at the centre of the incoming pulse, while the inversion behaves as usual, the Bloch vector is turned around by 2π. (Fig. 6).

There is an interesting limiting case, when an analytical solution for Eq. (4) can be obtained. If $\mathcal{E}=\frac{\tau+1}{\tau}$ sech $\frac{t-t_0}{\tau}$ then $\theta=2$ arctg $e^{(t-t_0)/\tau}$ is a solution which corresponds to the initial condition $\theta(0)=$ $=2$ arctg$e^{-t_0/\tau}$. The numerical results show however that essentially the same solution can be obtained if $\theta(0)=0$ (Fig. 7). In the numerical procedure the exciting pulse was set up with $t_0=5.5\tau$. In this case θ tends to π as the excitation decays (with other forms of excitations this could be achieved only by cutting them off when θ gets equal to π). The area of the exciting pulse is $(\tau+1)\pi$ which shows that in order to reach complete inversion one must have a pulse area larger than π, and this is the more so, the wider is the incoming pulse. The reflected and the transmitted waves are in opposite phase both of them having the same form as the exciting pulse, and the ratio of their amplitudes turns to be τ, *i.e.* independent of time.

Of course the $\theta=\pi$ value is not stable, the system will radiate spontaneously according to the sech $(t-t_1)$ law in both directions after a small perturbation. The characteristic time of this superradiating pulse is τ_R not depending on the excitation.

For pulses of area larger than 2π also a different behaviour can be obtained for different widths. For a 4π pulse and $\tau=4$ see Fig. 3. For $\tau=2$ however the inversion may increase once again after having decayed to -1. Accordingly the reflected wave

exhibits further oscillations. What is more interesting the transmitted pulse may be higher than the excitation, while it is narrower than the incoming pulse, thus showing up the effect of pulse compression (Fig. 8.)

For still shorter pulses the situation will be close to the case when the self field is neglected, though in all cases this self field turns back the system into its ground state.

These examples clearly show that the behaviour of the transmitted and reflected waves are very different for wide and short pulses of the same area. Beside the variations of the amplitudes of the secondary waves the changes in the phases also deserve attention. We note that measurements of similar phase jumps for choherent amplification, predicted at first time in [5] have been reported only very recently [6]. The results of our calculations show, at least in principle, the possibility to control the amplitude and phase of a coherent light pulse.

References

[1] *Allen L., J. H. Eberly:* Optical Resonance and Two-Level Atoms, Wiley, New York (1975).
[2] *de Costa L. C. T., G. A. P. Munguia:* Phys. Rev. **A14**, 1745 (1976).
[3] *Трифонов Е. Д., А. И. Зайцев, Р. Ф. Маликов:* ЖЭТФ **76**, 65 (1979).
[4] *Рупасов В. И., В. И. Юдсон:* Квант. элект. **9**, 2179 (1982).
[5] *Burnham D. E., R. Y. Chiao:* Phys. Rev. **188**, 667 (1969).
[6] *Varnavsky, O. P., A. N. Kirkin, A. M. Leontovich, A. M. Mozharovsky:* Opt. Comm. **49**, 71 (1984).

О ВЗАИМОДЕЙСТВИИ УЛЬТРАКОРОТКОГО СВЕТОВОГО ИМПУЛЬСА С ТОНКИМ РЕЗОНАНСНЫМ СЛОЕМ

М. Г. Бенедикт, и И. Демант

Оптически тонкая двухуровневая атомная система взаимодействует с резонансным электромагнитным импульсом. Исследуются пропущенная и отраженная волны в случае точного резонанса. Амплитуды и фазы во вторичных полях сильно зависят от площади и ширины возбуждающего импульса.

SPECIAL POINTS AND IDEAL-VACANCY-INDUCED DEEP LEVEL IN Si AND SOME III—V SEMICONDUCTORS

By

G. PAPP

Department of Theoretical Physics, Attila József University, Szeged

F. BELEZNAY

Research Institute for Technical Physics, Budapest

(Received July 3, 1984)

We show that the special points average technique is a suitable computational scheme to calculate the Green's function in the gap and we give a tight binding parameter set for Si.

Introduction

Vacancy induced localized defects in semiconductors have been the subjects of experimental and theoretical investigations for over two decades. Though not unambiguously identified experimentally, this simple lattice defect has attracted significant theoretical interest, mainly because of its conceptual simplicity as a prototype system to study localized defects. The knowledge of the deep level in the gap caused by localized defects in semiconductors is important in the understanding of many properties of a class of materials of major importance in most fields of pure and applied semiconductor physics.

To study the ideal vacancy induced levels in Si and in III—V compound semiconductors we have used an empirical tight binding scheme with linear combination of atomic orbitals in conjunction with the Green's-function technique [1]. As it was shown in [2], the levels caused by the vacancy in the gap, calculated by this method, are sensitive to the choice of the tight binding parameters. With different sets of parameters all of which give comparably good fits to the bulk band energies, the levels can vary through the whole range of the band gap. Clearly then, additional constraints on the fitting procedure are required to reduce ambiguity of the choice of the tight binding parameters.

A possibility to find a unique set of tight binding parameters [2] relied upon the established correlation between photothreshold and ionicity of the III—V compound semiconductors. The levels, obtained by these parameters provide trends as one goes from one material to another.

However the tight binding method with Green's function technique can be applied not only to vacancy induced deep levels in the gap but also to determining the surface and interface states [3] and in these cases finding a unique set of tight-

binding parameters is very important as well. In addition for the unrelaxed vacancy in some semiconductors there exist self-consistent Green's function calculations also [4], so it is natural to fit the TB parameters to these best results.

This fact, *i.e.* the knowledge of the "best" level would be a criterion to determine the tight-binding parameter system which might be useful for other calculation. But the calculation of the level induced by vacancy is rather cumbersome because of the time consuming integration over the Brillouin zone.

In this paper we will show that this integration can be reduced with the so-called special points average technique [5]. With this reduction we are able to determine a tight-binding parameter set which satisfies the requirement that the resulting level should agree with the level obtained from a self-consistent calculation and reproduce the bulk band structure.

I. The method for calculation of vacancy states

The basis of the Green's function method is the early work of KOSTER and SLATER [6], who showed that the electronic energy levels introduced in the band gap by a localized perturbation could be calculated from the knowledge of the Green's function for the perfect crystal and the matrix elements of the potential, both calculated in the Wannier representation.

LANOO and LENGLART [7] observed that the Green's function method is not limited to employing Wannier functions as a basis, but can be applied using a set of atomic orbitals and performing an LCAO band structure calculation. With this observation BERNHOLC and PANTELIDES [1] extended the method and showed that in an arbitrary localized representation the gap states introduced by the vacancy are given by the solution of

$$\det G^0_{\alpha\alpha}(E) = 0$$

where the matrix elements of the perfect-crystal Green's function are given by

$$G^0_{\alpha\alpha'}(E) = \sum_{n,\vec{k}} \frac{\langle \alpha | n\vec{k} \rangle \langle n\vec{k} | \alpha' \rangle}{E - E^0(n, \vec{k})}$$

where $|n\vec{k}\rangle$ are the Bloch states of the perfect crystal and $E^0(n, \vec{k}) - s$ are the corresponding energy bands and the $\{\varphi_\alpha\}$ is the set of orbitals which are localized about the site of the atom to be removed.

If the bulk solid electronic structure is sought within the LCAO approximation with s and p atomic basis set then the condition for the existence of a bound state can be rewritten as

$$\sum_{n,\vec{k}} \frac{|c_{\alpha j}(n, \vec{k})|^2}{E - E^0(n, \vec{k})} = 0$$

where $\{c_{\alpha j}\}$ are the coefficients of the expansion of the perfect crystal wave function, α, j refer to the αth-type (s, p_x, p_y, p_z) orbital located on the jth atom, n is the band index and $E^0(n, \vec{k})$ is the nth band energy at the wave vector $\vec{k}$.

The integration over $\vec{k}$ is carried out over the Brillouin zone of the material and the sum over n over all bands.

II. Average over Brillouin zone and results

As we have seen in Sec. I. the calculation of the vacancy-induced level in the gap requires an integration over Brillouin-zone. One of the most widespread methods is the so-called GILAT—RAUBENHEIMER [8] method, were used at first to calculate the frequency-distribution function in solids.

At this method we have to solve for the energy eigenvalues at evenly spaced points in reciprocal space and then to find other solutions in between by means of a TAYLOR expansion about each such point for each eigenvalue. By choosing the points for diagonalization sufficiently close together, all of the eigenvalues can be reached by linear extrapolation. In the application of the extrapolation method, the irreducible section of the first Brillouin zone is divided into a uniform simple cubic mesh of points $\vec{k}$, separated by a distance. Every $\vec{k}$ is at the center of a small cube throughout which extrapolation is carried out. In order to reach a reasonable result with this method a number of $\vec{k}$ is needed.

As it was shown in [9], a considerable simplification can be reached by introducing the mean value point or some special points [4], which are dictated by crystal symmetry, to calculate the approximate average values over Brillouin zone. The coordinates of these points were given for some lattices and possible applications of the method were suggested in the calculation of the electronic valence charge density and of the average one-electron valence-band energy [9]. The mean value point technique was also useful in evaluating the element of the dielectric matrix [10].

In this paper we have studied the possibility of the application of the method mentioned later to calculate the levels caused by the ideal vacancy in Si and some III—V semiconductor.

Since the question in this part is the applicability of the method therefore we have tested on the wellknown Si vacancy. We accepted for the tight binding parameter system given by PANDEY and PHILLIPS [11] which retains first and second nearest-neighbour interactions. Fig. 1 shows the function $G^0_{ss}(E)$, calculated with the mean value point and the two,- and ten special points. The zeros of $G^0_{ss}(E)$ in the regions of the band gap correspond to bound states of A_1 symmetry. As it can be seen there is no bound state in agreement with the calculation of Bernholc and Pantelides [1]. The Fig. 2 shows the function $G^0_{pp}(E)$ similar to $G^0_{ss}(E)$. The zeros of $G^0_{pp}(E)$ in the regions of the band gap correspond to bound states of T_2 symmetry. From this figure we can see that the $G^0_{pp}(E)$, obtained by ten points average becomes zero at $E=0.31$ eV (compared with 0.27 eV of [1]) and the other two do not give bound state. We have repeated this calculations using the parameters proposed by KAUFFER *et al.* [12]. We have obtained the same results, *i.e.* bound state is only in T_2 state ($E=0.25$ eV) with the help of ten representative points.

In Table I. the results of calculations for some III—V semiconductors are shown. The tight binding parameters are the same as in [2], and we compare the position of the levels in the fundamental gap region to the same levels previously calculated by hundred $\vec{k}$ point integration [2]. All energies are in eV and measured from the valence-band edge.

From the results we can establish that the one point and the two points average is not suitable, the ten point average agrees very well with the test data.

In particulary in the case of Ga series using the ten points good approximation can be reached. In the case of In series the gaps are so narrow for InSb and InAs

(0.24 eV and 0.38 eV, respectively) that there is no level in the gap, therefore the results are not informative, but for InP the agreement is suitable. Since from the calculations it was turned out that the ten points average over Brillouin zone is a succesful computational tool to determine the level caused by vacancy in the gap we tried to use this fact.

Knowing the position of the levels from other calculation (self-consistent calculations), we were able to determine the tight-binding parameters which gave a good

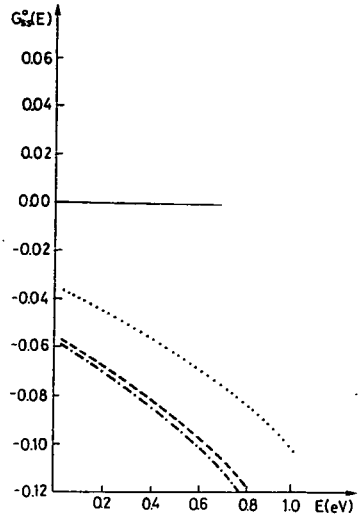

Fig. 1. The function of $G^0_{ss}(E)$, calculated by one point (dotted line), two points (dashed line), ten points (dashed dotted line) for Si.

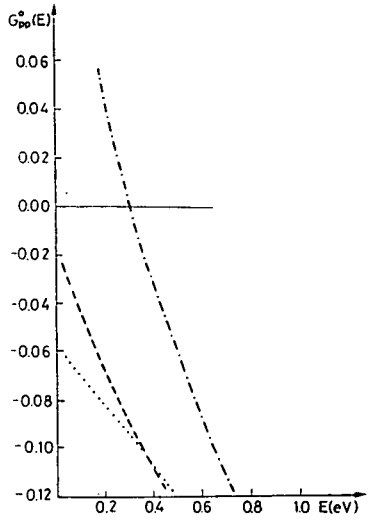

Fig. 2. The function of $G^0_{pp}(E)$ similar to Fig. 1

Table 1

A_1 and T_2 levels in the gap for anion vacancies (the energy zero is at the top of the valence band) as obtained with different calculations. A: mean value point; B: two points; C: ten points; D: from Ref. [2]. Energy in eV

	A_1				T_2			
	A	*B*	*C*	*D*	*A*	*B*	*C*	*D*
GaSb	—	0.67	0.49	0.56	—	0.39	0.59	0.76
GaAs	—	1.50	1.22	1.3	0.58	1.28	1.54	1.53
GaP	2.02	1.96	1.84	1.75	0.87	1.49	1.93	1.93
InSb	—	—	—	—	—	0.05	—	—
InAs	—	—	—	—	—	—	—	—
InP	—	—	1.29	1.35	0.33	1.06	1.37	1.47

Table II

Tight binding parameters for Si and the energies in the symmetry points. (The energies are in eV)

$E_{ss}(0, 0, 0)$	−4.24		−12.56
$E_{pp}(0, 0, 0)$	0.39		0.0
$E_{ss}\left(\frac{1}{2}, \frac{1}{2}, \frac{1}{2}\right)$	−2.08	Γ	3.59
$E_{xx}\left(\frac{1}{2}, \frac{1}{2}, \frac{1}{2}\right)$	0.428		3.92
$E_{xy}\left(\frac{1}{2}, \frac{1}{2}, \frac{1}{2}\right)$	0.95		−8.11
$\frac{1}{2}, \frac{1}{2}, \frac{1}{2}\Big)$	1.375	X	−3.2
$_s(1, 1, 0)$	0.00		2.54
$E_{xx}(1, 1, 0)$	0.19		4.54
$E_{xy}(1, 1, 0)$	0.34		−10.22
$_x(1, 1, 0)$	0.00		−7.79
$E_{xx}(0, 1, 1)$	−0.05	L	−1.0
			2.37
			2.50
			4.30

band structure and the energy level in the gap agrees with the level of self-consistent calculation [4].

We have generated such a parameter set for Si, shown in Table II., where the energies in symmetry points are also shown. This parameter system may be useful to solve other (for example vacancy system) problems.

III. Summary

In this paper using a linear combination of atomic orbitals description of the electronic structure of the perfect solid in conjunction with the Green's function technique we have shown that the ten points average over the Brillouin zone is a good approximation to determine the vacancy induced levels in semiconductors. Furthermore using this fact we have given a tight binding parameter set for Si.

References

[1] *Bernholc, J., S. T. Pantelides:* Phys. Rev. B **18**, 1780 (1978).
[2] *Das Sarma, S., A. Madhukar:* Phys. Rev. B **24**, 2051 (1981).
[3] *Pollmann, J., S. T. Pantelieds:* Phys. Rev. B. **18**, 5524 (1978).
[4] *Baraff, G. A., M. Schlüter:* Phys. Rev. B **19**, 4965 (1979).
Bernholc, J., N. O. Lipari, S. T. Pantelides: Phys. Rev. B **21**, 3545 (1981).
[5] *Chadi, D. J., M. L. Cohen:* Phys. Rev. B **8**, 5747 (1973).
[6] *Koster, F., J. C. Slater:* Phys. Rev. **95**, 1167 (1954). Phys. Rev. **96**, 1208 (1954).
[7] *Lanoo, M., P. Lenglart:* J. Phys. Chem. Solids **30**, 2409 (1969).
[8] *Gilat, G., L. J. Raubenheimer:* Phys. Rev. **144**, 390 (1966).
[9] *Baldereschi, A.:* Phys. Rev. B **7**, 5212 (1973).
[10] *Baldereschi, A., E. Tosatti:* Phys. Rev. B **17**, 4710 (1978).
[11] *Pandey, C., J. C. Phillips:* Phys. Rev. B **13**, 750 (1976).
[12] *Kauffer, E., P. Pêcheur, M. Gerl:* J. Phys. C **9**, 2913 (1976).

СПЕЦИАЛЬНЫЕ ТОЧКИ И ГЛУБОКИЕ УРОВНИ НАВЕДЕННЫЕ ВАКАНСИЯМИ В Si И В НЕКОТОРЫХ ПОЛУПРОВОДНИКАХ ТИПА III—V.

Г. Папп и Ф. Белезнаи

Показано, что техника усреднения в специальных точках является подходящим ме
тодом для вычисления функции Грина в запрещенной зоне, и задается множество параметро
сильной связи для Si.

DESIGN OF N_2 LASER PUMPED TUNABLE DISTRIBUTED FEEDBACK DYE LASERS WITH EXTENDED TUNING RANGE

By

J. HEBLING, ZS. BOR and B. RÁCZ

Institute of Experimental Physics, Attila József University, Szeged, Hungary

(Received 16th May, 1984)

The range in which N_2 laser pumped distributed feedback dye lasers can be tuned by turning mirrors is limited by the shift of the pump beams along the surface of the dye cell. In this article the pivot axis of the mirrors is determined for which the shift of the pump beams is minimized.

N_2 laser pumped distributed feedback dye lasers (DFDL-s) [1] are inexpensive and simple instruments capable of generating 6—40 ps long [2, 3], transform limited light pulses. Fig. 1 shows the scheme of a DFDL. The pump beam is diffracted by the grating and the DFDL structure is produced by the interference of the two diffracted beams. The period of the interference pattern is

$$\Lambda = \frac{d}{2} \tag{1}$$

where d is the period of the holographic grating. The wavelength of the DFDL is

$$\lambda_\ell = 2 \cdot n_s \cdot \Lambda \tag{2}$$

where n_s is the refractive index of the dye solution. According to equations (1) and (2) the wavelength of the DFDL does not depend on the wavelength of the pump beam, *i.e.* the pumping arrangement is achromatic. If the arrangement satisfies the

$$\frac{x}{y} = \left(\left(\frac{d}{\lambda_p}\right)^2 - 1\right)^{1/2} \tag{3}$$

geometrical condition — where λ_p is the wavelength of the pump beam —, then to each point of the dye cell the interfering beams are diffracted from the same point of the grating. This means that one can use pumping beams with poor spatial coherence. The DFDL can be tuned comfortably by turning the mirrors. The wavelength of the DFDL can be calculated from the equation

$$\lambda_\ell = \frac{n_s \lambda_p}{\sin(\alpha - 2\delta)} \tag{4}$$

where $\alpha = \arcsin(\lambda_p/d)$ is the angle of diffraction. The meaning of the angle δ is shown in Fig. 1. However, the DFDL wavelength now becomes dependent not only on δ, but also on λ_p, *i.e.* this arrangement is chromatic. This problem was investigated in [4], and it was shown that the chromatism is negligible in a tuning range of about 20 nm.

There is another problem, namely, with the turning of the mirrors the incidence points of the two diffracted beams with the surface of the dye solution shift in opposite directions. This can lead to significantly decreasing visibility of the interference pattern since the spatial coherence length of an N_2 laser beam is generally smaller than about 0.5 mm. The decreasing visibility may prevent lasing. This can be compensated by moving the grating or the dye cell during tuning, but then the whole set-up becomes too complicated. There is an alternative compensation utilizing the fact that the relative shift of the incidence point depends on the pivot axes of the mirrors.

Let us determine this dependence with reference to Fig. 2 (which shows only the right side of the DFDL). In the first case the pivot axis is located in the intersecting point (A) of the pump beam and the mirror. Turning the mirror between positions 1 and 2 causes a shift b of the incidence point. According to sine law

$$b = a\frac{\sin(2\delta)}{\cos(\alpha - 2\delta)} \tag{5}$$

where $a = \overline{AB}$. If the pivot axis is located in point 0 (the sign of mirror position and ray path are denoted by 3) then the distance b' can be calculated from the equation

$$b' = 2f\frac{\sin\alpha\cos(\alpha - \delta)}{\cos(\alpha - 2\delta)} \tag{6}$$

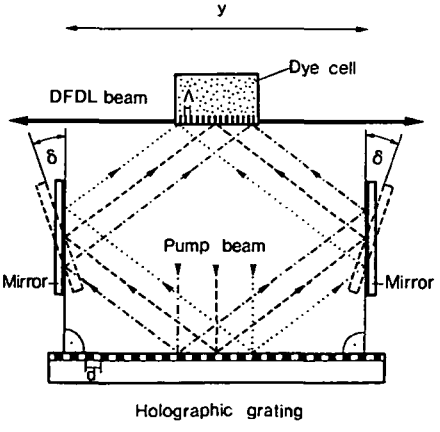

Fig. 1. Pumping arrangement of the DFDL

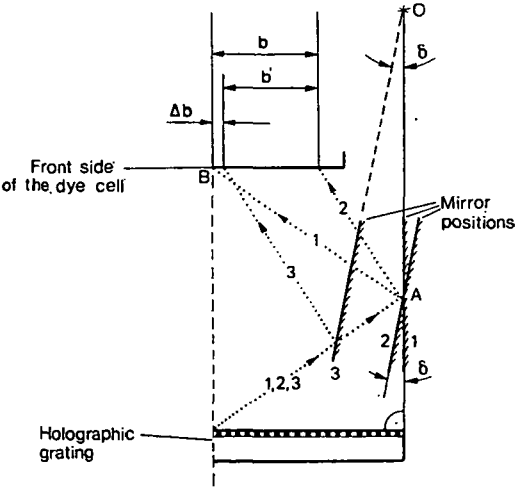

Fig. 2. Change of the ray path during mirror turning

where $f=\overline{AO}$ the arm length of the mirror. Finally the shift of the incidence point is

$$\Delta b = b' - b \tag{7}$$

when the mirror is turned about point 0 with an angle δ. Fig. 3 shows Δb as a function of δ with different arm lengths. The values of f are given in mm. As seen from Fig. 3 the mirror can be turned over a 50 mrad range while $|\Delta b|$ is smaller than 0.05 mm, which is one tenth of the spatial coherence length of the pump beam. Hence with such turning range the shift of the incidence points does not influence significantly the working condition of the DFDL. The curves shown in Fig. 3 were calculated using $a=40$ mm. In the case of $f=68.02$ mm the OB line is perpendicular to the AB line (see Fig. 2). The $\Delta b-\delta$ curves can be compressed vertically using smaller a and proportionally smaller f.

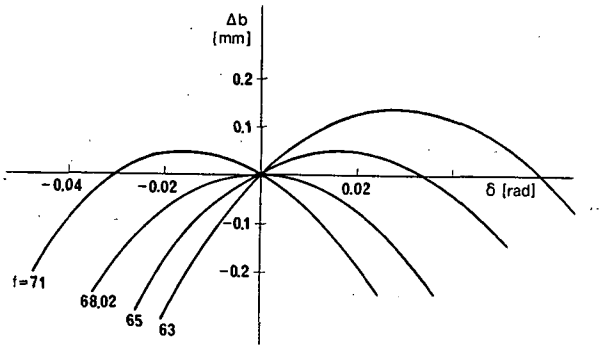

Fig. 3. The dependence of the incidence point shifting on the mirror rotating angle δ with four different arm lengths

According to the calculations for the chromatism [4] and the shift of the incidence point the DFDL is tunable simply by turning the mirrors in a range of few ten nm. This possibility was investigated experimentally. In the experiments a slightly different arrangement [5] as compared to the one shown in Fig. 1 was used (see inset of Fig. 4). The characteristic values of the DFDL were $a_1=50$ mm, $a_2=20$ mm, $f_1=83.8$ mm and $f_2=33.5$ mm. The active medium was a $6\cdot10^{-3}$ mol/ℓ solution of Rhodamine 6 G, dissolved in a 1:1 mixture of ethanol and DMSO. A 2400 ℓ/mm holographic grating was used. The pump source was a N_2 laser oscillator-amplifier system [6]. The pump beam was focussed onto the dye cell by a cylindrical lens having a focal length of 320 mm. In Fig. 4 the full line shows the calculated (from Eqs. (3)) and (4)) and the crosses (x) the measured value of the lasing wavelength as a function of rotation angle δ. The tuning range was 35 nm. In this range the difference between the measured and calculated wavelength was smaller than the accuracy of measurement. The threshold pump power was also measured during tuning. It was found that the change of the threshold was smaler than $\pm5\%$ in a 9 nm tuning range. This range was probably limited by the chromatism of the pumping since in the case of chromatically compensated pumping arrangement this tuning range was 25 nm [4].

In [4] a quartz prism was attached to the dye cell for chromatic compensation as shown in Fig. 5. (This figure displays only the right side of the symmetrical DFDL.)

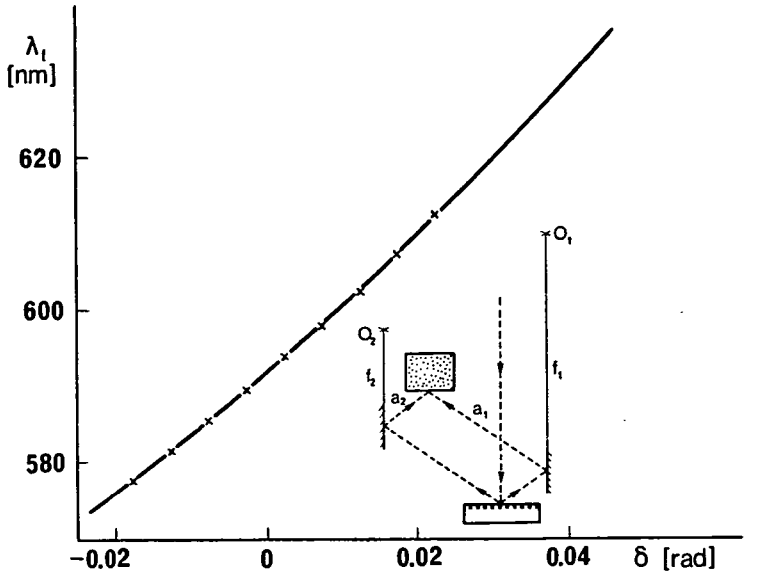

Fig. 4. Calculated (full line) and measured (x) lasing wavelength as a function of angle δ

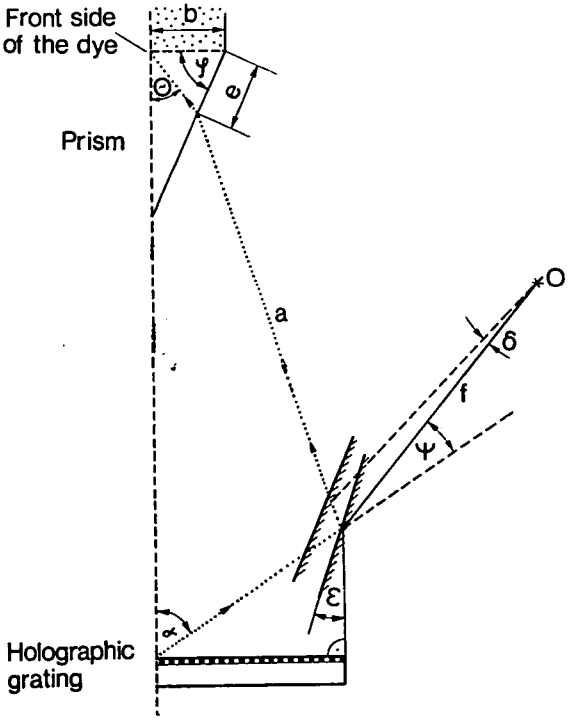

Fig. 5. Figure to define symbols used in equations (8)—(14)

In this case the shift of the pump beam on the surface of the dye during tuning is determined by the equation

$$\Delta b = \frac{\cos\gamma'}{\cos\Theta'} \cdot \tag{8}$$

$$\left[e + i\frac{\sin(2\varepsilon - 2\alpha)}{\cos(\alpha - 2\varepsilon - \varphi)} - \frac{\sin 2\delta}{\cos(\alpha - \varphi - 2\varepsilon - 2\delta)}\left(a + i\frac{\cos(\varphi + \alpha)}{\cos(\alpha - 2\varepsilon - \varphi)}\right)\right] - b$$

where

$$i = 2f\sin\left(\frac{\delta}{2}\right)\frac{\cos\left(\psi - \alpha + \varepsilon + \frac{\delta}{2}\right)}{\sin(\alpha - \varepsilon - \delta)}, \tag{9}$$

$$e = b\frac{\cos\Theta}{\cos\gamma}, \tag{10}$$

$$\gamma' = \arcsin\left(\frac{\sin(\varphi - \alpha + 2\varepsilon + 2\delta)}{n_p}\right) \tag{11}$$

$$\gamma = \arcsin\left(\frac{\sin(\varphi - \alpha + 2\varepsilon)}{n_p}\right) \tag{12}$$

$$\Theta' = \varphi - \gamma' \quad \text{and} \quad \Theta = \varphi - \gamma. \tag{13)—(16)}$$

The meanings of the symbols are defined in Fig. 5. n_p is the refractive index of the quartz prism. ε is the initial angle to which $\Delta b = 0$. Fig. 6 shows the $\Delta b - \delta$ functions

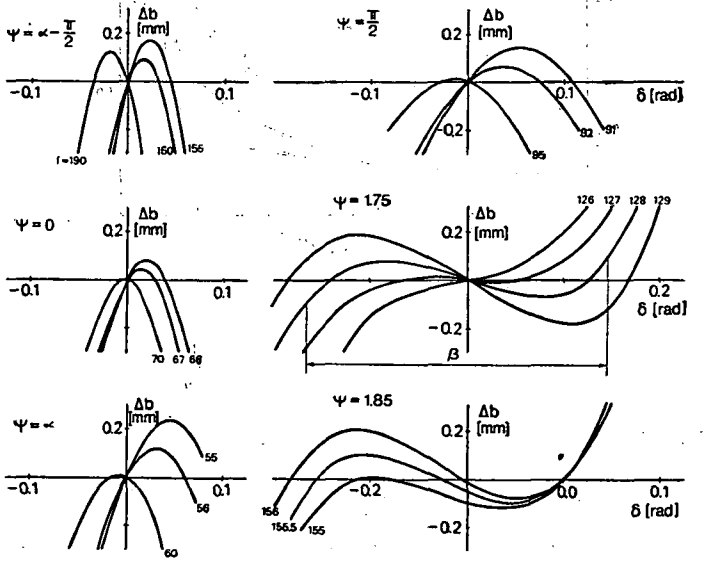

Fig. 6. Series of Δb *vs* δ curves (for six different ψ's) from which the optimal arm lengths can be selected and the values of β (shown only for $\psi = 1.75$ rad) are obtained

calculated with $\varepsilon=0.3299$ rad, $b=11.8$ mm, $a=40$ mm, $\varphi=1.1406$ rad, $n_p=1.4795$, $d^{-1}=2442$ mm^{-1}, $\lambda_p=337.1$ nm and different ψ and f values. $\varepsilon\neq 0$ was choosen because this arrangement is achromatic when $\varepsilon\neq 0$ opposite to the case which is shown in Fig. 2. In Fig. 5 the values of ψ and f are given in rad and nm, respectively. For each ψ we can select an optimal arm length, for which β is maximum. β is the mirror rotation angle range where $|\Delta b|$ is smaller than 0.1 mm (see Fig. 6). Fig. 7 shows the optimal arm lengths and the corresponding β as a function of ψ. Fig. 7 also shows the results of calculations, which were made using $b=5.9$ mm instead of $b=11.8$ mm. According to Figs. 6 and 7 with increasing ψ the value of β also increases, but the shape of the $\Delta b-\delta$ function becomes sensitive to the arm length. The optimal arm length have a minimum at $\psi\sim 0.6$ rad. If ψ is large f is significantly larger than its minimal value. This is disadvantageous because of increased demands on the mechanical stability of the mirror holding. In addition if $\psi>1.75$ rad during the turning the mirrors may touch the grating. Therefore, if large mirror tuning range is needed we must choose the pivot axis such that $\psi\lesssim 1.75$ rad is valid. It is advantageous to use a smaller quartz prism because in this case β is larger and f is smaller.

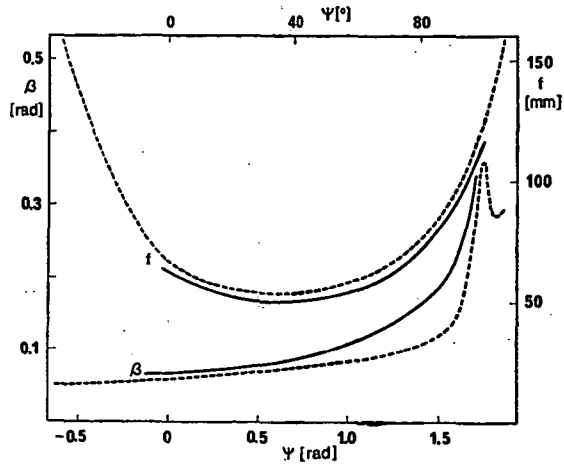

Fig. 7. Optimal arm length and β *vs* ψ with $b=11.8$ mm (broken lines) and $b=5.9$ mm (full lines)

In [4] a DFDL with the arrangement shown in Fig. 5 was investigated. The data were the same as in this article. Since the aim of that experiment was to cover the tuning range of a dye choosing $\psi=0$ rad proved to be satisfactory.

The turning range of a given arrangement can significantly be extended simply by reducing the sizes of the DFDL. From this and the fact that the limit of the chromatism is defined somewhat arbitrarily we can conclude that a tuning range of about 200 nm can be achieved without changing the refractive index of the dye solutions.

* * *

Acknowledgement

The authors wish to thank DR. G. SZABÓ for a critical reading of the manuscript.

References

[1] *Bor, Zs.:* Opt. Commun. **29,** 103 (1979).
[2] *Bor, Zs.:* IEEE J. Quantum Electron. QE-**16,** 517 (1980).
[3] *Bor, Zs., B. Rácz, A. Müller:* Appl. Opt. **22,** 3327 (1983).
[4] *Hebling, J., Zs. Bor:* To be published in Sci. Instruments.
[5] *Bor, Zs.:* Opt. Commun. **39,** 383 (1981).
[6] *Sánta, I., S. Szatmári, B. Németh, J. Hebling:* Opt. Commun. **41,** 59 (1982).

ПЛАНИРОВАНИЕ РОС ЛАЗЕРА, ВОЗБУЖДЕННОГО АЗОТНЫМ ЛАЗЕРОМ ДЛЯ ШИРОКОЙ ОБЛАСТИ НАСТРОЙКИ

Й. Хедлинг, Ж. Бор и Б. Рац

Область настройки РОС лазера, возбужденного азотным лазером настроенного вращением зеркала, ограничена сдвигом возбуждащих пучков на поверхности кюветы. Определена ось вращения, соотвествующая минимальному сдвигу возбуждающих пучков.

THE INFLUENCE OF DETERGENTS ON THE LUMINESCENCE PROPERTIES OF RHODAMINE B AND 6 G IN AQUEOUS SOLUTION

By

Z. KONEFAŁ

Institute of Experimental Physics University of Gdansk, Gdansk, Poland

(Received February 20, 1984)

The influence of detergents on the quantum yield of fluorescence and on the dimerization process in lasing dyes e.g. Rhodamine B and 6 G in aqueous solution, has been determined. The effect of the concentration quenching of the fluorescence by energy migration versus the concentration of the detergent have been studied. The optimal detergent concentration for the laser generation is given.

Introduction

For a complete understanding of dye lasers, a knowledge of the absorption and emission properties of dyes in solvent is very helpful. Water, which has a high heat capacity, is a highly desirable solvent for laser dyes. It is known that organic dyes in aqueous solution have a tendency to form dimers [1-3]. The equilibrium between monomers and dimers in the solution shifts towards the latter with increasing dye concentration. The dimerization of dyes like Rhodamine B and 6 *G* at ambient temperature and concentration of 10^{-4} *M* is enough to prevent laser action. The non-fluorescent dimers absorb the pump light and increase the cavity losses. The cavity losses are due to their long-wave absorption band which overlaps the fluorescence spectrum of the monomers.

The detergents are added to the lasing dye solution to prevent the dye molecules to form dimers and increase the efficiency of laser generation.

The present work deals with the fluorescence quantum yield and degrees of dimerization of the Rhodamine B and 6 G in aqueous solution containing various amounts of the following detergents:

1. Hostapon $C_{12}H_{25}SO_4Na$
2. Sulfapol $C_{12}H_{25}C_6H_4SO_3Na$
3. Triton X-100 $C_8H_{17}-C_6H_4-O(OCH_2CH)_{10}H$

Address: Instytut Fizyki Doswiadczalnej, Uniwersytet Gdanski, ul. Wita Stwosza 57, 80—952 Gdansk.

Experimental

The quantum yield η of Rhodamine B and 6 G at $2 \cdot 10^{-5}$ M concentration in aqueous solution with various concentrations of the above detergents was measured using the apparatus described earlier [4]. The results are illustrated in Fig. 1. It can be seen in Fig. 1 that in the solution for which the concentration of detergents is below the critical micelle concentration (*c.m.c.*) the quantum yield is smaller than for pure water solution. If the detergent concentration is increased above the c.m.c., the quantum yield is larger than for the pure solution.

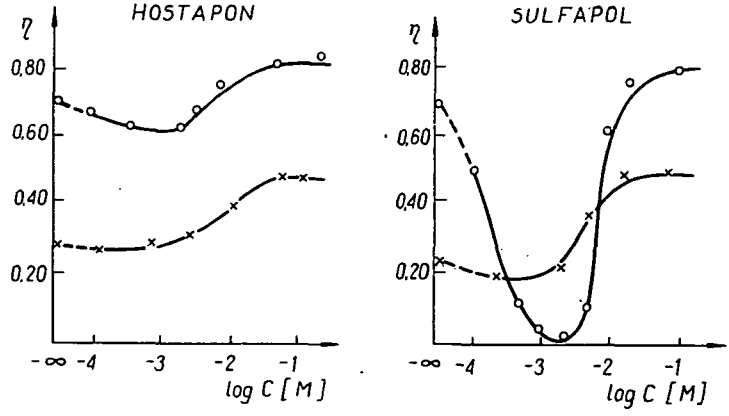

Fig. 1. The quantum yield of Rhodamine 6 G and Rhodamine B in aqueous solution versus the concentration of detergent. The dye concentration is $c = 2 \cdot 10^{-5}$ M

This effect was used for the determination of critical micelle concentration. The value of *c.m.c.* is about $3 \cdot 10^{-4}$ mol/l for Triton X-100 and 10^{-3} and $2 \cdot 10^{-3}$ mol/l for Hostapon and Sulfapol, respectively.

The quantum yield for solution at high dye concentration ($2 \cdot 10^{-4} - 2 \cdot 10^{-3}$ M) of Rhodamine B and 6 G was measured using a thin cuvette, in order to prevent reabsorption.

The fluorescence lifetime measurements for dye detergent solution were made by means of a phase shift fluoremeter [5].

The degree of dimerization of Rhodamine B and 6 G of this solution was calculated by means of the measured absorption spectrum [7-9].

The absorption spectra were recorded on a Zeiss-Jena type spectrophotometer using a quartz absorption cell with 0.01, 0.02, 1.0 cm path lengths. Fig. 2 shows the absorption spectra of Rhodamine B and 6 G in aqueous solution for $2 \cdot 10^{-3}$ M dye concentration at various concentrations of Triton X-100. It is noticable that 5% of Triton X-100 is enough to prevent Rhodamine dimerization.

Since the investigated solutions can be active media of dye lasers, it is useful to determine the lasing threshold. This was measured focusing the radiation from a nitrogen laser on a 1.0 cm cell containing the solution.

The results of the measurements as to the degree of dimerization (d), the relative value of the integrated intensity (f), and relative value of the lasing threshold (p) are illustrated in Fig. 3. As it can be seen from Fig. 3, if the detergent concentration increases, the degree of dimerization and the lasing threshold decreases but the fluorescence intensity increases. For both dyes, a volume concentration of 5% detergent increases the laser efficiency thus proving that this solution is a good laser medium.

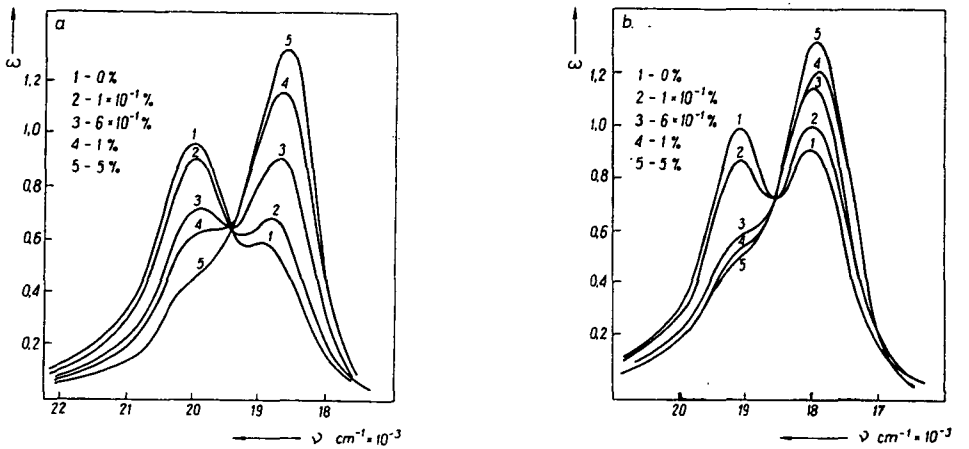

Fig. 2. Absorption spectra of Rhodamine B and 6 G in aqueous solution with various Triton X-100 concentration. Dye concentration is $c = 2 \cdot 10^{-3}$ M

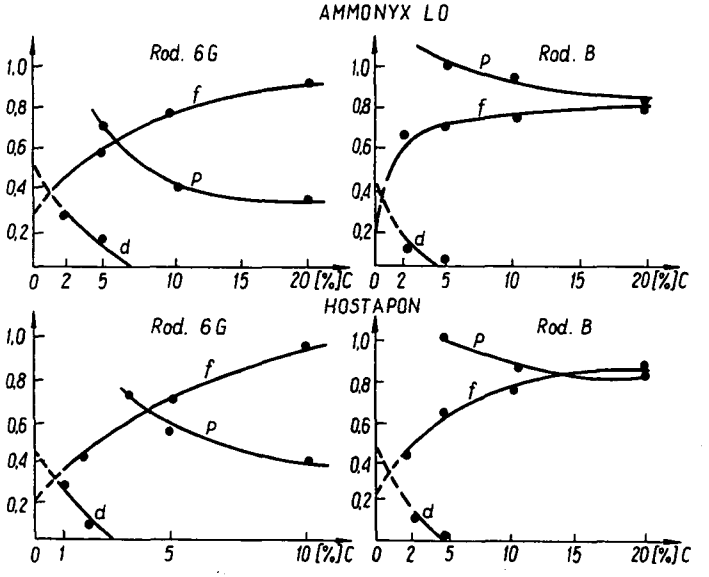

Fig. 3. The degree of dimerization d, relative value of the integrated lintensity f and lasing threshold p versus the detergent concentration. The concentration of Rhodamine B and 6 G was $c = 2 \cdot 10^{-3}$ M

Interpretation

In the region of critical detergent concentration the molecules of the dyes show the minimum quantum yield. This is due to the presence of insoluble dye-detergent complex salts in water.

The increase of quantum yield above the *c.m.c.* is due to the solubilization of the detergent complex salts [14].

The fact that the quantum yield of Rhodamine 6 G for aqueous solution without and with detergents increases from 0.71 to 0.80 is probably due to the solubilization of the dye dimers [7].

The quantum yield of Rhodamine 6 G in detergent solution increases almost by a factor of two. This increase cannot be explained in the same way as for the Rhodamine 6 G solution because the degree of dimerization of Rhodamine B at $2 \cdot 10^{-5}$ M dye concentration in aqueous solution is small.

The most important internal quenching mechanism for these dye molecules is connected with the mobility of the chromophore. In some xanthene dyes like Rhodamine B and Pyronine, potential mobility is connected with the mobility of the amino groups. The fluorescence efficiency of these dyes is reduced in most solvents (*e.g.* ethanol, water). The quantum yield can be increased considerably through the use of a solvent with strong molecular dipole moments which provide a microrigidity around the dye molecules [8].

The dye molecules introduced into the detergent solution are incorporated into micelles. The micelles strongly limit the mobility of the $N\langle^{Me}_{Me}$ groups in Rhodamine B which provide an increase in the quantum yield of these dyes.

The probability of nonradiative processes in Rhodamine B can be determined using the formula

$$W_{S_1S_0} + k_{ST} = (1-)\eta/\tau_f \tag{1}$$

where $W_{S_1S_0}$ and k_{ST} are the internal conversion rate and inter-system crossing rate respectively, τ_f is the mean lifetime of fluorescence.

Using the definition of the radiative transition probability given by the formula

$$A_{S_1S_0} = \eta/\tau_f \tag{2}$$

the influence of the detergent on the radiative processes $A_{S_1S_0}$ can be estimated. The results of the measurements and values of the estimated nonradiative and radiative transition rates of Rhodamine B in aqueous solution with various concentrations of Hostapon and Sulfapol are given in Table I.

It follows from Table I that the detergents prevent the nonradiative processes in Rhodamine B. For example, Sulfapol lowers the rate of the nonradiative processes by a factor of almost three.

Fig. 4 shows the dependence of the relative quantum yield and degree of monomerization of Rhodamine 6 G at $2 \cdot 10^{-4}$ M in aqueous solution with various concentration of Triton X-100. Knowing the molar absorption coefficient of the monomer $\varepsilon_M(\lambda)$ and dimer $\varepsilon_D(\lambda)$ for Rhodamine 6 G in aqueous solutions at excitation wavelength λ and the degree of monomerization X, one can determine the relative rate for "active" absorption.

"Active" absorption is defined as the ratio of the monomer absorption to the total absorption of the monomers and dimers as given by the following equation

$$\chi = \varepsilon_M X/\{\varepsilon_M + \varepsilon_D(1-X)/2\} \qquad (3)$$

Fig. 4 shows the dependence of χ versus the concentration of the detergents calculated using the formula (3). It follows from Fig. 4 that the χ curve does not fit to the curve of the relative quantum yield η/η_0. This can be explained by the effect of the concentration quenching of the fluorescence by energy migration.

This process is very effective for low detergent concentrations, since then, many dye molecules are incorporated into the same micelle. For solutions, where no concentration quenching processes appear, the relative quantum yield is equal to the "active" absorption. If the fluorescence is quenched by some processes then the dependence of η/η_0 versus χ is given by equation

$$\eta/\eta_0 = \chi \cdot \Phi \qquad (4)$$

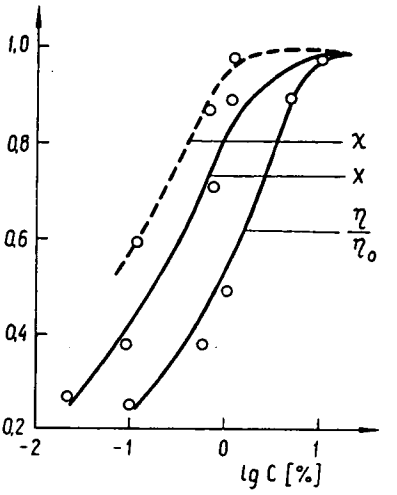

Fig. 4. The dependence of the relative value of quantum yield η/η_0, degree of monomerization X and the ratio of the monomer absorption to the total absorption of the monomer and dimer χ versus the Triton X-100 concentration. The concentration of Rhodamine 6 G is $c = 2 \cdot 10^{-4}$ M

where Φ describes the influence of all concentration quenching processes on the fluorescence quantum yield. If the quantum yield depends only on "active" absorption, the coefficient Φ is unity. From Fig. 4 it follows that the η/η_0 and χ curves differ and the differences are larger for higher detergent concentrations. As it can be seen from Fig. 4 the determined relative value of the quantum yield is three times smaller than the values of χ.

Table I

The τ_f and $W_{S_1S_0}+k_{ST}$ values of Rhodamine B ($2 \cdot 10^{-5}$ M aqueous solutions) versus different detergents concentration

	Detergent	c %	η	$\tau_f \cdot 10^{-9}$ s	$(W_{S_1S_0}+k_{ST}) \cdot 10^8$ s^{-1}
1.	Without detergent	—	0.25	2.1	3.6
2.	Hostapon	2	0.34	3.45	1.9
3.	Hostapon	5	0.41	3.55	1.6
4.	Hostapon	10	0.40	3.75	1.6
5.	Sufapol	2	0.43	3.9	1.4
6.	Sufapol	5	0.45	4.2	1.3

Summary

It has been shown that the quantum yield of Rhodanine B and 6 G depends on detergent concentration. Solutions with a detergent concentration below a critical value have a smaller quantum yield than pure aqueous solutions. This is due to the presence of insoluble dye-detergent complex salts. If the detergent concentration increases above the *c.m.c.*, the quantum yield increases also and reaches saturation for a detergent concentration of 10^{-2} M to 10^{-1} M.

The quantum yield for Rhodamine 6 G increases from 0.71 for pure aqueous solution to 0.80 for solution with detergent. The noted increase of η is due to the solublization of dye dimers. The quantum yield of Rhodamine B increases because the micelles strongly limit the mobility of the $N\begin{smallmatrix}Me\\Me\end{smallmatrix}$ groups in Rhodamine B. The detergents prevent the nonradiative processes in Rhodamine B almost by a factor of three.

Solution with high dye concentration and lower concentration of the detergent have a smaller quantum yield due to the concentration quenching of fluorescence by energy migration. From the performed investigations of the lasing threshold of Rhodamine B and 6 G at $2 \cdot 10^{-3}$ M in aqueous solution it follows that for both dyes a concentration of 5% detergent increases the laser efficiency thus proving that this solution is a good laser medium.

References

[1] *Levshin, W. L., I. S. Lonskay'a:* Opt. Spektr. **11,** 278 (1961).
[2] *Levshin, W. L., W. K. Groskhov:* Opt. Spektr. **10,** 759 (1967).
[3] *Levshin, W. L., E. G. Baranova:* Opt. Spektr. **10,** 362 (1961).
[4] *Marszałek, T.:* Praca habilitacyjna, UMK Torun.
[5] *Bauer, R. K., A. Kowalczyk:* Technical Report No. 3, (1974). UMK Torun.
[6] *Mukerjec, P., K. J. Mysels:* J. Am. Chem. Soc. **77,** 2937 (1955).
[7] *Levshin, W. L., W. G. Baranova:* Opt. Spektr. **6,** 55 (1959).
[8] *Drexhange, K. H.:* IEEE J. Quantum Electron. **QE—8,** 526 (1972).
[9] *Phillion, D. W., D. J. Kuizcuga, A. E. Siegman:* J. Chem. Phys. **61,** 3838 (1974).
[10] *Förster, Th., E. König:* Z. Elektrochem. Ber. Bunsenges. Phys. Chem. **61,** 344 (1957)
[11] *Kenney-Wallace, G. A., J. H. Flint, S. C. Wallace:* Chem. Phys. Lett. **32,** 71 (1975).
[12] *Konefal, Z., E. Lisicki, T. Marszalek:* Acta Phys. Polon. **A52,** 149 (1977).
[13] *Konefal, Z.:* Z. Naturforsch. **34a,** 551 (1979).
[14] *Bálint, E., E. Lehoczki, J. Hevesi:* Zhur. Prikl. Spektr. **19,** 68 (1973).

ВЛИЯНИЕ ДЕТЕРГЕНТОВ НА ЛЮМИНЕСЦЕНТНЫЕ ХАРАКТЕРИСТИКИ РОДАМИНА Б И 6Ж В ВОДНОМ РАСТВОРЕ

З. Конефал

Исследовалось влияние детергентов на выход флюоресценции и на процесс димеризации в лазерных кристаллах таких как Родамин Б и 6 Ж в водном растворе.

Определен эффект концентрационного тушения флюоресценции как функции концентрации детергента.

Установлены оптимальные концентрации детергентов для лазерной генерации.

THE RELATIVE PERMITTIVITY CHANGE OF $Ce(NO_3)_3 \cdot 6H_2O$ AND $Y(NO_3)_3\ 6H_2O$ BETWEEN 193—353 K

By

F. KOCZÓ, N. DULIĆ and L. HORVÁTH

Technical High School, Subotica, Yugoslavia

(Received May 16, 1984)

Recently many articles were published on the structure of cerium(III)-nitrate and yttrium(III)-nitrate supplied by Merck. Some of the investigations proved that the bound water is the same in these compounds. Our investigations support the bound water differences indicated by Merck, as well as the first bound water release temperature, which had been found to be (341—343) K cerium(III)-nitrate and (331—333) K in the case of yttrium(III)-nitrate.

Introduction

During our experiments regarding the dielectric behaviour of these substances, we have examined the relative permittivity change of cerium(III)-nitrate and yttrium(III)-nitrate. The temperature range was between 193—353 K at $\omega = 10^4$ 1/s constant angular frequency. Both substances are known to contain bound water, although this amount of water varies, depending on temperature.

We tried to find discrete temperatures at which an unambiguous phase transition or change in structure could be detected, due to change in the amount of absorbed water. For this purpose, we have examined the relative permittivity temperature dependence of the above mentioned substances, assuming that the changes in structure are followed by a sudden change of permittivity.

We have kept the tested, highly hygroscopic substances at 40 °C for few days, then they were dried in a desiccator at ambient temperature for two months. The conductivity of the substances prepared in such a manner was an order of nS, while their conductivity was an order of mS prior to drying.

The tested substances have not been purified. According to the data of the producer (Merck) the quality of yttrium(III)-nitrate was laboratory pure, while the cerium(III)-nitrate contained 1.5% of other rare-earth metals.

Measuring equipment

We determined the permittivity by measuring the capacitance of a measuring condenser (Fig. 1). This capacitance was measured by means of an a.c. bridge. As a basic instrument we used a $\omega \sim 10^4$ 1/s angular frequency (1591.5 Hz) bridge, type B331 MK from WAYNE KERR, while a signal generator type 3310 A from HEW-

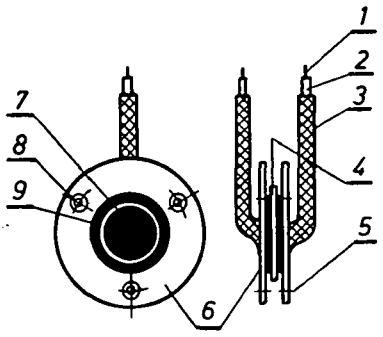

Fig. 1. 1 — copper wire, 2 — teflon insulation, 3 — shielding, 4 — sample, 5 and 8 — coupling bolt holes, 6 — insulation material, 7 and 9 — shielding harness and measuring armature

LETT PACKARD served as an external source. As a signal detector we used an ORTHOLOC SC™—9505 TWO PHASE LOCK-IN ANALYSER from EGG BODKREAL. Its output signal was transmitted to a HP 7046 A X—Y recorder.

In such a manner we obtained the plot of the capacitance of the measuring condenser and the thermo-voltage on the output. At the same time we could also measure the conductivity using the equipment (Fig. 2). The measuring condenser together with the thermostat was placed in the internal part of a VÖTSCH VMT II test chamber, where the temperature could be varied continuously between 193—353 K.

We measured the temperature with a thermocouple and its hot spot was directly at the measuring condenser while its cold juntion was at water freezing point. From the capacitance of the measuring condenser, filled with the substance to be tested, the permittivity can be determined by means of a calibration curve. For recording the calibration curve a substance of known permittivity was placed in the measuring condenser.

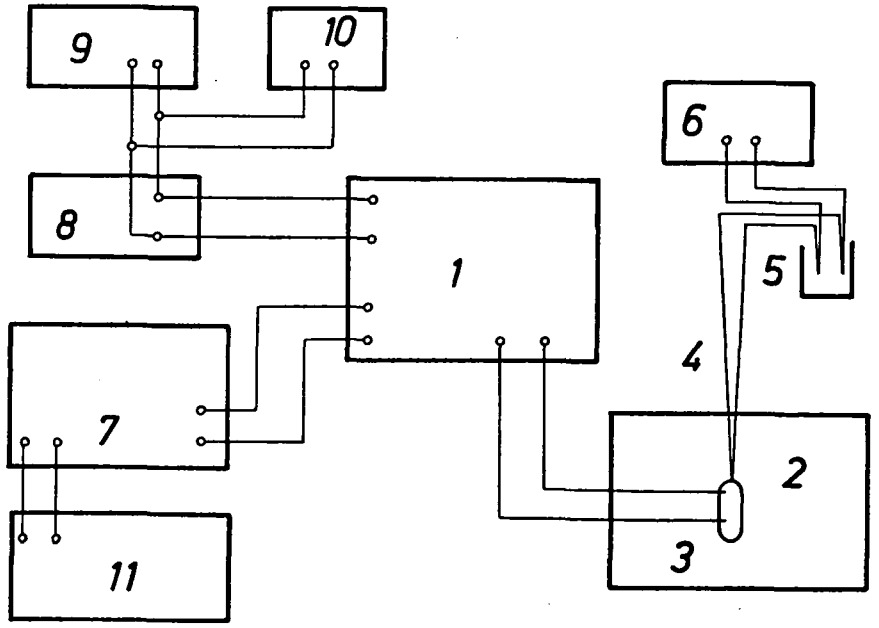

Fig. 2. 1 — WK, 2— test chamber, 3 — thermostat, 4 — thermocouple, 5 — cold junction, 6 — multimeter, 7 — lock-in analyser, 8 — multimeter, 9 — signal generator, 10 — fequency meter, 11 — X—Y recorder

The curve obtained in such a manner properly agreed with the curve, which was drawn on the basis of a theoretically derived formula [1,2] for this type of condenser. The difference was below 1%.

For the substance tested, pellets have been pressed under 15 MPa pressure. The results of the measurements have been affected by the parallelism of the sample surfaces, their roughness and changes in the solidity by each specimen. If the sample surfaces were not parallel and the circumference of the surfaces was rough an air gap could appear between the measuring condenser and the circumference of the sample. The existence of such an air gap could be an important source of errors during the permittivity measurements, so we made measurements for the evaluation of errors. The known permittivity for the pellet dispersion of substances having various thicknesses was 1.5% at 95% reliability.

Results of measurements

The results of the tested substances are shown in Fig. 3. For the temperature dependence of the relative permittivity of cerium(III)-nitrate we have shown two

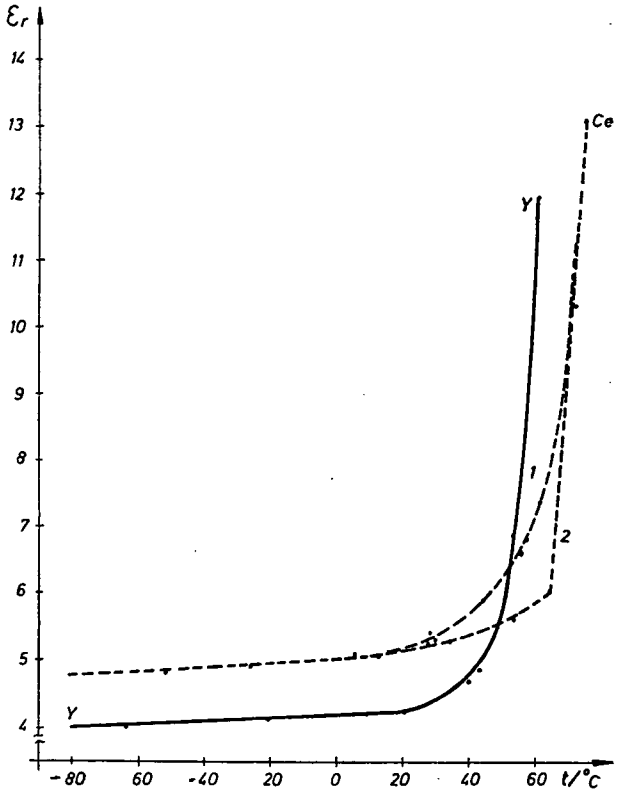

Fig. 3.

curves heated in two different ways. In the case of curve **1** the temperature change was about 1 °K /min., while in the case of curve **2** the the temperature change was so slow, that the reading has practically happened at a complete thermal equilibrium. In the case of yttrium(III)-nitrate the heating rate was the same as at curve **1** of the previous sample.

Analysis of results

The relative permeability of yttrium(III)- and cerium(III)-nitrates shows a slight change in the low temperature range which proves that there is a dominant induced polarization.

The relative permittivity of cerium(III)-nitrate at such temperatures is higher at about 20% than that of yttrium(III)-nitrate. This difference is due to the fact, that there are more water molecules near the cerium ion than near the yttrium ion. This assumption is supported by the sample-structure test results [3, 4].

The relative permittivity of yttrium(III)-nitrate shows a jump at about 323 K which is followed by a sudden increase in conductivity. The same phenomenon happens in the case of cerium(III)-nitrate at about 333 K. The increase of permittivity can be explained by the orientation polarization of the releasing water molecules. Neither does this method provide any information regarding the release of water quantity nor does it give details of the occuring change in structure. The structural change of the cerium(III)-nitrate is supported by the crystallographic tests [5] while there is no indication in literature about the structural changes of yttrium(III)-nitrate at 333 K. Another change of structure at higher temperature (361 K) has already been reported [6].

References

[1] *Von Hippel, A. R.:* Dielectric Materials and Applications, M. I. T. Press, Cambridge, Mass., 1966.
[2] *Frõlich, H.:* Theory of Dielectric, Dielectric Constant and Dielectric Loss, Oxford and the Clarendon Press, 1968.
[3] *Milinski, N., B. Ribar and M. Satarić:* Cryst. Struct. Comm. **9**, 473 (1980).
[4] *Ribar, B., N. Milinski, Ž. Budovalčev, I. Krstanović:* Cryst. Struct. Comm. **9**, 203 (1980).
[5] *Milinski, N., P. Radivojević, B.—Ribar, and S. Djurić:* Cryst. Struct. Comm. **11**, 1241 (1982).
[6] *Radivoiević, P., N. Milinski, B. Ribar and D. Lazar:* Cryst. Struct. Comm. (in press).

ИЗМНЕНИЯ ДИЭЛЕКТРИЧЕСКОЙ ПРОНИЦАЕМОСТИ В $Ce(NO_3)_3 \cdot 6H_2O$ И $У(NO_3)_3 \cdot 6H_2O$ В ИНТЕРВАЛЕ ТЕМПЕРАТУР 133—353 К

Ф. Коцо, Н. Дулич и Л. Хорват

Измерены изменения диэлектрической проницаемости в $Ce(NO_3)_3 \cdot 6H_2O$ и $У(NO_3)_3 \cdot 6H_2O$ в интервале температур 193—353 К. Полученные результаты подтверждают различное количество и различие в характере связывания кристаллизационной воды, предположенное фирмой изготовителем препаратов (Мерк).

INHIBITORY EFFECTS OF SOME HETEROCYCLIC DERIVATIVES OF MERCAPTANS, CORRELATED TO THEIR ACIDITY EXPRESSED AS A PROTON LEVEL, J

By

HIGAZ NADER ALI

College of Education, University of Aden, Aden, P. D. R. Yemen

(Received 26th October, 1983)

A quasipotentiostatic polarization method has been applied for study of the inhibitory effects of some heterocyclic dervatives of mercaptans on the corrosion behaviour of pure copper in deaerated solutions containing chloride ions. This study showed the inhibitory effectiveness to be a function of the acidity of the inhibitor, expressed as a proton level, **J**.

Introduction

The corrosion of copper is a common problem; it is frequently encountered in cooling systems that use hard water containing soluble chlorides. The inhibition of copper corrosion in similar media has been investigated with the use of some organic inhibitors [1—3]. Among the organic inhibitors applied for the inhibition of copper corrosion in acetic and chloroacetic acid solutions, 2-Mercaptobenzothiazole **(2-MBt)** proved to be an excellent inhibitor [4]. In connection with the inhibition of the corrosion of pure copper in neutral solutions containing chloride ions, our aim was to study the relative inhibitory effects of some heterocyclic derivatives of mercaptans by means of a quasipotentiostatic polarization method, and also to examine whether the relative inhibitory effects of the investigated inhibitors were related to their acidity.

Experimental

Cylindrical copper electrodes, made from high-purity copper rods supplied by Johnson Matthey Ltd., were used for the electrochemical investigations. The electrodes were abraded with 600 emery paper, degreased with acetone, washed with a jet of tap water, and finally rinsed with distilled water. The inhibitors investigated were selected from those previously applied for the inhibition of the corrosion of 316 L stainless steel [5].

The selected inhibitors were 2-mercaptobenzimidazole **(2-MBi)**, 2-mercaptobenzothiazole **(2-MBt)**, and 2-mercaptobenzoxazole **(2-MBo)**. These were chosen because of the similarity of their chemical structures, which are shown in Table I.

Table I

Chemical structures of the investigated inhibitors

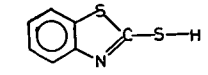

2-Mercaptobenzothiazole

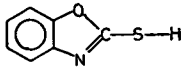

2-Mercaptobenzoxazole

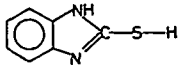

2-Mercaptobenzimidazole

The inhibitory effectiveness was determined at a constant concentration of 10^{-3} mol dm^{-3} in deaerated solution containing 0.10 mol dm^{-3} of Cl^- ions. The chosen inhibitor was dissolved in methanol so that 50 cm^3 of the prepared solution gave the desired concentration, when diluted to 1 dm^3. The neutral chloride solution without inhibitor contained the same amount of methanol.

In the case of **2-MBt** the inhibitory effects was also determined in a slightly acidic solution (pH=4). The experiments were conducted in the same electrolytic cell as used in our previous investigations. [5]. Prior to the electrochemical measurements, deaeration was accomplished by bubbling highly-purified nitrogen gas through the solution. A nitrogen atmosphere was maintained during the measurements by passing nitrogen gas above the solution. The measurements were made at 25±1 °C. The polarization experiments were performed with a PRT—100—1X Tacussel Potentiostat. The electrodes were polarized from the stationary potentials in the noble direction at a scanning rate of 25 mV/5 min (0.30 V/hr). Though the electrode potentials were measured with respect to the saturated calomel electrode, here they are given with respect to the normal hydrogen electrode.

Results and discussion

In the absence of inhibitors, both in slightly acidic (pH=4) and in neutral (pH=7) chloride solutions, copper was found to exhibit only general corrosion. No pitting corrosion was observed, up to 500 mV. This was also checked after the completion of the electrochemical measurements under a magnifying microscope. Copper exhibited active anodic dissolution at low electrode potentials, in agreement with the results found by TAYLOR ET AL [6]. The Tafel slope established in the active domain was found to be equal to 60 mV, a value close to that found by KISS ET AL [7]. Copper initially dissolves in chloride solutions as monovalent copper [8—11]. Figure 1 shows the quasipotentiostatic polarization curves of pure copper in slightly acidic chloride solutions in the absence and in the presence of **2-MBt**.

Similarly, in slightly acidic (pH=4) chloride solutions in the presence of **2-MBt**, copper was found to exhibit only general corrosion. This was checked after the comple ion of the electrochemical measurements, using the magnifying microscope. The electrodes were found to be unpitted. In the presence of **2-MBt**, as it can be seen from

Fig. 1, the anodic dissolution of copper was significantly depressed. The anodic Tafel slope in the presence of **2-MBt** was found to be equal to 75 mV.

The inhibitory effect of **2-MBt** proved to be better at pH=7 than at pH=4. As can be seen from Fig. 2, in neutral chloride solutions in the presence of **2-MBt**, the active domain of copper was completely depressed. However, at electrode potentials more noble than 475 mV, pitting corrosion occured. After the completion of the electrochemical measurements, a few small pits were detected in the electrodes under the magnifying microscope.

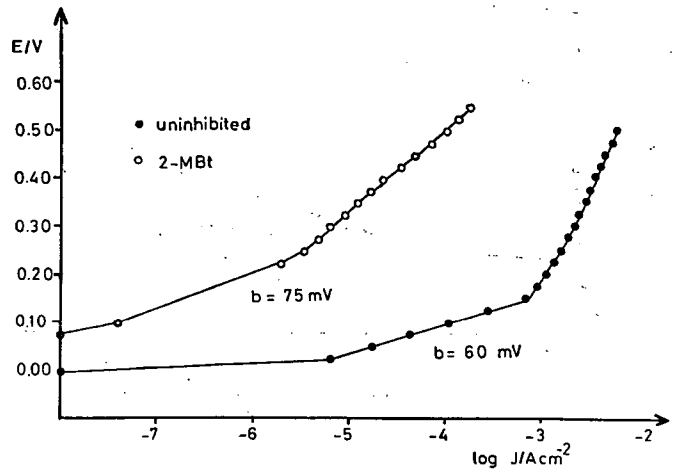

Fig. 1. Quasipotentionstatic anodic polarization curves of pure copper in the absence and in the presence of **2-MBt**, at pH=4.

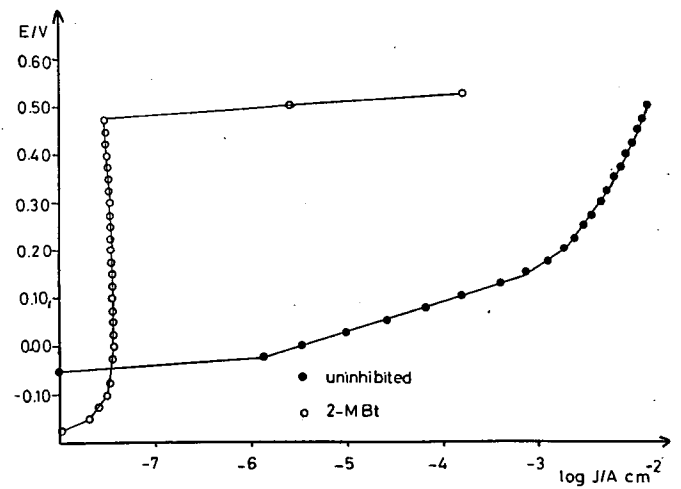

Fig. 2. Quasipotentiostatic anodic polarization curves of pure copper in the absence and in the presence of **2-MBt**, at pH=7.

The investigated inhibitors have a common functional group (—SH) in addition to two donor atoms bonded to the carbon atom to which the —SH group is bonded. Since **2-MBt** proved to be more effective at pH=7 than at pH=4, the inhibitory effects of the investigated inhibitors were determined at pH=7.

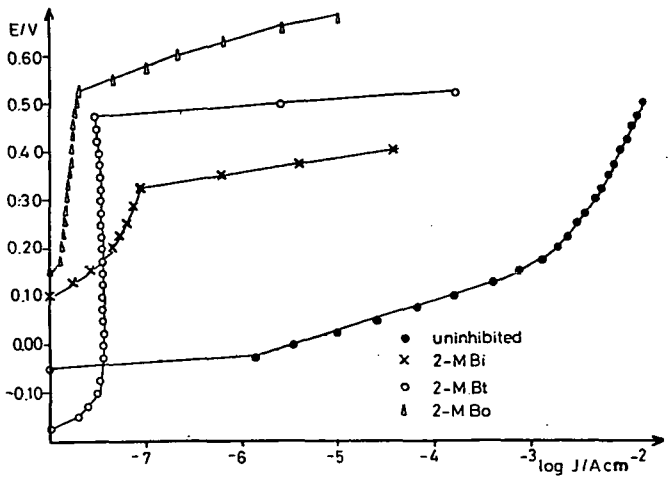

Fig. 3. Quasipotentiostatic anodic polarization curves of pure copper in the absence and in the presence of the investigated inhibitors

Fig. 3 shows the anodic polarization curves of pure copper in the absence and in the presence of the investigated inhibitors. As can be seen from Fig. 3, in the presence of the investigated inhibitors the active anodic dissolution of copper was significantly depressed, especially in the case of **2-MBo**. In the presence of the investigated inhibitors, copper was found to exhibit passivation and pitting corrosion. After the electrochemical measurements, a number of small pits were found in the electrodes.

Table II. shows the corrosion data, reflecting the relative inhibitory effects of the investigated inhibitors. As can be seen from Table II, the average current densities, j_p, established in the passivation domain in the presence of the investigated inhibitors, lay in the following sequence:

$$j_p(\text{2-MBo}) < j_p(\text{2-MBt}) < j_p(\text{2-MBi}).$$

It seems reasonable that the lower the current density in the passive state, the higher the stability of the passive films, *i.e.* the more noble the breakdown potential is expected to be. This assumption seems to fit in with our results. Thus from Table II, Fig 3. and the above comparisons, it can be seen

Table II

Corrosion data reflecting the relative inhibitory effects of the investigated inhibitors in solution containing 0.10 mol dm^{-3} Cl^- *ions at* pH=7

Inhibitor	$E_{corr.}/V$	J_p $\mu A\ cm^{-2}$	E_b/V
—	−0.05	—	—
2-MBi	0.10	0.04	0.325
2-MBt	−0.175	0.03	0.475
3-MBo	0.15	0.012	0.525

that the relative effectiveness of the investigated inhibitors displayed the following sequence:

2-MBi < 2-MBt < 2-MBo.

Using the weight loss method, PRAPAJATI ET AL [4] found **2-MBt** to be an excellent inhibitor of the corrosion of copper in acetic and chloroacetic acid solutions. They attributed the effectiveness of **2-MBt** to the very high stability of the copper-**2-MBt** complex. Further, they also reported [12] that the ionic species of **2-MBt** form an insoluble complex salt [Cu(**2-MBt**)$_2$] with copper cations. This acts as a protective coating on the metal surface.

Similarly, the potentiodynamic method showed that **2-MBt** is effective in inhibiting the anodic dissolution of copper in 0.10 M NaCl. According to TRABANELLI ET AL [13], the inhibitory effect is due to an adherent and protective film formed by the binding between **2-MBt** and copper cations through the sulphur atom of the —SH group and by means of bonds coordinated with the electron pairs of the other sulphur atom or of the nitrogen atom. However, the IR data suggested that the bonding occured only the sulphur atom [14].

Because of their common features and their similar chemical structures, **2-MBi**, **2-MBt** and **2-MBo** were expected to exhibit similar inhibition mechanisms. This accounts for the fact that in their presence only pitting corrosion was observed to take place at more noble potentials. Thus, the inhibitory effects of each of them may be attributed to the interaction of the ionic species of the inhibitor with the copper cations in the metallic substrate, leading to the formation of an insoluble protective film. The bonding is achieved mainly between the negatively charged sulphur atom of the —SH group and the copper cations. This would explain the better effectiveness of **2-MBt** at pH=7 than at pH=4, for the ionic concentration of **2-MBt** is greater at pH=7 than at pH=4, and as a result the protective film is more stable at pH=7 than at pH=4. That the protective film is more stable at pH=7 than at pH=4 can also be inferred from a comparison of the anodic polarization curves of pure copper in the presence of **2-MBt** at pH=4 and pH=7.

At pH=7 and at a constant inhibitor concentration of 10^{-3} mol dm^{-3} in our case, the concentration of any of the ionic species is expected to be higher if the acidity is greater, probably leading to the formation of a more stable passive film and consequently to a more noble break-down potential. To check this assumption, the break-down potentials recorded in the presence of the investigated inhibitors were compared with their acidity expressed as a proton level, **J**, given by the VERMILYEA equation [15].

VERMILYEA ET AL [15] reported that the inhibitory effectiveness is a function of the acidity of the inhibitor, expressed as a proton level, **J**:

$$-\mathbf{J} = 0.059\,(1.744 - \log K_a)$$

where K_a is the acid dissociation constant of the inhibitor. Since $-\log K_a = pK_a$, the above equation may also be written in the following form:

$$-\mathbf{J} = 0.059\,(1.744 + pK_a).$$

Table III shows the pK_a and the caculated **J** values. The pK_a values of the investi-

Table III

pK_a and J data on the investigated inhibitors

Inhibitor	pK_a	J
2-MBi	9.2	−0.65
2-MBt	7.2	−0.53
2-MBo	6.6	−0.49

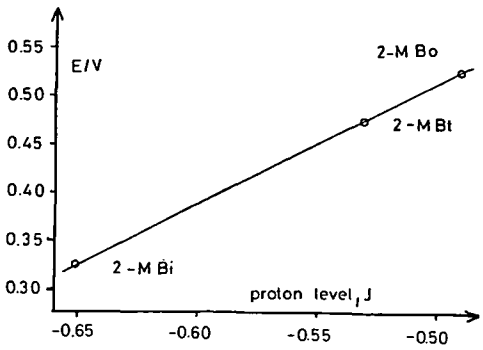

Fig. 4. Dependence of the break-down potentials of copper on the acidity of the investigated inhibitors, expressed as a proton level, **J**

gated inhibitors have been quoted from [4].

Fig. 4 shows the dependence of the break-down potentials on the acidity of the investigated inhibitors, expressed as a proton level, **J**.

As can be seen from this Figure, the coordinates (J, E_b) of the investigated inhibitors fall on a straight line, indicating that these inhibitors have a common inhibition mechanism. The break-down potential becomes linearly more noble as the acidity of the inhibitor increases. This result illustrates the importance of the acidity of the inhibitors in the corrosion inhibition mechanism

Conclusions

The investigated heterocyclic derivatives of mercaptans appreciably inhibited the corrosion of pure copper in deaerated neutral solutions containing chloride ions. The active anodic dissolution of copper in such agressive media was significantly depressed in their presence, especially in the case of **2-MBo**. The inhibitory effect of each of them is propably due to the formation of an insoluble protective surface film. A simple relation correlating the effectiveness of these inhibitors has been obtained, based on the break-down potentials. The higher the acidity of the inhibitor, expressed as a proton level, **J**, the more effective the inhibitor proved to be. This result illustrates the importance of the acidity of the inhibitors in the corrosion inhibition mechanisms. Of the investigated inhibitors, **2-MBt** and **2-MBo** proved to be very effective for inhibition of the corrosion of copper in neutral chloride solutions.

References

[1] *Ken Nobe:* Corrosion **29,** 5 (1975).
[2] *Đessi, N. N., S. S. Rana:* Compt. Rend. du 2eme Symp. Europeen Sur les Inhibiteurs de Corrosion, Annali Univ. Ferrara, N. S., Sez. V. Suppl. 849 (1966).
[3] *Kobayashi, T.:* Besheku Gijutsu **13,** 246 (1964). C. A. **63,** 318 (1965).
[4] *Prajapati, S. N. et al:* J. Electrochem. Soc. India **25'** 175 (1976).
[5] *Rauscher, Á., Higaz Nader Ali, J. Horváth, M. I. Bán and I. Bálint:* Acta Phys. et Chem. Szeged **27,,** 59 (1981).
[6] *Taylor, H.:* J. Electrochem. Soc. **118,** 6, 854 (1975).
[7] *Kiss, L., J. Farkas, A. Kores:* Acta Chim. Hung. **67,** 179 (1971).
[8] *Turner, M., P. A. Brook:* Corrosion Sci **13,** 12, 973 (1975).
[9] *Flat, R. K., Brook, P. A.:* Corrosion Sci. **11,** 185 (1971).
[10] *Sugawara, H., H. Ebike:* Corrosion Sci. **7,** 513 (1967).

[11] *Rothenbacher, P.:* Corrosion Sci. **10,** 391 (1970).
[12] *Prajapati, S. N., et al:* Indian J. Technol. **10,** 73 (1972).
[13] *Fontana, M. G., R. W. Staehle:* Adv. in Corrosion Sci. and Technol. Vol. 1 191. Plenum Press, N. Y. 1970.
[14] *Khan, M. M., A. U. Malik:* Inorg. Nucl. Chem. **34,** 1847 (1972).
[15] *Vermilyea, D. A., W. Vedder:* Trans. Faraday Soc. **66,** 2644 (1970).

ИНГИБИРУЮЩИЙ ЭФФЕКТ НЕКОТОРЫХ ГЕТЕРОЦИКЛИЧЕСКИХ ПРОИЗВОДНЫХ МЕРКАПТАНОВ В СОПОСТАВЛЕНИИ С ИХ КИСЛОТНОСТЬЮ

Хигаз Надер Али

С применением квазипотенциостатического метода было изучено ингибирующее действие некоторых гетероциклических производных меркаптанов на коррозию чистой меди в растворах, содержащих постоянные концентрации хлоридов. Результаты работы показывают, что эффективность ингибиторов является функцией их кислотности.

ÜBER PEPTISIERUNG UND OBERFLÄCHENMODIFIZIERUNG VON ILLIT AUS FÜZÉRRADVÁNY

Von

Á. PATZKÓ, F. SZÁNTÓ

Institut für Kolloidchemie der Attila József-Universität, Szeged

(Eingegangen am 23 Mai 1984)

Es wurde die Adsorption von CPCl an Illit-Fraktionen aus Füzérradvány geprüft. Die Fraktionierung des Tones wurde unter Zuhilfenahme der Peptisation mit Natriumkarbonat durchgeführt. Die Adsorptionsisothermen weisen auf chemische und physikalische Adsorption hin. Aus den Isothermen wurden die Werte der organischen Kationenaustausch und der spezifischen Oberfläche berechnet. Die Sedimentvolumina und die relative Viskosität der Suspensionen der Organokomplexe wurden in Benzol gemessen und festgestellt, dass diese sich mit der Adsorptionsmenge einer Maximum-Kurve entsprechend ändern. Diese mit der zunehmenden Organophilität des Illits parallel eintretende Änderung kann mit der Benetzung, Quellung und der Desaggregation der Organokomplexe erklärt werden.

Einleitung

Seit Jahrzehnten befasst man sich mit der Adsorption von Stoffen verschiedener Molekülstruktur an Tonmineralien. Aus der Literatur ist bekannt, dass die Adsorptionskapazität in der Reihe Montmorillinit, Illit, Kaolinit abnimmt [1—6].

Aus Tonmineralien können mit kationaktiven Stoffen in organischen Flüssigkeiten gut benetzende organophile Produkte hergestellt werden. Die Modifizierung der Oberfläche ist bei Illit nur an den äusseren Oberflächen möglich, bei Montmorillonit aber können die Moleküle des kationaktiven Stoffes zwischen die Basisoberflächen eindringen [7—9]. Das Verhalten des organophilen Illits in organischen Flüssigkeiten wird durch die Benetzung, im Falle des organophilen Montmorillonits aber in erster Reihe durch die Quellung und Desaggregation beeinflusst. Dies alles wird durch die Eigenschaften des organophilen Stoffes, sowie durch die Polarität und Zusammensetzung des Dispersionsmittels bestimmt [10].

Unsere früheren Untersuchungen [11] haben wir jetzt mit Illiten fortgesetzt. Unser Ziel war, es einen Zusammenhang zwischen den Eigenschaften der organophilen Illitsuspensionen und Adsorption des kationaktiven Stoffes zu finden.

Versuchsmaterialen und Methoden

Als Modellsubstanz wurden drei Illite aus Füzérradvány verwendet. Um die groben Tonminerale und ihre Beimineralien trennen zu können, benötigen wir zur Peptisierung und Desaggregierung des Illits Natriumkarbonat in optimalen Mengen. Die Natriumkarbonatmenge wurde so gewählt, dass sie auf das Illit berechnet zwi-

schen 1 und 1,5 Gev.-Prozent lag. Zu den konzentrierten, wässrigen Suspensionen wurde das Natriumkarbonat in Form einer wässrigen Lösung (50 g pro dm^3) hinzugegeben. Die zu Gelen erstarrten Systeme wurden mehrmals umgerührt und einen Tag lang stehen gelassen. Die 2-prozentigen wässrigen Suspensionen wurden nach eintätigem Stehenlassen in grossen Flaschen sedimentiert. Diese Sedimente setzen sich überwiegend aus Teilchen mit einem Äquivalentradius von grösser als 1 μm zusammen.

Die weitere Zerlegung der übergebliebenen Suspensionen wurde mit der Laboratoriumszentrifuge mit 10 000 Umdrehungen pro Min. 15 Minuten lang durchgeführt. Der sich in der Zentrifuge absetzende relative grobdisperse Anteil wird „mittlere Fraktion", die hochdisperse Fraktion „kolloide Fraktion" genannt.

Die röntgenographische Untersuchung der einzelnen Fraktionen* hat gezeigt, dass die kolloide Fraktion von Illit 1. zwischenschichtliche Illit-Montmorillonit enthielt. Im Illit 2. lassen sich neben der Basisreflexion von Illit, mit kleinerer Intensität auch Montmorillonit-Reflexionen erkennen. Im Illit 3. ist nur die Basisreflexion des Illits erkennbar. In den mittleren Fraktionen können Kaolinit und Quartz nachgewiesen werden.

Die Adsorptionsversuche mit Cetylpyridiniumchlorid (CPCl) führten wir auf folgende Weise durch: Es wurde die 10 g pro dm^3 wässrige CPCl-Lösung zu Illitsuspensionen bekannter Konzentration (5 g pro dm^3) zugegeben. Dies löste die Koagulation der Systeme aus. Der voluminöse Niederschlag wurde getrocknet, gemahlen und durch ein Sieb von 60 μm Lochbreite durchgelassen. Die Konzentration des kationaktiven Stoffes wurde durch die sog. Zweiphasen-Titrierung bestimmt, vor und nach der Adsorption [13]. Die Berechnung der adsorbierten Menge geschah nach der Formel:

$$n^{a(v)} = \frac{V}{m}(c_0 - c_g)$$

wo V das Lösungsvolumen, c_0 die Anfangs-, c_g die Gleichgewichtskonzentration des Adsorptivs und m die Menge des Adsorbens bedeuten.

Das Sedimentvolumen des organophilen Illites wurde in 10 cm^3 Proberöhren mit je 0,1 cm Einteilungen bei Zimmertemperatur in Benzol durchgeführt. Die Ausflusszeit der Suspensionen wurde nach zwei Wochen unter Zuhilfenahme eines Ostwaldschen Viskosimeters gemessen. Das Suspendieren und die Sedimentation wurde mehrmals wiederholt.

Versuchsergebnisse

Die Adsorptionsisothermen (siehe Abb. 1) wurden an den mittleren und kolloiden Fraktionen der Illit-Proben aufgenommen. Diese zeigen, dass bis gewissenen zugegebenen Mengen von CPCl die ganze Menge irreversibel quantitativ adsorbiert wird, bis ein kritischer Wert erreicht ist. CP^+-Ionen werden als Kationen eingetauscht, im Austausch gegen die austauschfähigen Kationen des Illits. Das organische Kationenaustausch-Vermögen an verschiedenen Fraktionen zeigt Tabelle I.

* Die Röntgenprüfungen wurden an dem Lehrstuhl für Mineralogie, Geochemie und Gesteinskunde der Attila József-Universität und an dem Lehrstuhl für Mineralogie der Universität für Chemische Industrie Veszprém ermittelt, wofür wir unseren Dank ausdrücken.

Tabelle I

Die Werte der Adsorptionsisothermen

Adsorbens	Organische Austausch-kapazität mäqu./100 g	Spezifische Oberfläche, a_s m²/g		zu V_{max} gehörende Werte	
				$n^{\sigma(v)}$ mäqu./100 g	a_s m²/g
Kolloide Fraktion					
CP-Illit 1.	14,5	269	550	30	218
CP-Illit 2.	12,5	219	405	23	167
CP-Illit 3.	4,0	182	—	12	79
Mittlere Fraktion					
CP-Illit 1.	6,0			8	58
CP-Illit 2.	5,5	97,5	—	8	58
CP-Illit 3.	2,5			—	—

Bei höheren CPCl-Konzentrationen nimmt die Adsorption eigenartigerweise weiter zu. Diesen Isothermen-Ast schreiben wir einer physikalischen Adsorption zu. Die Isothermen der kolloiden Fraktionen von Illit 1. und 2., die auch quellfähige Gitter enthalten, steigen am höchsten an. Das Mass der physikalischen Adsorption hängt von der Struktur des Adsorbens ab.

Die Adsorptionsisothermen wurden auch in linearisierter Form dargestellt. In Abb. 2. geben wir als Beispiel die auf die einzelnen Fraktionen bezüglichen Daten an. Die Werte $1/n^{\sigma(v)}$ nehmen für die mittleren Fraktionen und die Kolloid-Fraktion ohne Montmorillonit im untersuchten Bereich mit der Menge $1/c_g$ praktisch linear zu. Bei den übrigen kolloiden Fraktionen sind zwei Stufen zu erkennen. Aus dem Schnittpunkt der Ordinatenachse wurde die Oberfläche nach PHAM und BRINDLEY [13] bestimmt. Für dem Oberflächenbedarf eines CPCl-Moleküls wurde der Wert 1,21 nm² verwendet. Die erhaltenen Daten sind in Tabelle I. zusammengefasst. Aus den Daten

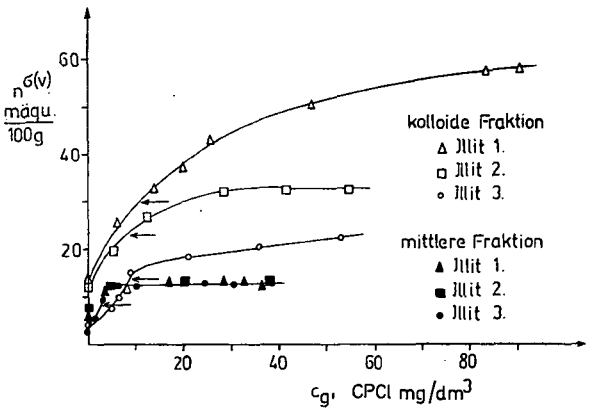

Abb. 1, Die Adsorptionsisothermen von Illit-Fraktionen aus Füzérradvány

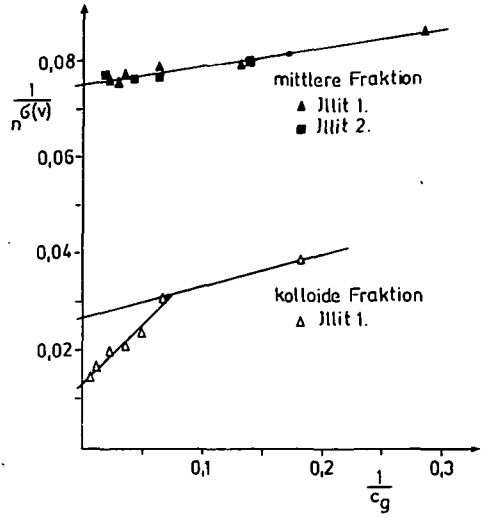

Abb. 2. Die in der linearisierten Form Adsorptionsisothermen

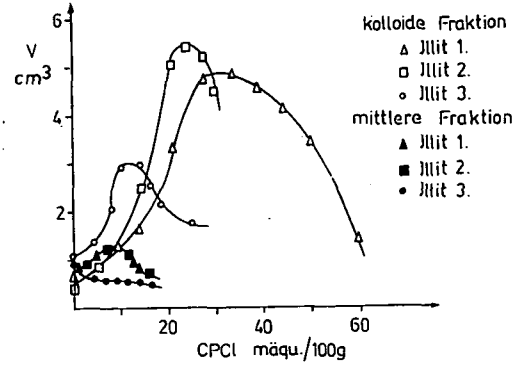

Abb. 3. Änderung des Sedimentvolumens der organophilen Illite in Benzol

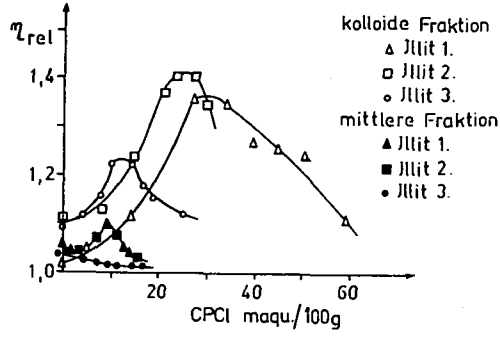

Abb 4. Änderung der relativen Viskosität der organophilen Illite in Benzol

ist ersichtlich, dass sich auf den ersten monomolekularen Adsorptionsschicht möglicherweise noch eine zweite mit umgekehrter Orientierung aufbaut.

Abb.-en 3—4. zeigen die charakteristische Änderung des Sedimentvolumens und der relativen Viskosität in Benzol mit zunehmender Menge des kationaktiven Stoffes. Die Kurven steigen zuerst langsam, dann steiler an, um nach einem Maximum zu fallen. Wenn die adsorbierte Menge so gross ist, dass sich auf die erste Adsorptionsschicht noch eine zweite mit umgekehrter Orientierung aufbaut, wird die Oberfläche wieder weniger hydrophob, dementsprechend nimmt das Sedimentvolumen ab. Die Quellung, das heisst, die Lage und Höhe des Maximums sind praktisch von der Adsorptionsfähigkeit abhängig. Die Lage des Maximums wurde mit Pfeil an der Adsorptionsisothermen (in Abb. 1.) gekennzeichnet. Es erleuchtet, dass das maximale Sedimentvolumen bei beginnender physikalischen Adsorption gefunden werden kann. Aus der dem V-Maximum entsprechenden adsorbierten Menge wurden auch die spezifischen Oberflächen der Illit-Fraktionen bestimmt. Die so berechneten Werte sind kleiner als die aus dem Schnittpunkt der Ordinatenachse erhaltenen Werte siehe (Tabelle I.).

Die Änderung des Sedimentvolumens läuft parallel mit der in Benzol gemessenen relativen Viskosität. Die Benetzung der Illit-Fraktionen in Benzol wird mit zunehmender Organophilität immer besser, da die Möglichkeit der Quellung und der Desaggregation in der Suspension zunimmt. Ein ähnliches Verhalten lässt sich auch beim Sedimentvolumen und bei der relativen

Viskosität erkennen. Nach Durchlaufen des Maximums wird die Benetzung immer schlechter, gleicher Weise nimmt die Quellung und die Desaggregation ab (Abb. 3—4.).

Die aus der mittleren Fraktion des Illits 3. hergestellten organophilen Stoffe verhalten sich in Benzol so, wie die Systeme aus kompakten, ungeqollenen Teilchen. Das Sedimentvolumen und die relative Viskosität nimmt mit zunehmender Organophilität ab, weil mit etwas besserer Benetzung die organophilen Illitteilchen sich einander nähern. Zugleich wird das Volumen des Sediments kleiner und auch die Viskosität nimmt ab (Abb. 3—4).

Aus den Untersuchungen ergibt sich, dass die Eigenschaften der Suspension von organophilen Illiten sich mit der Adsorptionskapazität parallel ändern, und dies wird von der mineralischen Zusammensetzung beeinflusst, wobei die relative Menge der quellenden Schichten eine entscheidende Rolle spielt.

References

[1] *Pinck, L. A., W. F. Holton and F. E. Allison:* Soil Sci., **91,** 22 (1961).
[2] *Frissel, M. J. and G. H. Bolt:* Soil Sci., **94,** 284 (1962).
[3] *Greenland, D. J., R. H. Laby and J. P. Quirk:* Trans. Faraday Soc., **61,** 2013 (1965).
[4] *Greenland, D. J., R. H. Laby and J. P. Quirk:* Trans. Faraday Soc., **61,** 2024 (1965).
[5] *Thompson, T. D. and G. W. Brindley:* Am. Mineralogist, **54,** 858 (1969).
[6] *Bansal, O. P., Singhal, J. P. and S. U. Khan:* J. Colloid Interface Sci., **81,** 180 (1981).
[7] *Weiss, A.:* Clays Clay Minerals, **10,** 191 (1963).
[8] *Weiss, A.:* Organic derivatives of clay minerals, zeolites and related minerals. In: G. Eglinton and M. T. J. Murphy (Editors), Organic Geochemistry, Springer Verlag, Berlin, pp. 737—781. 1969.
[9] *Lagaly, G.:* Clay Minerals, **16,** 1 (1981).
[10] *Szántó, F., S. Veres:* Acta Phys. et Chem. Szeged, **9,** 157 (1963).
[11] *Szántó, F., B. Várkonyi, Á. Patzkó:* Settling properties of clay minerals in presence of cation active substances. 1st Conference on Colloid and Surface Chemistry, Mátrafüred, 111—113. 1971.
[12] *Szántó, F., M. Gilde-Farkas, B. Várkonyi, J. Balázs:* Acta Geol. Hung., **11** (4), 409 (1967).
[13] *Hummel, D.:* Tenside, **1,** 116 (1964).
[14] *Pham, T. H., G. W. Brindley:* Clays Clay Minerals, **18,** 203 (1970).

МОДИФИКАЦИЯ ПОВЕРХНОСТИ И ПЕПТИЗАЦИЯ ИЛЛИТА МЕСТОРОЖДЕНИЯ ФЮЗЕРРАДВАНЬ

А. Пацко и Ф. Санто

Изучена адсорбция цетил-пиридиний-хлорида на трех фракциях иллита месторождения Фюзеррадвань. Сопутствующие породы удалены фракционированием, проведенными после пептизации с Na_2CO_3. Найдено, что на изотермах адсорбции можно отделить участки химической и физической адсорбции. На основании изотерм адсорбции определены ионообменная емкость с органическими катионами и величины удельной поверхности.

Измерены объемы осадков и вязкость суспензий органокомплексов в бензоле, которые имеют зависимость от степени покрытия поверхности, проходящий через максимум. Это объясняется происходящимии изменениями явлений смачивания, набухания и дезагрегации иллита наряду с повышением его органофильности.

X-RAY DIFFRACTION EXAMINATION OF INTERCALATED ALKYLAMMONIUM HUMATE COMPLEXES

By

E. TOMBÁCZ, I. DÉKÁNY, Á. PATZKÓ

Department of Colloid Chemistry, Attila József University Szeged, Hungary

(Received 5th June 1984)

By exchange of the cations of humate extracted from brown coal with an equivalent quantity of long-chain organic cations, the following organophilic humate samples were prepared: *n*-decyl, *n*-dodecyl, *n*-tetradecyl, *n*-hexadecyl and *n*-octadecyl-ammonium humate. X-ray diffraction examination of the humic acid and the alkylammonium humates revealed behaviour similar to that of smectite-type clay minerals. The results clearly support the theory of the layer structure of humic acid. Calculations on the basis of the Brindley model indicate that the humate layers are 4.65 Å thick and that the double layer of the alkylammonium cations bound to the carboxyl and phenolic hydroxyl groups in the interlayer space is oriented at 53.25° relative to the planes.

Introduction

Humic substances are of natural origin. They are dark brown, hydrophilic, acidic, high molar mass, polydisperse substances. They contain acidic functional groups, such as carboxyl and phenolic hydroxyl, which dissociate to varying degrees depending on the pH of the solution and the concentration of the electrolyte. As concerns physical-chemical characteristics, they display features of both polyelectrolytes [1], and association colloids [2].

Several research workers [3] have examined the chemical structures of humic substances with different methods for a long time. No exact structure can be given, as a result of the chemical complexity of humic substances. Various conceptions have been put forward. BURGES ET AL. [4] consider that their structure is similar to that of other natural macromolecules and they are polycondensates of a random collection of phenolic units. HAWORTH [5] thinks that the basis of their structure is a complex aromatic nucleus, to which polysaccharides, proteins, simple phenols and metals are attached physically or chemically. According to SCHNITZER [3], fulvic acids (a group of humic substances) are built up from aromatic oxycarboxylic acids. These "building blocks" are attached to each other through hydrogen-bonds.

The steric structure of the particles of humic substances is questionable. Are they linear, flexible chains which, depending on the dissociation of the functional groups, roll up to various extents? Do they form a statistical coil? Or are they planar aromatic ring systems which can arrange themselves in certain circumstances?

From their examinations of humic acids by ultracentrifugation, FLAIG and BEUTELSPACHER [6] came to the conclusion that they are spherical colloids. On the

basis of small angle X-ray scattering, WERSHAW ET AL. [7] propose that larger particles of humic acid are elliptical, while smaller ones are spherical. Humic substances have been examined by means of viscosity measurements by several authors [3]. The substances uniformly showed polyelectrolyte characteristics. The polyanions of humic substances are linear chains and/or spherical colloids.

X-ray diffraction examination of solid humic substances of natural origin demonstrated that they are not crystalline [3]. In the X-ray diffraction pattern of a powder specimen of fulvic acid, KODAMA and SCHNITZER [8] found a diffuse band at 4.1 Å, accompanied by a few minor humps. These humps were similar to those given by carbon black, which contains graphite-like layers. With respect to the carbon skeleton of fulvic acid, they stated that it was a network of poorly condensed aromatic rings. From X-ray examinations KASATOCHKIN ET AL. [9] concluded that humic substances contain a flat condensed aromatic network, to which side-chains and functional groups are attached.

The X-ray examinations reported in the literature, which could indicate the steric structure, the globular or lamellar shape of the molecules of humic substances, or the planar structure of the condensed aromatic ring system, are not convincing. The result usually is that very uncharacteristic, diffuse diffraction patterns are formed, since the flakes, even if they existed in a dissolved state, are not satisfactorily arranged in the solid sample. PFIRRMANN and WEISS [10, 11] made an X-ray diffraction study of humates organophilized by long alkyl-chain cation-active compounds. They obtained sharp reflexions at angles depending on the length of the alkyl chain.

Though the crystal structure of montmorillonite is that of a layer silicate built up from two SiO_4 tetrahedral sheets and one AlO_4 octahedral sheet, the basal spacing (d_{001}) X-ray diffraction peak is diffuse [12]. Sharp peaks are found, however, if the cations in exchangeable positions are exchanged for long-chain organic cations, since as a result of the interaction between the alkyl chains the flakes lie in order on top of each other [13].

Our starting point was that by reacting the negatively charged functional groups of humates with long-chain organic cations, we should observe behaviour similar to that of montmorillonite organocomplexes if the humate particles were originally planar in structure.

Experimental

The humic acid sample examined was extracted from Hungarian brown coal (Tatabánya) with 0.1 mol dm^{-3} potassium hydroxide. Purification of the crude humic acid was carried out in the usual way, as described by SCHNITZER and KHAN [3]. The elementary composition of the humic acid was C: 54.01%, H: 4.32%, O: 34.86%, N: 3.08%, its ash-content was 3.72%, and its cation exchange capacity was 4.1 meq g^{-1}. By means of membrane osmometry and extrapolation as applied in the measurement of the molar mass of polyelectrolytes [14], the number-average molecular weight of the sample was found to be $\overline{M}_n = 10\,600$.

Preparation of n-alkylammonium organocomplexes

Humic acid was dissolved in an equivalent quantity of sodium hydroxide to give a 1 g/100 cm^3 sodium humate solution. The alkylammonium chlorides were made by dissolution of alkylamines in an equivalent quantity of HCl. With increase of the length of the alkyl chain, the alkylammonium become less soluble in water, so the solution were made at 60 °C. 0.1 mol dm^{-3} *n*-decyl, *n*-dodecyl and *n*-tetradecylammonium chloride, 0.05 mol dm^{-3} *n*-hexadecylammonium chloride and 0.03 mol dm^{-3} *n*-octadecylammonium chloride solutions were made. The organocomplexes were also made at 60 °C, equivalent quantities of alkylammonium salts being added to sodium humate solution. The suspensions were kept at 60 °C for one day, then filtered and washed chloride-free with approx. 60 °C distilled water. The substances were dried under infrared light and then ground. The powder samples were examined by X-ray diffraction with a DRON-3 Soviet-made diffractometer.

Results

Diffractograms of humic acid and the various alkylammonium humates (2—12° angle range) can be seen in Fig. 1. The alkylammonium humates, especially with those with longer alkyl chains, give high-intensity sharp peaks, in contrast with the diffuse, uncharacteristic diffraction pattern of humic acid. With increase of the length of the alkyl chain, the reflexions shift towards lower 2θ values and become sharper. The distances between the humate flakes were calculated from the reflexion values *via* the Bragg equation, supposing clay mineral analogy and regarding the peaks as d_{001} distances:

$$d_{001} = \frac{\lambda}{2}\frac{1}{\sin\theta}$$

where $\frac{\lambda}{2}$=0.77092 (CuKα).

The results are given in Table I.

When the distance between the humate flakes was plotted as a function of the length of the alkyl chain in the alkylammonium cations (see Fig. 2), a linear connection was found, similarly to those for the alkylammonium intercalation complexes of montmorillonite and vermiculite [13].

With regard to the analogous behaviour, the results were evaluated on the basis of the Brindley model [15] for the primary alkylammonium complexes of montmorillonite and vermiculite. The model considers the geometry (the orientation relative to the flakes) of the straight-chain alkylammonium cations in the space between the clay mineral layers from the distances (d_{001}) between the

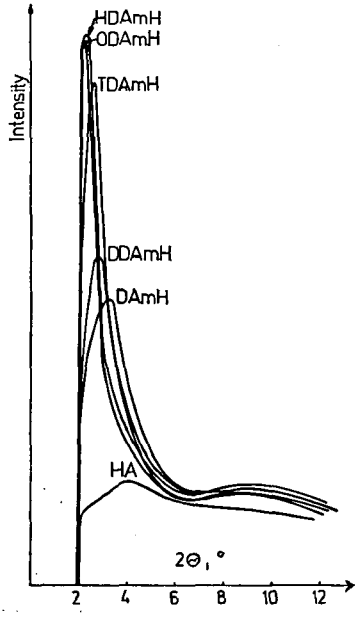

Fig. 1. X-ray diffraction patterns of primary alkylammonium humates and humic acid

Table I

Sample	Quantity of alkyl-ammonium cations %	2θ, °	d_{001}, Å		Relative intensity
			experimental	calculated	
Humic acid (HA)	0	4	—	—	0.06
n-Decylammonium humate (DAmH)	50.8	3.200	27.61	27.59	0.42
n-Dodecylammonium humate (DDAmH)	54.8	2.800	31.55	31.67	0.53
n-Tetradecylammonium humate (TDAmH)	58.3	2.485	35.55	35.74	0.88
n-Hexadecylammonium humate (HDAmH)	61.2	2.125	41.58	39.81	1
n-Octadecylammonium humate (ODAmH)	63.8	2.075	42.57	43.88	0.98

layers, determined as a function of the chain length. In the Brindley model the slope of the function $d_{001}=f(n_C)$ is a projected distance-increase related to the increase in chain length. Its value for an alkyl chain orientation perpendicular to the flakes, and taking into consideration the valence angle of 109°28′ between the carbon atoms, is 1.27 Å. At smaller inclination angles the values can only be smaller. However, if the experimental $\Delta d_{001}/\Delta n_C$ is higher than above, the alkylammonium cations form a double layer in the space between the flakes. The slope of the line in Fig. 2 is 2.035 Å, so a double layer is formed, *i.e.* the increase in the two alkyl chains occurs additively. The inclination angle of the humate flakes and the alkyl chains (φ) can be calculated from simple geometrical reasoning. d_{001} is the perpendicular distance between the flakes. The perpendicular projected length of two C—C distances is 2.54 Å. The experimentally determined 2.035 Å is also two

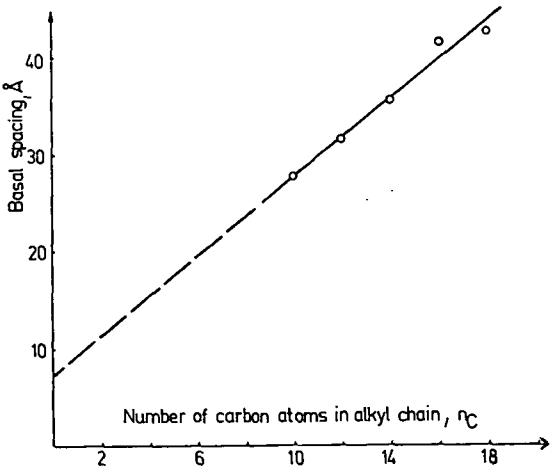

Fig. 2. Variation in basal spacing with length of alkyl chain in primary alkylammonium humates

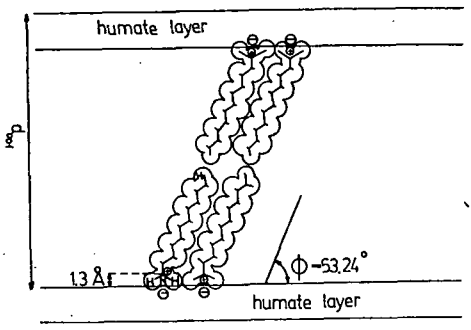

Fig. 3. Scheme of intercalated alkylammonium humate complex

C—C distances, *viz.* a perpendicular projection of the projected C—C distance of 2.54 Å for a given alkyl chain orientation (see Fig. 3). In the present case the angle of inclination of the alkyl chain and humate flakes is as follows:

$$\sin\varphi = \frac{\Delta d_{001}/\Delta n_C}{2.54} = \frac{2.035}{2.54},$$

$$i.e. \quad \varphi = 53.24°.$$

On the basis of the model, the most likely angle of inclination of the alkyl chains, taking into consideration the valence angles, is 55°. There is good agreement between the two values. With a similar method, the value for montmorillonite complexes was 65° [15].

With the $\lim_{n_C \to 0} d_{001}$ extrapolation, the thickness of the humate flakes can be calculated. Twice the distance between the imaginary plane of the humate flakes and the N atom of the ammonium cation (which the Brindley model gives as 1.3 Å) must be subtracted from the extrapolated value (7.25 Å). On this basis, the thickness of the humate flakes is 4.65 Å. The scheme based on the model can be seen in Fig. 3. The d_{001} distances calculated in the case of alkyl chain orientation for the alkylammonium humate intercalation complexes in terms of the Brindley model are given in Table I. Comparison of the experimental and calculated values demonstrates very good agreement.

Conclusions

The experimental results and the useful application of the Brindley model for lamellar-structure clay minerals seem to indicate clearly that the examined humic acid has a layer structure. If originally there had not been lamellae, but spheres or statistical coils in the humate solution, then the ion-exange of the alkylammonium cations would not have resulted in a change like this in the X-ray diffractograms. The reason why the diffraction pattern of the humic acid is so diffuse (see Fig. 1) is that there are not enough parallelly arranged lamellae in the powder samples to result in X-ray interference of satisfactory intensity. In the alkylammonium humates, however as a result of the van der Waals interaction between alkyl chains longer than 8 carbon atoms the lamellae become arranged in parallel. The fact that the X-ray reflections become more and more intense and sharp with increase of the alkyl chain length indicates the formation of more ordered structures.

The thickness of the humate layers can be calculated by extrapolation, but also from the experimental results which can be evaluated subsequently. The value 4.65 Å is realistic and corresponds to the structure conceived by HAWORTH [5] and SCHNITZER [3] (a polycondensed aromatic ring system bound by hydrogen-bonds).

Acknowledgement

The authors express their thanks to the Department of Applied Chemistry of Attila József University for taking the X-ray diffractograms.

References

[1] *Steelink, C.:* J. Chem. Educ. **54,** 599 (1977).
[2] *Tombácz, E., S. Sipos, F. Szántó:* Agrokémia és Talajtan **30,** 365 (1981).
[3] *Schnitzer, M., S. U. Khan:* Humic Substances in the Environment, Marcel Dekker, New York (1972).
[4] *Burges, N. A., H. M. Hurst, S. B. Walkden:* Geochim. Cosmochim. Acta **28,** 1547 (1964).
[5] *Haworth, R. D.:* Soil Sci. **111,** 71 (1971).
[6] *Flaig, W. A. J., H. Beutelspacher:* in Isotope and Radiation in Soil Organic-Matter Studies, International Atomic Energy Agency, Vienna, 23 (1968).
[7] *Wershaw, R. L., P. J. Burcar, C. L. Sutula, B. J. Wiginton:* Science **157,** 1429 (1967).
[8] *Kodama, H., M. Schnitzer:* Fuel **46,** 87 (1967).
[9] *Kasatochkin, V. I., M. M. Kononova, N. K. Larina, O. I. Egorova:* Trans. 8th Int. Congr. Soil. Sci., Bucharest, **3,** 81 (1964).
[10] *Pfirrmann, G. L.:* Thesis, Heidelberg (1968).
[11] *Weiss, A.:* personal communication.
[12] *Nemecz, E.:* Agyagásványok, Akadémiai Kiadó, Budapest (1973).
[13] *Theng, B. K. G.:* The Chemistry of Clay-Organic Reactions, Hilger, Bristol (1974).
[14] *Morawetz, H.:* Macromolecules in Solution High Polymers **21,** Interscience, New York (1966).
[15] *Brindley, G. W.:* Clay Minerals **6,** 91 (1965).

РЕНТГЕНОГРАФИЧЕСКОЕ ИЗУЧЕНИЕ ИНТЕРКАЛЯЦИОННЫХ КОМПЛЕКСОВ АЛКИЛАММОННЫХ-ГУМАТОВ

Э. Томбац, И. Декань и А. Пацко

Заменили гуматные катионы эквивалентными количествами алкиламмониевых катионов с длиной цепи алкильного радикала C_{10}—C_{18}. Рентгенографическое исследование полученных образцов показало, что образующиеся структуры аналогичны минералам смектитного типа. Рассчитаны расстояния между слоями гуматов и определены углы наклона алкильных цепей к плоскостям структуры.

THE EFFECTS OF Na-SALICYLATE AND Na-FULVATE ON THE STABILITY AND RHEOLOGICAL PROPERTIES OF Na-MONTMORILLONITE SUSPENSIONS

By

E. TOMBÁCZ, M. GILDE, F. SZÁNTÓ

Department of Colloid Chemistry, Attila József University Szeged, Hungary

(Received 5th June, 1984)

Na-salicylate and Na-fulvate in small quantities adsorb on the edges of Na-montmorillonite particles (adsorption capacities: 20 and 14.5 μeq g^{-1}).

The negative zeta potentials (determined by microelectrophoresis) and the critical coagulation concentrations increase with increase in the quantity of the organic anions. These anions interact with the octahedral aluminium ions on the edges of the montmorillonite particles, the charge of the edges thereby being reversed, and the negative charge of the particles increases. The experimental results are supported by calculations made according to the DLVO theory and Stern's theory.

In the presence of organic anions, the neutralization of the edge charge means that only face-to-face aggregation and no edge-to-face aggregation can be formed. These various structures are shown in scanning electronmicroscopic pictures.

The changes in the structure of the suspensions are proved by rheological measurements. As an effect of the small quantity of organic anions, the Bingham yield stress of the suspensions decreases significantly.

Introduction

The peptizing effects of various anions, mainly phosphate, polymetaphosphate and carbonate, which influence the stability and rheological properties of clay mineral suspensions, have been examined mainly from a practical point of view. Relatively few systematic studies have been carried out on the effects of organic anions, although many polyanions of natural origin are used to increase the suspension stability and to modify the flow properties.

The questions arise as to whether organic anions are bound to certain surface parts of clay mineral particles in a similar way to inorganic anions and have a similar effect as a result of this, and whether a more negative charge, *i.e.* the complete dissociation of more functional groups of the molecule, is needed for the above effects to occur.

There are extreme opinions in the technical literature about the interactions between clay minerals, mainly montmorillonite, and organic acids and their salts. Certain authors [1, 2] question the occurrence of adsorption altogether or regard it as very slight, while others [3, 4], who have examined mainly humic substances of natural origin, describe significant adsorption. The problem is that, as a result of isomorphous substitution in their crystal lattice, the clay mineral particles have a negative charge and thus repel organic anions.

However, interaction may occur in the case of a highly retarded dissociation state (*e.g.* in the case of a weak acid at low pH) [3]. Further, if the lattice charge is compensated by multivalent cations, then interaction may also occur through these [4] and with the broken bonds on the edges of the particles, which (depending on the circumstances) can be in a given hydrated and charged state [5, 6, 14].

Depending mainly on the pH, but to a smaller extent on the electrolytes [7], phosphate anions bind to the aluminium ions on the edges of clay particles [6, 7]. They reverse the positive charge of the edges and may increase their negative charge, thereby impeding the formation of edge-to-face aggregation [8]. In the presence of multivalent anions (*e.g.* diphosphate anions), the stability of clay suspensions increases considerably, since only a face-to-face aggregated structure can be formed and this needs a considerably greater quantity of coagulating electrolytes [8].

The flow improving effects of various supplementary anionic materials on ceramic mashes were examined by WEIAND [9] from a practical aspect.

The present paper considers the interactions between Na-montmorillonite and the Na-salts of salicylic acid (as a simple aromatic oxycarboxylic acid) and synthetic fulvic acid (as a model of natural humic substances), as well as their effects on the stability and rheological properties of a Na-montmorillonite suspension.

Experimental materials and methods

Montmorillonite was obtained from Kuzmice bentonite by fractionation following Na_2CO_3 peptization. From this, H-montmorillonite was produced with the Barshad method [10], and the monocationic Na-montmorillonite was made by neutralization with an equivalent quantity of NaOH. Particle size: $d \leqq 1$ μm, cation exchange capacity: 800 μeq g^{-1}.

For the experiments Na-salicylate of analytical purity was used. The fulvic acid was made from gallic acid in the presence of Ca-montmorillonite as heterogeneous catalyst [11]. The number-average molar mass of the product was 840, calculated by means of vapour pressure osmometry with the pH correction method of HANSEN and SCHNITZER [12]. The total acidity of the fulvic acid was 10.1 meq g^{-1}; this is the quantity of negatively charged functional groups in the material. From these data it can be seen that an average of 8.5 acidically dissociating functional groups are to be found on the molecules of fulvic acid.

Adsorption isotherms were determined under the following conditions:

Na-montmorillonite concentration: 5 g dm^{-3}

Adsorption time: 2 days at room temperature

Initial concentration of adsorptives: 0.1—1.0 meq dm^{-3}.

So that the results could be compared, we calculated in terms of concentration units (given in equivalents) referred to negative charges, and not in terms of molar concentrations. The two different concentration units are the same for Na-salicylate since the dissociation of Na-salicylate gives one negative charge per molecule if the pH of the medium is not too high (dissociation constants of salicylic acid: $K_1 = 1.06 \cdot 10^{-3}$, $K_2 = 3.6\ 10^{-14}$).

The equilibrium concentrations were determined spectrophotometrically following sedimentation of the montmorillonite particles in a preparative ultracentrifuge

(20 000 RPM, 30 minutes). The Fe(III) salicylate complex was measured at 525 nm, and Na-fulvate at 450 nm.

The zeta potentials of 1 g dm^{-3} Na-montmorillonite suspensions containing Na-salicylate or Na-fulvate in increasing quantities were measured with a Japanese-made Laser Zee Meter microelectrophoresis apparatus. In parallel with this, the critical coagulating concentrations *(c.c.c.)* of suspensions of the same type were determined by observing coagulation series with increasing NaCl concentrations. The results were measured on materials after a 96-hour standing. This differs from the customary 24 hours in the literature [6, 8]. The reason is that after a 24-hour standing the examined structures were not close to the equilibrium state, whereas after 96 hours the observations did not change quantitatively compared to those throughout the total observation period of 240 hours.

The edge-to-face or face-to-face aggregated structures formed by coagulation of the suspensions were examined with a scanning electronmicroscope (JEOL, Japan). The samples were made from 5 g dm^{-3} Na-montmorillonite suspensions which contained 0 or 1 meq dm^{-3} Na-salicylate or Na-fulvate, as well as 200 mmol dm^{-3} NaCl, with the freeze-drying technique proposed by O'BRIEN ET AL. [13]. The suspension-film on the disc was dipped into isopentane cooled with liquid-air to approx. −140 °C, and the water was then sublimed in a freeze-drying instrument. With this method the suspension structure can be preserved even in the solid state.

Rheological examinations were carried out with a Rheotest-2 (GDR) rotational viscometer. To 7.4 g/100 g Na-montmorillonite suspensions, 0, 16, 33 or 66 μeq g^{-1} Na-salicylate or Na-fulvate was added. The flow curves were measured after a 2-day standing.

Results and discussion

The adsorption isotherms in Fig. 1 show the quantitative relationships of the interactions of Na-salicylate and Na-fulvate with Na-montmorillonite. Figure 1 also gives the equilibrium pH values, which do not display a monotonous change with increasing concentration of the adsorptives; they are about pH = 7. In the case of Na-salicylate the isotherms is of regular Langmuir-type, while it is a little different for Na-fulvate. The linear regression data and the adsorption capacity values calculated from the linearized form of the Langmuir isotherms equation are listed in Table I.

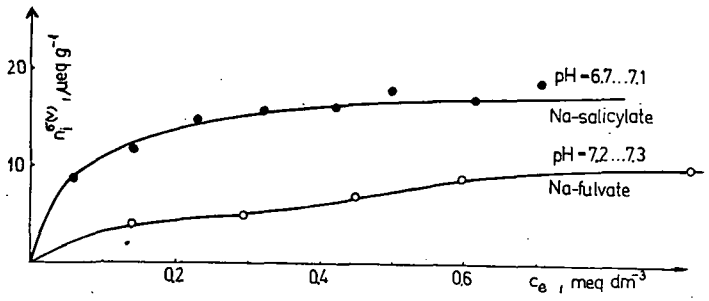

Fig. 1. Isotherms for the adsorption of Na-salicylate and Na-fulvate by Na-montmorillonite at room temperature

Table I

Adsorption system	Equilibrium pH	Adsorption capacity μeq g^{-1}	Linear regression
Na-montmorillonite + Na-salicylate	6.7—7.1	20.0	0.989
Na-montmorillonite + Na-fulvate	7.2—7.3	14.5	0.951

The degree of adsorption is small; it is only a few per cent of the quantity of adsorbed organic cations. GREENLAND and MOTT [14] describe the amounts of positive and negative charge on various clay minerals and oxides in their review. In the case of montmorillonite prepared from Wyoming bentonite, the quantity of negative charge was 980 μeq g^{-1}. The pH-dependent positive charge at pH=7 was 2 μeq g^{-1}, and at pH=3 was 12.5 μeq g^{-1}. These data suggest that the very low adsorption capacities we calculated are realistic. We made calculations of whether, on purely quantitative considerations, bonds on the edges are possible. The approximate quantity of octahedral Al ions on the edges of 500—100 nm montmorillonite particles is 3.12—31.3 μmol g^{-1}. The magnitude of the calculated adsorption capacity (see Table I) is the same. Thus, the salicylate anions are most likely to be bound to the Al ions on the edges (as we described in detail in our previous study [15]), probably by complex bonds. Since fulvic acid is a polycondensed aromatic oxycarboxylic acid, fulvate is bound to the surface in a similar way to salicylate.

We confirmed the bonding of salicylate and fulvate anions on the edges of montmorillonite particles by various examinations and calculations. Depending on their nature and quantity, the adsorbed anions change the stability of the montmorillonite suspension. In connection with this, the change in the structure of the electric double layer can be followed macroscopically by measurement of the zeta potential.

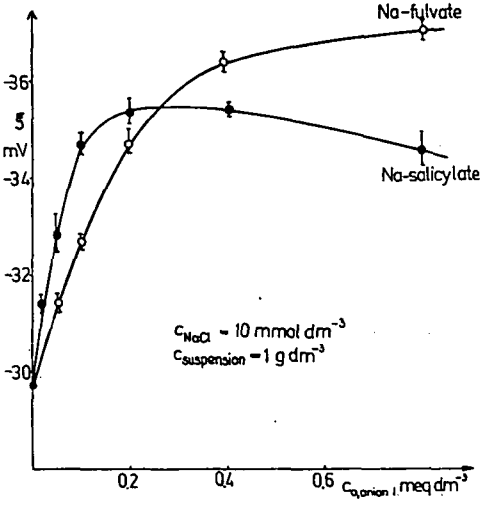

Fig. 2. The zeta potential of montmorillonite suspensions as a function of Na-salicylate and Na-fulvate concentration

The measured zeta potentials are presented in Fig. 2 as functions of the concentration of salicylate and fulvate. It can be seen that both anions increase the negative zeta potential to a small extent (about 1.15—1.20 of the original). In our estimations the effect of Na-fulvate is higher. Because of the several (8.5) negatively charged functional groups, only a few can bind by adsorption (steric block); the others increase the negative charge of the particle. In the case of salicylate, even if only the coverage of the positive

charge of the edges is assumed, the small increase in the gross charge of the particle, and macroscopically the increase in the zeta potential, become understandable. If the negative surface or Stern potentials are calculated from the original surface charge density of the montmorillonite and from the increased charge density, taking into consideration the adsorption data, the difference will be similar to the experimental zeta potential increase. In the case of Na-hexadecyl-sulphate kaolin systems, similar results (the increase of the electrophoretic mobility of the particles) were reported by FLEGMANN and OTTEWILL [16].

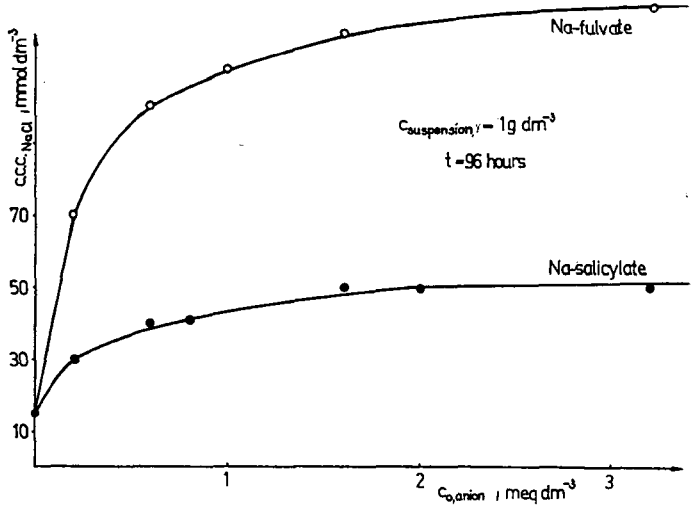

Fig. 3. The critical coagulation concentration of montmorillonite suspensions as a function of Na-salicylate and Na-fulvate concentration

The *c.c.c.* values (see Fig. 3) show the increased stability of montmorillonite suspensions following treatment with salicylate and fulvate. The stabilizing effect of salicylate was much smaller than that of fulvate. This contradicts VAN OLPHEN'S [6] results. Van Olphen considers that there must be at least 3 phenolic hidroxyl groups in the aromatic molecule for it to have a stabilizing effect. FREY and LAGALY [8] determined a *c.c.c.* of 200 mmol dm^{-3} for montmorillonite suspensions stabilized by diphosphate. This value is roughly 1.5 times the *c.c.c.* of a suspension stabilized by Na-fulvate.

Taking into consideration the results of adsorption measurements on the basis of the zeta potential and the coagulation data, the stabilizing effects of Na-salicylate and Na-fulvate can be explained analogously to that of multivalent phosphate anions [8].

The organic anions bound on the edges of the particles modify their charge. The Stern potential of montmorillonite (ψ^*_{St}), which is characteristic of a double layer of the platelets, was calculated at various electrolyte concentrations on the basis of the Stern model by means of the following equations referring to a flat double layer [6]. The surface charge density (σ) is the sum of the charge densities of the Stern layer

(σ_1) and the diffuse layer (σ_2):

$$\sigma = \sigma_1 + \sigma_2$$

$$\sigma = (\varepsilon'/4\pi\delta_{St})(\psi_0 - \psi_{St})$$

where δ_{St} = 5 Å (the thickness of the Stern layer)
ε' = dielectric constant of the medium in the field of the molecular condenser
ψ_0 = surface potential
ψ_{St} = Stern potential

$$\sigma_1 = \frac{N_1 ve}{1 + (N_A/Mn)\exp(-(ve\psi_{St} + \varphi)/kT)}$$

where
N_1 = 10^{15}/cm², the number of adsorption sites on 1 cm² of the wall,
φ = specific adsorption potential of the counter-ions (with our calculations $\varphi = 0$)
e = elementary charge ($e = 4.77\ 10^{-10}$ esu)
v = valency of the ion
N_A = Avogadro number
M = molecular weight of the solvent

$$\sigma_2 = (2\varepsilon nkT/\pi)^{1/2} \sinh(ve\psi_{St}/2kT)$$

where
ε = dielectric constant of the medium
k = Boltzmann constant
T = temperature
n = ion concentration in number of ions/cm³

The average surface charge density of montmorillonite was calculated from the cation exchange capacity (*c.e.c.* = 800 μeq g^{-1}) and the dimensions of the unit cell (surface: $F = 46.5 \cdot 10^{-16}$ cm², relative weight: M = 720):

$$\bar{\sigma} = Mc.e.c.10^{-6}\, e/2F = 2{,}954\ 10^4 \text{ esu/cm}^2$$

The condition of coagulation at the *c.c.c.* is the equality of the differential quotients of the attractive and repulsive potentials with respect to distance [17]:

$$\frac{dV_R}{dd} = \frac{d(-V_A)}{dd} \quad \text{and} \quad V_R = -V_A$$

where

$$V_R = \frac{64nkT}{\varkappa}\gamma^2 e^{-2\varkappa d}$$

$$V_A = -\frac{\delta^2 A}{32\pi d^4} \quad \text{(in the case of plates } \delta \text{ thick)}$$

where
$\delta = 6.6$ Å (the thickness of montmorillonite plates) in the case of $\varkappa d = 2$ condition it can be deduced [18].

$$c.c.c. = 4.1 \cdot 10^{-6} \frac{\gamma^{4/3}}{A^{2/3} v^{10/3}} \quad (\text{mmol dm}^{-3})$$

A = Hamaker constant (10^{-12} or $2 \cdot 10^{-12}$ erg)

$$\gamma = \frac{\exp(z/2) - 1}{\exp(z/2) + 1} \quad \text{and} \quad z = \frac{ve\psi_{St}}{kT}$$

The Stern potential (ψ_{St}^{**}) which can be calculated from the experimental *c.c.c.* data using the above equations shows the realistic behaviour of the systems. The *c.c.c.* values determined at 3.2 meq dm^{-3} anion concentrations, the Stern potentials (ψ_{St}^{**}) calculated from the *c.c.c.* values, and the potentials (ψ_{St}^{*}) calculated on the basis of Stern's theory at the same electrolyte concentrations, are given in Table II.

Table II

System	c.c.c. mmol dm^{-3}	ψ_{St}^{*} mV	ψ_{St}^{**}, mV	
			$A = 10^{-12}$ erg	$A = 2 \cdot 10^{-12}$ erg
Na-montmorillonite	15	−109	−8.4	−11.9
Na-montmorillonite + Na-salicylate	50	−80.3	−20.9	−30.1
Na-montmorillonite + Na-fulvate	130	−56.5	−45.1	−68.9

A comparison of the data in Table II; clearly reveals the differences. The montmorillonite particles can be aggregated by edge-to-face (low *c.c.c.*) and face-to-face (high *c.c.c.*) interactions [8, 18], depending on the electrolyte concentration and the charge of the edges. In the case of montmorillonite, from the high Stern potential ($\psi_{St}^{*} = 109$ mV) characteristic of a double layer of the plates a significantly greater stability could be expected. The difference in magnitude of ψ_{St}^{*} and ψ_{St}^{**} (the latter can be calculated from the *c.c.c.*) is a contradiction which can only be solved by assuming formation of the edge-to-face heterocoagulation structure. Edge-to-face aggregation is blocked in the presence of materials which adsorb on the edges and recharge them [6, 8]. It can be supposed that in the case of salicylate this occurs partially, but with fulvate the edges become negative and hydrated completely due to the non-bound, ionized and therefore negatively charged functional groups. Thus, in the presence of fulvate, only a face-to-face aggre-

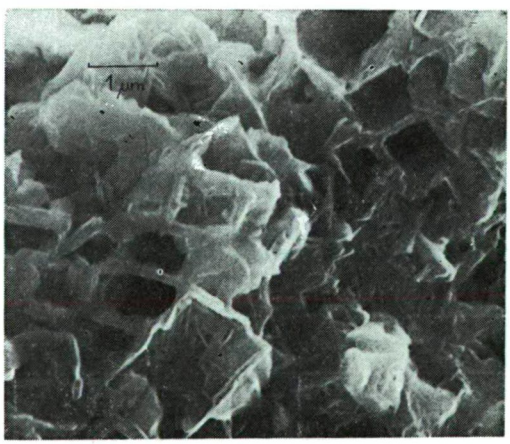

Fig. 4. Scanning electronmicrograph of house-of-cards structure in montmorillonite suspension (uncompressed, freeze-dried sample of montmorillonite suspension coagulated with 200 mmol dm^{-3} NaCl)

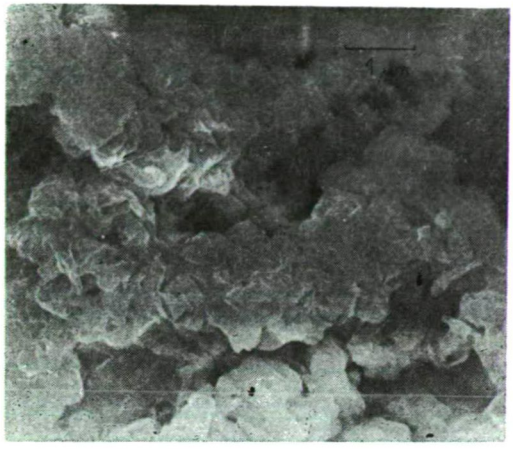

Fig. 5. Scanning electronmicrograph of montmorillonite suspension in the presence of Na-salicylate (uncompressed, freeze-dried sample of montmorillonite suspension containing 1 meq dm^{-3} Na-salicylate, coagulated with 200 mmol dm^{-3} NaCl)

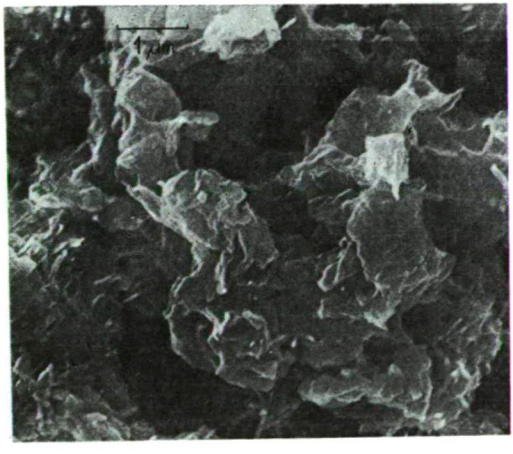

Fig. 6. Scanning electronmicrograph of montmorillonite suspension in the presence of Na-fulvate (uncompressed, freeze-dried sample of montmorillonite suspension containing 1 meq dm^{-3} Na-fulvate, coagulated with 200 mmol dm^{-3} NaCl)

gated structure can be formed and therefore the ψ_{St}^{*} value characterizing the double layer of the plates is quite near the ψ_{St}^{**} values characterizing the real stability of the system. Similar results were given in the case of Na-gallate and Na-humate in earlier examinations [19].

Marked evidence for the formation of structures aggregated in different ways is provided by the electronmicroscopic photographs shown in Figures 4—6. The house-of-cards structure formed by an edge-to-face connection can be seen very well in the sample which does not contain any organic material. On the other hand, the picture of the sample containing salicylate and fulvate is rather indistinctive and furry; one can only guess that the plates have slid on top of each other.

We examined the effects of Na-salicylate and Na-fulvate on the rheological properties of a montmorillonite suspension. The flow curves of suspensions containing different specific quantities of organic anions are shown in Figures 7—8.

The shearing stress (τ) plotted as a function of the rate of shear (D) is the highest for suspensions which do not contain organic anions. At higher velocity gradients (D) the flow curves become linear and run almost parallel with each other. By extrapolation of these straight lines the Bingham yield stress (τ_B) can be obtained. τ_B is shown in the $a-\tau$ plane of spatial Figures 7 and 8 as a function of the specific amount of organic material (a, $\mu eq\ g^{-1}$). It can be seen that with increasing amount of organic material τ_B first decreases significantly, then reaches a minimum and subsequently increases slightly. The yield-stress minima exhibited quite good agreement with the adsorption capacities (for Na-salicylate: approx. 20 $\mu eq\ g^{-1}$; for Na-fulvate: lower than 20 $\mu eq\ g^{-1}$). These materials also cause a reduction of the

Bingham yield stress, similarly to inorganic and some natural organic compounds used in the ceramics industry [9]. This effect is a result of the bonding of the anions on the edges. The completely negatively charged particles repel each other,

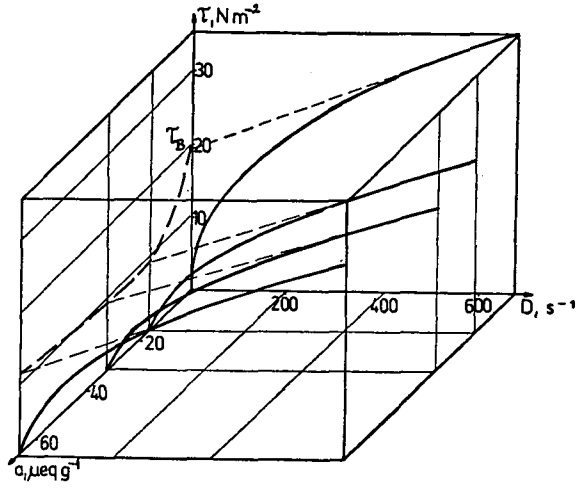

Fig. 7. Flow curves of Na-montmorillonite suspensions with different Na-salicylate contents, and the Bingham yield stress as a function of the specific amount of added Na-salicylate

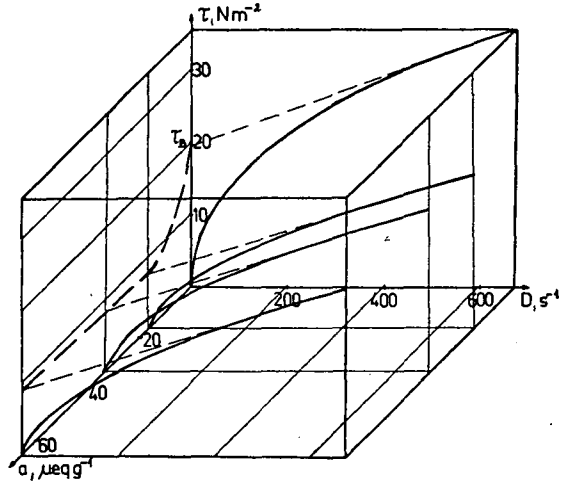

Fig. 8. Flow curves of Na-montmorillonite suspensions with different Na-fulvate contents, and the Bingham yield stress as a function of the specific amount of added Na-fulvate

and therefore an edge-to-face house-of-cards structure cannot be formed; thus, a smaller shearing force is enough to form independent flow units.

To summarize, it can be stated that a uniform interpretation of results obtained from different experimental methods is possible if adsorption on the edges is assumed, similarly as for inorganic anions.

Acknowledgements

The authors express their thanks to the Development Laboratory of the Paper Mill in Dunaujváros for making possible the zeta potential measurements, and to the Electronmicroscope Laboratory of the Central Silicate Research and Planning Institute for taking the photographs.

References

[1] *Theng, B. K. G.:* The Chemistry of Clay-Organic Reactions, Hilger, Bristol (1974).
[2] *Mortland, M. M.:* Adv. Agron. **22,** 75 (1970).
[3] *Schnitzer, M., S. U. Khan:* Humic Substances in the Environment, Marcel Dekker, New York (1972).
[4] *Greenland, D. J.:* Soil Sci. **111,** 34 (1971).
[5] *Kapoor, B. S.:* Clay Minerals **9,** 425 (1972).
[6] *Van Olpen, H.:* An Introduction to Clay Colloid Chemistry, New York (1963).
[7] *Hingston F. J., R. J. Atkinson, A. M. Posner, J. P. Quirk:* Nature **215,** 1459 (1967).
[8] *Frey, E., G. Lagaly:* J. Coll. Interface Sci. **70,** 46 (1979).
[9] *Weiand, W.:* Sprechsaal **109,** (1976).
[10] *Barshad, I.:* Soil Sci. **108,** 38 (1969).
[11] *Wang, T. S. C., Song Wu Li:* Z. Pflanzenernachr. Bodenkd. **140,** 669 (1977).
[12] *Hansen, E. H., M. Schnitzer:* Anal. Chim. Acta **46,** 247 (1969).
[13] *O'Brien, N. R., M. Arakawa, E. Suito:* J. Electronmicroscopy **19,** 277 (1970).
[14] *Greenland, D. J., C. J. B. Mott:* Surface of Soil Particles (Ch. 4.), in Chem. Soil Const. Hillary Birmingham, Wiley: Chichester, England (1978).
[15] *Tombácz, E.. M. Gilde, F. Szántó:* Proceedings of the 3rd Conference on Colloid Chemistry, Siófok, 61 (1981).
[16] *Flegmann, A. W., R. H. Ottewill:* Proceedings of the IVth International Congress on Surface Active Substances, Brussels, **2,** 1271 (1964).
[17] *Verwey, E. J. W., J. Th. G. Overbeek:* Theory of the Stability of Lyophobic Colloids, Elsevier, New York (1948).
[18] *Frey, E.:* Untersuchungen zur Kolloidchemie von Tonmineralen, Diss., München (1977).
[19] *Tombácz, E., F.-né, Gilde, F. Szántó:* Conference on Colloid Chemistry, Eger, Abstracts p. 110 (1983).

ВЛИЯНИЕ САЛИЦИЛАТА И ФУЛЬВАТА НАТРИЯ НА СТАБИЛЬНОСТЬ И РЕОЛОГИЧЕСКИЕ СВОЙСТВА НАТРИЕВОГО МОНТМОРИЛЛОНИТА

Э. Томбац, М. Гильде и Ф. Санто

Значения зета потенциалов и критических концентраций коагуляции возросают с увеличением адсорбированного количества названных соединений. Экспериментальные данные подтверждены рассчетами произведенными на основании моделя Штерна и теории ДЛВО. Представлены сканинг электронно-микроскопические снимки полученных образцов. Реологические свойства суспензий подтверждают предполагаемые структурные изменения в суспензиях.

ВЛИЯНИЕ ГИДРОДИНАМИЧЕСКИХ УСЛОВИЙ НА КИНЕТИКУ ДИСПЕРСИОННОЙ ПОЛИМЕРИЗАЦИИ И СОПОЛИМЕРИЗАЦИИ МЕТИЛМЕТАКРИЛАТА

И. А. АНДОР и И. ДРЕВЕНИ
Кафедра общей и физической химии университета им. Аттилы Йожефа, Сегед

(Поступило в редакцию 17 апреля 1984 г.)

Изучено влияние интенсивности перемешивания на кинетику безэмульгаторной дисперсионной полимеризации метилметакрилата и его сополимеризации с бутилметакрилатом и стиролом. Обсуждены причины наблюдавшихся явлений и предложен механизм образования полимера и полимерных частиц при инициировании реакции персульфатом калия.

В настоящее время среди способов промышленного крупнотоннажного производства ряда высокомолекулярных технических материалов, доминирующим является гетерогенная, проводимая в водной среде дисперсионная полимеризация. При ее использовании открываются широкие возможности в регулировании процесса полимеризации по скорости и по качеству получаемых продуктов. О продолжающемся и в последние годы интересе исследователей и производственников к вопросам теории дисперсионной полимеризации, свидетельствует недавнее издание монографии по эмульсионной полимеризации и ее применении в промышленности [1]. Несмотря на то, что научных публикаций по разным видам дисперсионной полимеризации очень много [2—4], ряд важных вопросов кинетики и топохимии полимеризационного процесса в гетерогенных и микрогетерогенных системах остается еще невыясненным.

О влиянии интенсивности перемешивания на кинетику гетерогенной полимеризации впервые сообщили еще в 1953 г. [5]. Вопрос о механизме воздействия гидродинамических условий проведения на дисперсионную полимеризацию различных мономеров, под действием водорастворимых инициаторов, не рассматривался интенсивно исследователями и в литературе относительно мало данных, касающихся этого вопроса [6—8].

Некоторые технологические и экономические преимущества способа безэмульгаторной эмульсионной полимеризации и ее пригодность для использования в качестве модели, вследствие относительной простоты системы, для изучения влияния различных факторов на кинетику дисперсионных полимеризационных процессов, побудили нас к продолжению наших работ, опубликованных ранее [9—11].

Задача данного исследования состояла в выяснении влияния интенсивности перемешивания на начальную скорость полимеризации малорастворимого в воде мономера и его сополимеризации с нерастворимыми в воде мономерами в присутствии персульфатного инициатора.

Объекты и методы исследования

Технические мономеры очищались от ингибитора (гидрохинона) обычными методами, аналогично описанному в предыдущем сообщении [11]. Для опытов были применены мономеры: метиловый эфир метакриловой кислоты (ММА), н-бутиловый эфир метакриловой кислоты (БМА) и стирол. Очищенные мономеры имели показатель плотности, коэффициент преломления и температуру кипения, соответствующие литературным данным.

В качестве инициатора применялся персульфат калия — $K_2S_2O_8$ (ПСК) с чистотой 99.8%, определенной иодометрически. Концентрация ПСК (C_{in}, $mol\,dm^{-3}$) рассчитывалась относительно водной фазы.

В качестве определяющего гидродинамического параметра системы, при прочих равных условиях, была принята интенсивность перемешивания, характеризуемая числом оборотов мешалки n, (s^{-1}). За кинетикой полимеризации в начальных стадиях следили дилатометрически с применением магнитного перемешивания. Постоянство температуры поддерживалось водяным ультратермостатом (333.15 K $\pm$0.1). Соотношение мономерной и водной фаз по массе составляло 1:4.

Перед полимеризационными опытами обе фазы освобождались от растворенного в них кислорода вакуумированием и барботированием азота высокой чистоты, пропущенного через катализатор *BTS (Flüka)*. Воспроизводимость кинетических опытов по скорости полимеризации была в пределах $\pm$5%.

Относительную молекулярную массу полученного полиметилметакрилата определяли вискозиметрически по характеристической вязкости бензольных растворов.

Экспериментальные данные

Для выяснения влияния скорости перемешивания системы на конверсию ММА в полимер, нами были проведены полимеризации в закрытых дилатометрах. При строгом соблюдении постоянства всех условий (в том числе формы и объема дилатометров) мы изменяли только число оборотов мешалки в единицу времени и по сокращению объема системы рассчитывали конверсию в заданный момент времени. Полученные результаты представлены на *рис. 1.* Из данных рисунка следует, что при низких степенях конверсии (5—15%) зависимость последней от времени, при исследованных скоростях перемешивания, носит прямолинейный характер. Поэтому на основании полученных аналогичных данных, по тангенсу угла наклона можно было рассчитать начальные скорости полимеризаций в применяемых нами условиях.

На *рис. 2.* представлены рассчитанные начальные скорости полимеризации ММА при разных числах обротов мешалки. Как видно из данных *рис. 2.* скорость полимеризации с увеличением числа оборотов мешалки сначала возрастает, затем, достигнув максимума при $n=6$, постепенно снижается. При данной концентрации ПСК ($C_{in}=0.05\,mol\,dm^{-3}$) наблюдается возрастание

начальной скорости полимеризации с повышением интенсивности перемешивания, примерно в 5 раз.

Представлял интерес изучить влияние концентрации инициатора на начальную скорость полимеризации ММА при постоянной, оптимальной по предыдущим данным, скорости перемешивания реакционной системы. Как видно из представленных на *рис. 3* данных, начальная скорость полимеризации резко увеличивается с повышением концентрации инициатора только до определенного предела (C_{in}=0.005 *mol dm*$^{-3}$), затем наблюдается экспоненциальное снижение скорости полимеризации при более высоких концентрациях ПСК.

Ввиду того, что зависимость начальной скорости полимеризации ММА проходит через максимум, как от скорости перемешивания, так и от концентрации инициатора, мы изучили совместное влияние обоих факторов. Полученные результаты видны на *рис. 4*, из которых следует, что при оптимализации изучаемых параметров, скорость полимеризации может превосходить скорость дифузионного гетерогенного процесса, т. е. проходящего без перемешивания системы, примерно на 1.5 порядка.

Наблюдаемые нами явления в процессе образования полиметилметакрилата (ПММА) в присутствии ПСК, могут объясняться либо изменениями условий растворения и транспорта мономера к местам инициирования и роста цепей, либо изменением места элементарных актов полимеризации в микрогетерогенной дисперсной системе. Выяснению этих вопросов может оказать большую помощь изучение влияния интенсивности перемешивания на начальные скорости сополимеризации ММА с такими нерастворимыми в воде, но отличающимися друг от друга по природе мономерами, как бутилметакрилат и стирол. Экспериментальные данные, полученные при проведенных сополимеризациях представлены на *рис. 5* и *6*. В случае сополимеризации ММА с обо-

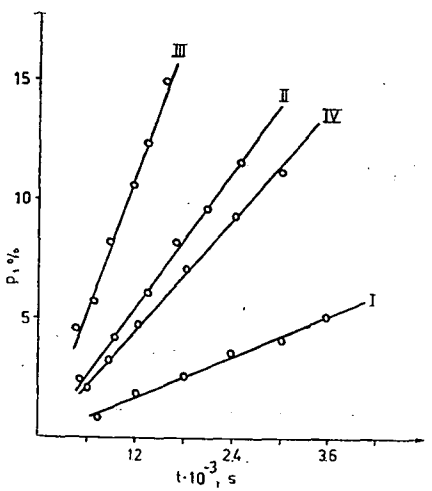

Рис. 1. Зависимость конверсии ММА (p) от времени (t) при разных интенсивностях перемешивания реакционной системы (обороты мешалки — n, s^{-1}): I — 0, II — 2, III — 6, IV — 18 (C_{in}=0,05 *mol dm*$^{-3}$).

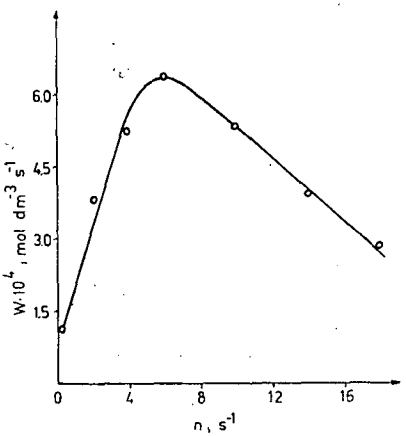

Рис. 2. Зависимость начальной полимеризации (W) ММА от интенсивности перемешивания (n) при C_{in}=0,05 *mol dm*$^{-3}$.

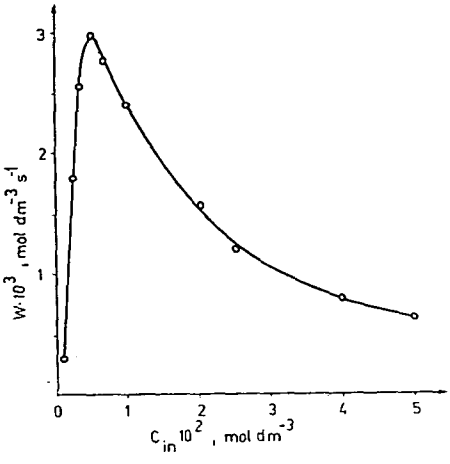

Рис. 3. Зависимость начальной скорости полимеризации (W) ММА от концентрации инициатора (ПСК) при $n=6$.

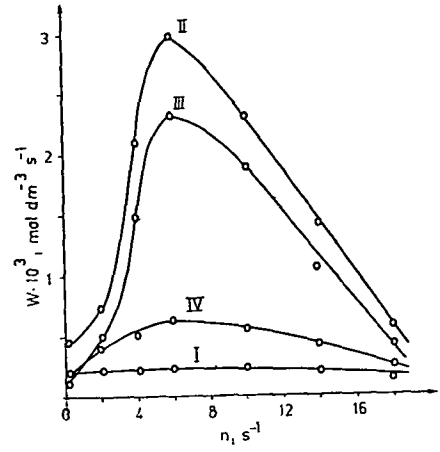

Рис. 4. Зависимость начальной скорости полимеризации (W) ММА от интенсивности перемешивания (n) при разных концентрациях инициатора (ПСК), *mol dm*$^{-3}$: I — $1 \cdot 10^{-3}$, II — $5 \cdot 10^{-3}$, III — $1 \cdot 10^{-2}$, IV — $5 \cdot 10^{-2}$.

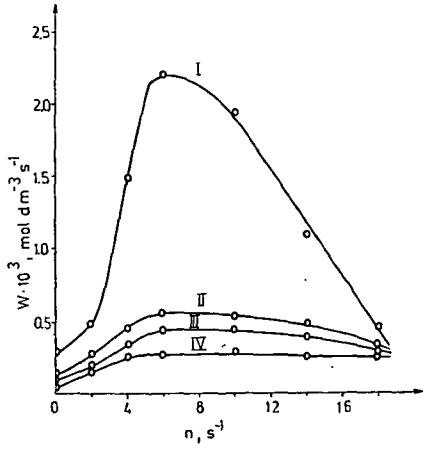

Рис. 5. Зависимость начальной скорости сополимеризации (W) ММА с БМА от интенсивности перемешивания (n) при разных содержаниях БМА (масс. %): I — 0, II — 10, III — 30, IV — 50 ($C_{in}=0.01$ *mol dm*$^{-3}$).

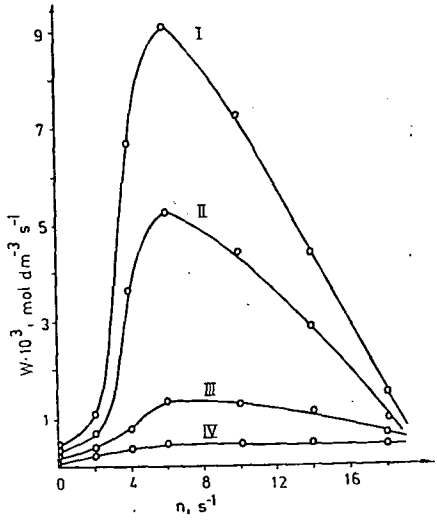

Рис. 6. Зависимост начальной скорости сополимеризации (W) ММА со стиролом от интенсивности перемешивания (n) при разных содержаниях стирола (масс. %): I — 25, II — 50, III — 75, IV — 100 ($C_{in}=0.004$ *mol dm*$^{-3}$, T=348 K).

ими сомономерами, наблюдаются аналогичные закономерности, найденным при гомополимеризации ММА, однако, с увеличением доли гидрофобных мономеров в полимеризующейся смеси, происходит постепенный переход к зависимостям, характерным для дисперсионной полимеризации последних.

Обсуждение полученных результатов

Выяснение влияния гидродинамических условий проведения на кинетику дисперсионной безэмульгаторной полимеризации различных мономеров и установление механизма происходящих при этом явлений, оставались за пределами внимания большинства исследователей. Это может объясняться, прежде всего, несравненно большим промышленным значением мицеллярной и гранульной полимеризаций, в которых гидродинамические условия вовсе не имеют, или имеют только второстепенное значение, а также и тем, что гидродинамические условия проведения процесса являются почти невоспроизводимыми за пределами одной лаборатории. Таким образом, полученные данные могут носить только относительный характер, что затрудняет теоретическое обобщение экспериментальных данных. Однако, некоторые явления, происходящие во всех дисперсионных полимеризационных процессах, могут быт обнаружены и выяснены именно в более простых безэмульгаторных системах.

Авторы [6, 7], исследовавшие влияние интенсивности перемешивания на скорость полимеризации хорошо растворимого в воде мономера акрилонитрила ($\sim 1.4\ mol\ dm^{-3}$ при 303 К) показали, что с повышением скорости вращения мешалки происходит уменьшение скорости полимеризации. В работах [5, 8] также было найдено, что полимеризация ММА (растворимость в воде $\sim 0.6\ mol\ dm^{-3}$ при 303 К) замедляется с повышением интенсивности перемешивания. Нами [11] было показано ранее, что как начальная, так и стационарная скорости безэмульгаторной дисперсионной полимеризации стирола (растворимость в воде $\sim 0.04\ mol\ dm^{-3}$ при 303 К) в присутствии ПСК сначала возрастают с увеличением числа оборотов мешалки в единицу времени, затем, выше определенного числа, остаются постоянными.

Вопрос о причинах снижения скорости дисперсионной полимеризации акрилонитрила носит особый характер, поскольку при этом различие от наших систем наблюдается не только в степени водорастворимости мономера, но и в полном отсутствии растворения полимера в своем мономере.

Представлял интерес проведение изучения влияния интенсивности перемешивания на начальную скорость полимеризации ММА в условиях, обеспечивающих более тонкое регулирование скоростей сдвига в системе, чем в работе [8]. Это достигалось малыми размерами перемешивающего магнита и отсутствием в дилатометре отражающих выступов. Из данных *рис. 1* следует, что при принятых нами предосторожностях подготовки полимеризационных систем, в процессе не наблюдается выраженный индукционный период (экстраполяция прямых конверсии приводит к началу координат). Аналогичные прямые были получены во всех испытуемых нами системах и расхождения в рассчитанных скоростях полимеризации в повторных опытах не превышали 10%-ов.

Представленная на *рис. 2* зависимость рассчитанных начальных скоростей

полимеризации ММА от числа оборотов мешалки в единицу времени, отличается от данных работы [8] тем, что при использованных нами малых интенсивностях перемешивания, найдено возрастание скорости полимеризации. Наблюдаемое увеличение начальной скорости полимеризации является следствием увеличения скорости транспорта мономера в водную фазу, что, как известно, является прямой функцией степени дисперсности капель. Поскольку свободные радикалы инициатора находятся в воде, первоначально акт инициирования происходит в молекулярном водном растворе мономера. Там же происходит сначала рост цепей, затем с образованием полимерных частиц и адсорбированием ими мономера, образуются полимерно-мономерные частицы в которых продолжается процесс полимеризации с наиболее вероятным инициированием и обрывом цепей в их поверхностном слое. Такой механизм был предложен нами, в согласии с литературными представлениями, и на основании данных полученных при безэмульгаторной дисперсионной полимеризации стирола инициированной ПСК [11]. Очевидно, в случае полимеризации ММА, при относительно малых интенсивноцтях перемешивания, механизм процесса не отличается от изложенного.

Однако, со значительным увеличением сдвиговых напряжений, вследствие меньшей вязкости и меньшего пограничного натяжения ММА с водой, чем у стирола, в системе более интенсивно происходит деформация и дробление капель мономера и увеличивается число микрокапель (осколки дробления макрокапель). Резко возросшая дисперсность мономера приводит к увеличению вероятности захвата каплями и микрокаплями полимерно-мономерных частиц. В этих условиях, во-первых, может увеличиваться скорость обрыва растущих полимерных цепей вследствие увеличения вероятности попадания одновременно большего числа радикалов в капли, и, во-вторых, не проявляется столь характерный для полимеризации ММА «гель эффект». В действительности, при скоростях оборотов мешалки, превышающих определенное значение (6 оборотов в секунду в наших условиях), наблюдается постепенное уменьшение начальной скорости полимеризации ММА, что видно из данных *рис. 2.*

Если предложенный выше механизм происходящих явлений соответствует действительности, то молекулярная масса полимеров должна уменьшаться не только с увеличением скорости полимеризации, но и при ее дальнейшем снижении с возрастанием интенсивности перемешивания. С целью проверки этого положения, было проведено выделение образовавшегося ПММА и определены относительные молекулярные массы полимеров, приготовленных при разных интенсивностях перемешивания системы. Полученные данные (приведены в *Таблице*) подтверждают изложенные, на основании данных *рис. 2,* представления о причинах появления максимума в скорости полимеризации в зависимости от интенсивности перемешивания.

В предыдущей нашей работе [11] мы отметили, что при подкрашивании олеорастворимым красителем «Суданом III» мономера стирола, после проведения безэмульгаторной полимеризации в присутствии ПСК, дисперсия полистирола была бесцветной и лишь 5—10% по массе полимера была окрашеной и находилась в агрегированном состоянии. Из этого наблюдения бесспорно следовало наличие механизма с переходом мономера из капель в растущие полимерно-мономерные частицы. С этой же целью было проведено в данной

Таблица

*Скорость полимеризации ММА (W) и относительная молекулярная масса полимеров (M_r), полученных при разных интенсивностях перемешивания (обороты мешалки — n)**

Интенсив. перемеш. n, s^{-1}	Скорость полим. $W \cdot 10^4$ $mol\ dm^{-3}\ s^{-1}$	Молекух. масса $M_r \cdot 10^{-6}$
0	1.79	2.2
2	4.78	1.4
4	14.7	1.2
6	24.0	1.1
10	18.8	0.95
14	11.5	0.85
18	4.01	0.80

* $T = 333.15$ K, $C_{in} = 0.01\ mol\ dm^{-3}$

работе подкрашивание мономера ММА «Суданом III» и проведены полимеризации при разных скоростях перемешивания систем. Образовавшиеся дисперсии ПММА были розоватого цвета, наряду с небольшим количеством (10—15% по массе) более крупных красных частиц. Установить количественную зависимость между скоростью перемешивания и распределением краски в дисперсии ПММА нам не удалось. Основная причина этого состояла в том, что дисперсные частицы были слипшиеся и неоднородны. В целом, наблюдаемые нами явления при полимеризациях с окрашенными мономерами, находятся в соответствии с описанным механизмом образования частиц в работе [1, ст. 96] для неполярных и полярных мономеров. Таким образом, полученные нами результаты по опытам с подкрашиванием мономера, также подтверждают развитые выше представления о механизме происходящих явлений в полимеризующихся системах под действием перемешивания.

Изучение влияния концентрации инициатора ПСК на начальную скорость безэмульгаторной полимеризации ММА, привело к несколько неожиданному результату. В более широком интервале концентраций ПСК, обнаружен максимум на кривой зависимости скорости полимеризации от концентрации инициатора *(рис. 3)*. Однако, снижение скорости полимеризации при повышенных концентрациях инициатора можно объяснить высаливающим действием ПСК, что приводит к уменьшению растворимости мономера и замедлению его транспорта к местам полимеризации.

Из сложной зависимости начальной скорости полимеризации от скорости перемешивания и концентрации ПСК, получается общая зависимость, представленная на *рис. 4*. Из данных этого рисунка следует возможность оптимализации безэмульгаторных процессов полимеризации, при знании закономерностей влияния названных факторов на скорость реакции.

Ввиду большого значения степени водорастворимости мономера на безэмульгаторный процесс полимеризации, представлял интерес изучить влияние интенсивности перемешивания на кинетику сополимеризации ММА с такими мономерами, которые имеют очень малую растворимость в воде, как, например, стирол ($\sim 0.04\ mol\ dm^{-3}$) и БМА ($\sim 0.005\ mol\ dm^{-3}$). Условия проведения

полимеризаций, разультаты которых представлены на *рис. 5* и *6*, были подобраны таким образом, чтобы начальные скорости сополимеризаций были примерно одного порядка. Из данных приведенных на этих рисунках следует, что с увеличением доли менее гидрофильных мономеров в полимеризующейся смеси, характерная, проходящая через максимум, зависимость скорости полимеризации ММА от интенсивности перемешивания, постепенно переходит в вид с достижением предельной скорости, найденного ранее для стирола [11]. Замечательным является то обстоятельство, что, в соответствии с меньшей растворимостью БМА в воде, уже при 50%-ном содержании его в полимеризующейся смеси, наблюдается зависимость скорости полимеризации от интенсивности перемешивания полностью соответствующая характерной для неполярных мономеров. В противоположность этому, даже при 75%-ном содержании стирола в смеси с ММА, все еще обнаруживается максимум скорости полимеризации от интенсивности перемешивания системы.

Таким образом, подытоживая изложенные выше результаты, можно прийти к выводу, что в безэмульгаторных дисперсионных полимеризациях, осуществляемых в присутствии ПСК, гидродинамические условия проведения процесса в значительной мере влияют на скорость образования и молекулярную массу получаемых полимеров. Очевидно, что наибольшее значение из физических свойств мономеров имеет их водорастворимость, в определении характера влияния гидродинамических условий проведения процесса на кинетику и топохимию прохождения полимеризации или сополимеризации, для растворяющих свой полимер мономеров.

Авторы выражают свою благодарность Т. П. Пановой и Л. А. Корытной за участие в выполнении экспериментальной части работы.

Литература

[1] *Eliseeva, V. I., S. S. Ivanchev, S. I. Kuchanov, A. V. Lebedev:* Emulsion polymerization and its applications in industry, Plenum Publ., New York, 1981.
[2] *Кучер, Р. В., В. И. Карбан:* Химические реакции в эмульсиях, «Наукова думка», Киев, 1973.
[3] *Lissant, K. J.* (Editor): Emulsions and emulsion technology, Academ. Press, London—New York, 1974.
[4] *Smith, A. L.* (Editor): Theory and practice of emulsion technology, Academ. Press, London—New York, 1976.
[5] *Рутовский, Б. Н., Г. С. Гончаров:* Ж. прикл. хим., **26**, 426, 434 (1953).
[6] *Thomas, W. M., E. H. Gleason, G. Mino:* J. Polym. Sci., **24**, 43 (1957).
[7] *Роскин, Е. С.:* Ж. прикл. хим., **30**, 1030 (1957), **32**, 676 (1959).
[8] *Цветков, Н. С.:* Вестн. Львовского унив., сер. хим., вып. 6, 13 (1963).
[9] *Андор, И. А., А. И. Юрженко, А. Э. Шамракова:* (Сборн.) Проблемы синтеза, исследования свойств и переработки латексов, «Химия», Москва, 1971. ст. 41.
[10] *Иванчев, С. С., И. А. Андор, Н. И. Соломко:* Ж. прикл. хим., **46**, 1724 (1973).
[11] *Андор, И. А., И. Древени:* Acta Phys. Chem. Szeged, **24**, 491 (1978).
[12] *Липатов, Ю. С., А. Е. Нестеров, Т. М. Гриценко, Р. А. Веселовский:* Справочник по химии полимеров, «Наукова думка», Киев, 1971. ст. 52.

EFFECT OF HYDRODYNAMIC PARAMETERS IN THE DISPERSION POLYMERIZATION AND COPOLYMERIZATION OF METHYLMETHACRYLATE

J. A. Andor and I. Dreveni

The effect of stirring intensity was studied in the polymerization of methylmethacrylate without emulsifier, and in the copolymerization of methylmethacrylate with buthylmethacrylate and styrene. The experimental results are interpreted and a mechanism is described for the formation of polymer and of polymer particles, in the reaction, initiated by $K_2S_2O_8$.

INVESTIGATION OF CRUDE OIL-WATER EMULSIONS IN PRESENCE OF NON-IONIC SURFACTANTS, II.

Behaviour of emulsions at elevated temperatures, and emulsification of crude oil fractions

B. FELIÁN, J. BALÁZS*, J. LAKATOS-SZABÓ, I. LAKATOS
Chemical Research Laboratory for Mining, Hungarian Academy of Sciences, Miskolc-Egyetemváros, Hungary

(Received 29th May, 1984)

The investigations were focussed on the determination of the stability and rheological properties of emulsions prepared from natural crude oil and its fractions, using ion-free water and aqueous tenside solutions. The effects of temperature on the stability and rheological properties of the emulsions were tested in the presence of tensides and in surfactant-free systems.

The experimental results permit the conclusion that with increasing temperature the originally plastic emulsion first assumes pseudoplastic properties, and later Newtonian flow behaviour. The change in the rheological properties is attributed to the paraffin crystals present at low temperature in Algyő-2 crude oil, which also stabilize the emulsion structure. In the presence of non-ionic tensides, the oil external emulsions have a complex nature [O/W/O type], and demulsify readily at elevated temperatures.

The emulsification of the crude oil fractions indicates that asphaltenes not only stabilize the tenside-free emulsions, but play a decisive role in shaping the rheological properties as well. No clear-cut relation was found between the interfacial tension and the stability of the emulsions, whereas it is probable that the interfacial rheological properties (viscosity, elasticity, film-forming ability) can be correlated with the spontaneous demulsification.

Introduction

In part I [1], the emulsion-forming abilities of surfactants to be applied in enhanced oil recovery were investigated at constant temperature (363 K). However, in order to clarify the properties of emulsions that may be formed under reservoir conditions, it was necessary to study how the stabilities and viscosities of emulsions change when the temperature is increased. The effect of temperature is also important when the crude oil is brought to the surface in the form of an emulsion, and the latter has to be demulsified. Moreover, from the experimental findings outlined in the first paper, it seemed unavoidable to determine which of the crude oil components, presumably the natural surfactant, basically shapes the rheological properties of the emulsions.

* Department of Colloid Chemistry, Attila József University, Szeged, Hungary

Experimental

The crude oil and surfactants used in the experiments were the same as described earlier [1]. Separation of the crude oil into its fractions was carried out as follows: After distillation up to 473 K under atmospheric conditions, the atmospheric residue was subjected to vacuum distillation at 53.32 Pa and 523 K. These two fractions together represented the oil phase designated **T**. Addition of *n*-pentane resulted in the precipitation of the asphaltenes from the vacuum residue. The *n*-pentane-free malthene was then adsorbed on a Kieselgel, from which the resins and the residual fractions were extracted with benzene and methanol.

In the fractions obtained, the following phases maintained the concentrations of the different components at the same level as in the original crude oil.

phase **a**: T+0.3 w.% resin,
phase **b**: T+3.5 w.% asphaltene,
phase **c**: T+0.3 w.% resin+3.5 w.% asphaltene,
phase **d**: T+10.7 w.% asphaltene-free and resin-free residue,
phase **e**: T+resin-free fraction (3.5 w.% asphaltene +10.7 w.% asphaltene-free and resin-free residue),
phase **f**: synthetic (reconstituted) crude oil.

The interfacial tension between the oil and distilled water was determined by the pendent drop method. A Contraves Low Shear 30 viscometer was used to study the interfacial rheological properties of the two-phase system [2].

Results and discussion

1. Effects of temperature on stabilities and rheological properties of emulsions in tenside-free systems

In this test series, the emulsions contained equal phase volumes of crude oil and ion-free water. The dispersed systems were prepared at a given temperature and maintained under these circumstances for 24 hours.

It was observed that all emulsions were of W/O type, independently of temperature, and their thermal treatment did not lead to any phase separation. Notwithstanding this, the emulsions cannot be regarded unequivocally as stable ones. At room temperature, the significant difference in viscosity between the two liquid phases tends to prevent the disperse portion from separating from the system. The emulsified drops are stabilized by the natural emulsifiers present in the crude oil, and the emulsion structure is stabilized by crystals of the high molecular weight paraffins still in solid form at 298 K. As the temperature was elevated to 323, 348 and 363 K, the increase in the drop size and their settling could be observed visually. The reduction in oil viscosity with increasing temperature made it possible for the drops to settle, resulting in a lower distribution stability of the system. As the temperature rises, the solid paraffin particles melt, and they ceases to have any role whatever in the apparent stabilization of the emulsion.

The flow curves measured at constant temperature after thermal treatment are illustrated in Fig. 1. It is clear that any shift in temperature leads to a change in the

flow behaviour of the emulsions. The dispersed system, that exhibits plastic properties at room temperature, becomes pseudoplastic at 323 and 348 K, and behaves essentially as a Newtonian liquid at 363 K. At the same time, a considerable change also takes place in the plastic viscosity and the Bingham yield value, as shown in Fig. 2.

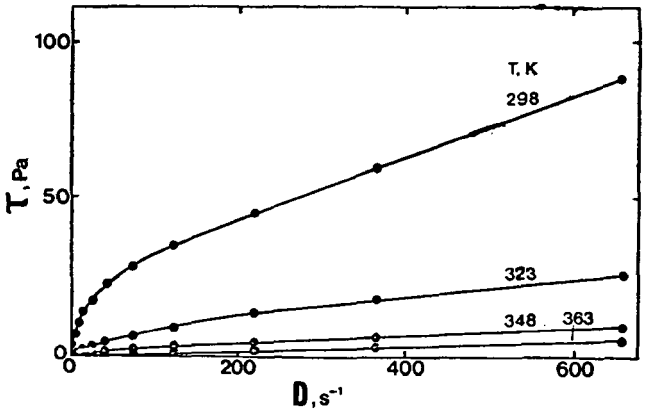

Fig. 1. Ascending legs of flow curves at 298, 323, 348 and 364 K, for emulsions containing 50 vol. % crude oil and 50 vol. % distilled water

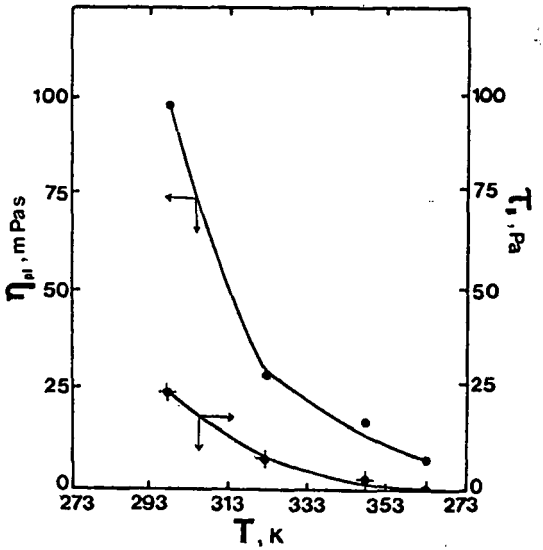

Fig. 2. Bingham yield value (τ_B) and plastic viscosity (η_{pl}) vs. temperature for emulsions of 50 vol. % crude oil and 50 vol. % distilled water

From Fig. 2, it may be stated that the greatest change in the emulsion viscosity is caused by raising the temperature from 298 K 323 K. It is presumably, in this range that a large proportion of the long-chain paraffins melt and dissolve in the dispersion medium.

2. *Effects of temperature on stabilities and rheological properties of emulsions containing tenside*

Tensides containing 8 or 20 ethylene oxide groups were chosen as model compounds. The concentration of surfactant was selected so that an oil external emulsion formed in one case and a water external emulsion formed in the other when equal volumes of oil and water were mixed at 298 K [1]. Tenside solutions of 0.5 g dm^{-3} and 40 g dm^{-3}, from surfactants NPE_8 and NPE_{20}, respectively, were therefore used to produce an O/W emulsion at rcom temperature. The emulsions were prepared at the given temperature and allowed to stand for 24 hours under thermostated conditions, after which the flow curves were measured. The apparent viscosities obtained at different temperatures are shown in Figs 3 and 4.

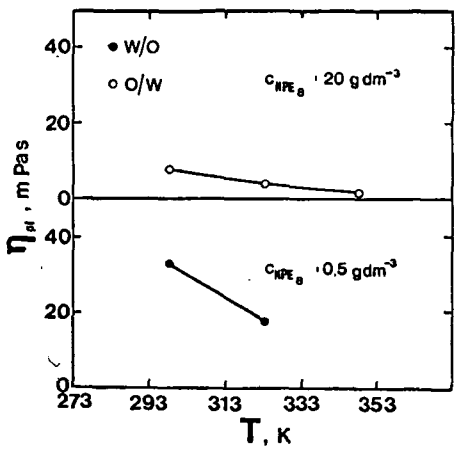

Fig. 3. Temperature-dependence of emulsions stabilized with tenside NPE_8.

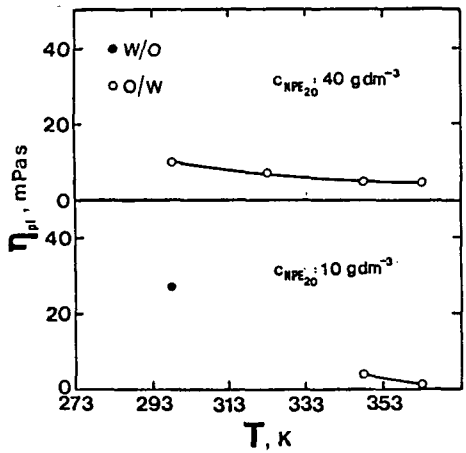

Fig. 4. Temperature-dependence of emulsions stabilized with tenside NPE_{20}

It is obvious from Fig. 3 that on increase of the temperature by 25 K the viscosity decreased from 33 mPas to 17 mPas. On the other hand, the emulsions obtained at 348 and 363 K underwent full demulsification after 24 hours and they separated, in accordance with their initial composition, into 50 vol. % oil and 50 vol. % aqueous phase.

When the emulsions were prepared with a solution having a tenside concentration of 20 g dm^{-3}, each of them proved to be of the O/W type. It is apparent from Fig. 3 that the viscosity of the emulsion is already below 10 mPas at 298 K, and it diminishes to 2 mPas if the temperature is increased to 348 K. After thermal treat-

ment for 24 hours, separation of neither the dispersed portion nor the dispersion medium could be observed up to 348 K. On the other hand, at 363 K (the highest temperature used) the emulsion demulsified into 3 phases, with formation of an O/W emulsion in the middle zone. Its volume comprised 23% of that of the initial emulsion.

SHINODA and ARAI [3] have studied in detail the relationship between the cloud point and the phase inversion temperature. On the basis of their experimental results it can be stated that for a given tenside the phase inversion temperature depends to a large extent on the composition of the oil phase. It also depends on the oil phase whether the phase inversion temperature is lower or higher than the cloud point. For an oil phase abundant in aromatic compounds, the phase inversion temperature is usually lower than the cloud point, while it tends to exceed the latter in the cases of normal and cycloparaffins. For a given tenside (for a given cloud point), the phase inversion temperature increases if a compound containing a longer hydrocarbon chain is present in the oil phase. This may explain why a water external emulsion occurs well above the cloud point (318 K) when NPE_8 is used, while the O/W emulsion becomes unstable at 348 K.

According to SHINODA and SAGITANI [4], the stability of the O/W emulsion drops against coalescence is greatest if the storage temperature is 20 to 55 degrees lower than the inversion temperature. Thus, the value of 363 K may be near the phase inversion temperature above which a W/O emulsion may already occur.

The emulsions prepared with 10 g dm^{-3} NPE_{20} solution (Fig. 4) are of W/O type at room temperature and 323 K, and of O/W type at 348 and 363 K. The viscosity of an emulsion stored at 298 K for 24 hours does not differ significantly from that of an emulsion prepared with 0.5 g dm^{-3} NPE_8 (Fig. 3). At higher temperatures, the viscosity of water external emulsions is small, amounting to merely a few mPas.

After thermal treatment at 323 K, the originally W/O emulsions separated into 3 phases. The amount of the O/W emulsion between the boundaries of the oil and aqueous phases is about 5% of the initial volume. This water external emulsion can only be a result of the demulsification of the initially complex O/W/O type system.

After 24 hours, the O/W emulsions thermally treated at 348 and 363 K showed diffuse opalescence. The emulsions prepared with 40 g dm^{-3} NPE_{20} were of the O/W type at any temperature. At room temperature, the viscosity level was about 10 mPas, and it decreased only slightly as the temperature increased. It could also be stated that, on standing at a given temperature, the stability of the emulsified drops against coalescence was high and neither the dispersion medium nor the dispersed phase separated from the system as a discrete liquid. At the same time, the distribution stability of the emulsions is low (as usual other O/W emulsions) and they show diffuse distribution at any temperature.

It seems a contradiction that when these non-ionic tensides are used, a W/O emulsion can be produced at low temperatures, and an O/W emulsion at higher temperatures, whereas just the opposite might be expected on the basis of theoretical considerations. An explanation of this question must be sought in the composition of the hydrocarbon phase. According to the experimental results of SHINODA and ARAI [3], the phase inversion occurs at a temperature higher than the cloud point if the oil phase contains mainly paraffins. Typically, Algyő-2 crude oil is rich in paraffins of different chain lengths [5], *i.e.* in components which may increase the phase inversion temperature above the cloud point. It can be seen from the data in Table I that up to

373 K no opalescence of the aqueous solution of tenside NPE_{20} takes place. Thus, the phase inversion temperature should be higher than 373 K. The experimental fact that a W/O emulsion forms at low tenside concentrations and temperatures, and an O/W emulsion at higher temperatures [6], is not connected directly with the phase inversion that might be expected from the change in the HLB of non-ionic tensides due to increased temperature. The alteration in emulsion character observed as a result of increased tenside concentration and that effected by temperature may possibly be explained by the chemical nature of compounds present in Algyő-2 crude which stabilize the oil external system. This possible interaction leads to destabilization of the initial emulsion. At lower temperature, the solid particles also take part in the apparent stabilization of the dispersed system. They melt when the temperature increases, and a stable emulsion can be formed only if a sufficient amount of tenside is present in the system; on the other hand, the emulsion demulsifies if this is not the case.

3. Stability of emulsion prepared from crude oil fractions

The different phases (**T**, **a**—**e**, listed earlier) were mixed with an equal volume of distilled water at 298 K. No stable emulsion was obtained by emulsifying phase **T**, and separation of the phases occurred immediately on preparation. The emulsification of phase **e**(**T**+resins) did not result in a stable emulsion either, and breaking of the system started even at room temperature. At 323 K and on standing over 1 hour, 4% of the initial volume remained in emulsion from. The respective values for 348 and 363 K were 2 and 1%. Addition of asphaltenes to phase **T** (phase **b**) led to an extremely stable emulsion, with neither the dispersed portion nor the dispersion medium separating out of the system under identical circumstances.

On emulsification of phase **c** (**T**+resins+asphaltenes), breaking of the emulsion could not be observed at room temperature. However, the dispersion medium began to separate at 323 K, and its volume amounted to 22% of the initial emulsion. It could also be observed that the drop size increased with rising temperature.

The emulsion was stabilized only slightly by the asphaltene-free and resin-free residue, and separation of the two phases became complete at 323 K. Emulsification of the resin-free phase (phase **e**) gave a stable emulsion. No increase in the water drop size was visible to the naked eye. At 363 K, after a standing time of 1 hour, oil separated from the emulsion, its volume amounting to 10% of the original volume of the emulsion. Emulsification of phase **f** (the reconstituted synthetic oil) gave a very stable emulsion, similar to that prepared from phase **e**; at 363 K, only oil separated from the emulsion, but its volume was less than 10% of the initial volume.

Previously, the interfacial tension was regarded as the factor playing the crucial role in emulsification and emulsion stability [7]. For instance, MARSZALL [8] suggests that a low interfacial tension is a necessary, but insufficient condition of stability. On the other hand, the studies of interfacial rheological properties revealed a relatively close correlation between the stability and viscosity of the emulsions. BOYD ET AL. [9] found that the stability depends highly on the elasticity of the rigid films formed at the water/oil interface. WASAN ET AL. [10] found that in systems with an ultralow interfacial viscosity the drop coalescence occurs very rapidly, *i.e.* the emulsions are unstable.

Table I

Characteristic interfacial tension, interfacial and plastic viscosity, and Bingham yield value for different oil/water systems

Hydrocarbon phase	σ $\times 10^{-3}$ N m^{-1}	η_s $\times 10^{-3}$ N s m^{-1} 4 h, D = 5.14 s^{-1}	η_{pl} $\times 10^{-3}$ N s m^{-2}	τ_B N m^{-2}
T	14.65	—	—	—
a	11.06	3.22	—	—
b	17.51	18.90	92.7	21.4
c	16.33	11.03	62.5	15.0
d	14.13	24.60	38.4	2.2
e	18.62	28.70	114.3	54.6
f	16.60	30.71	113.1	36.5
Crude oil	22.10	45.76	103.2	34.8

Of the interfacial film properties, interfacial tension and interfacial viscosity were measured at 298 K in a system composed of various crude oil fractions and distilled water. The build-up of an interfacial layer is a time-consuming process, which cannot be followed through the interfacial tension alone, as the latter comes into equilibrium after 10 to 20 minutes, regardless of the chemical composition of the oil phase (Fig. 5).

In the first column of Table I the equilibrium interfacial tensions are listed. Comparison of these data with those measured during the stability tests shows that the interfacial tension in the case of the most stable emulsions does not constitute the lowest value. The lowest interfacial tension was found for phase **a**, which forms a read-

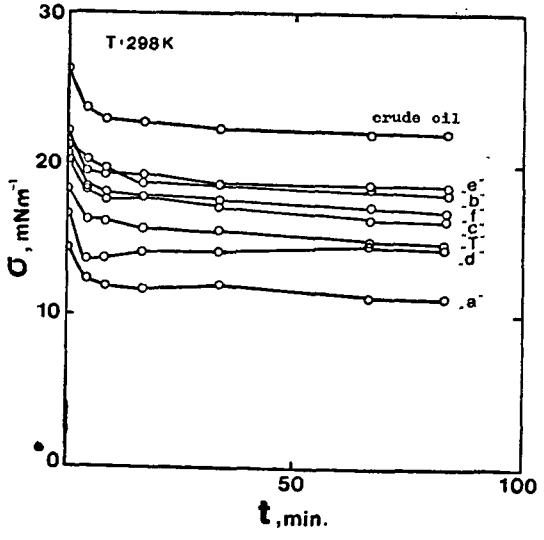

Fig. 5. Time-dependence of interfacial tension in oil/water system

ily breaking emulsion. However, it should be noted that certain crude components and compounds undergo autoxidation during the preparation of the different fractions, which leads to the formation of compounds active at the interfaces. The fact that the interfacial properties of the original crude and the "synthetic " (reconstituted) oils are different is attributed to this phenomenon.

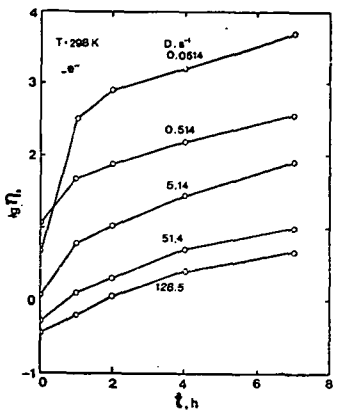

Fig. 6. Change of interfacial viscosity *vs.* shear rate in phase *e*/water system

Formation of the interfacial layer can be followed better through the change in the interfacial viscosity as a function of time. Figure 6 presents data on the viscosity of the interface between phase **e** and distilled water at different shear rates.

The shapes of the curves in Fig. 6 are similar to those obtained for the other fractions, *i.e.* the greatest change is measured within 1 hour, and the build-up of the interfacial layer continues even after 4 hours.

The characteristic interfacial viscosities measured after 4 hours and at $D=5.14\ s^{-1}$ are also included in Table I. Analysis of the data revels a correlation between the interfacial viscosity and the properties of the emulisons. It is quite reasonable that the emulsion prepared from phase **a**, having an interfacial viscosity of merely 3.22×10^{-3}, is unstable. However, a highly stable emulsion is formed in the asphaltene-containing system, where the interfacial viscosity is relatively high.

Unfortunately, we are faced with special experimental circumstances which hinder the establishment of a close correlation between the emulsion stability and the interfacial rheological properties. The problems stem from the fact that, when a rheometer is used in the rotation mode of operation, the highly elastic, rigid films formed at the interface in asphaltene-containing systems are usually ruptured at very low ($<0.1\ s^{-1}$) shear rate and therefore the values reported in Table I are probably far below the actual interfacial viscosities existing at a state of rest or at very low shear forces. Thus, it seems unavoidable to complement the present studies with oscillation rheometric measurements and to seek relationships between the emulsion stability and the elastic properties (stronge modulus, shear rigidity, compliance, etc.).

4. *Rheological properties of emulsions prepared from different crude oil fractions*

The ascending leg of the rheograms for the emulsions containing oil phases of different compositions is shown in Fig. 7; the plastic viscosity and the Bingham yield values of the emulsions are listed in Table I.

It is obvious from the flow curves presented in the Figure that asphaltenes play a key role in the plasticity of the emulsions. If only the asphaltenes of the heavy cut are present in the oil phase of the emulsion (curve **b**), the plastic viscosity is reduced slightly and the yield value decreases to a greater extent than for the emulsion prepared from the original crude oil (Table I). The presence of resins besides the asphaltenes reduces the plasticity, while if only the resin is absent from the oil phase (curve **e**)

the flow curve over the entire range of measurement will run above the curve for the emulsion prepared from the initial crude and distilled water, whereas the Bingham yield value increases from 34.8 Pa to 54.6 Pa and the plastic viscosity from 103.2 to 114.3 mPa s. When neither resins nor asphaltenes are present in the oil phase (curve **d**), a drastic change takes place in the emulsion structure: adhesion forces scarcely exist between the dispersed drops, and the viscosity of the emulsion is 38.4 mPa s. If the oil from the various fractions is reconstituted and mixed with an equal volume of distilled water, an emulsion is obtained whose flow curve approximates fairly well to that of the emulsion prepared from the initial crude oil, but it runs above it for the reasons mentioned earlier.

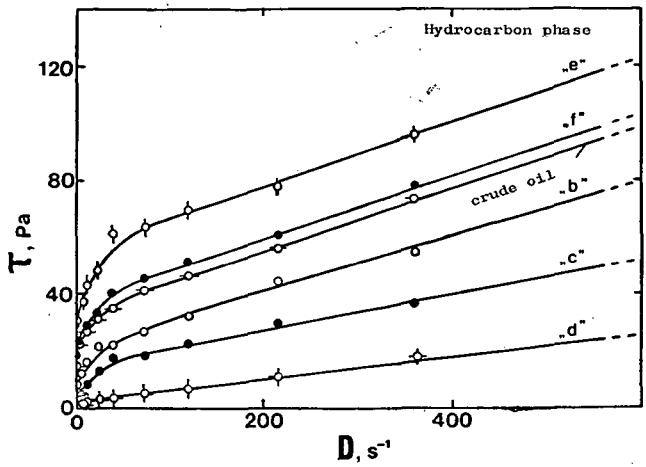

Fig. 7. Flow curves of different emulsions containing 50 vol. % hydrocarbon and 50 vol. % ion-free water

These experimental results agree with the literature observations [11—13]. Accordingly, of all the oil components, it is the asphaltenes that primarily stabilize natural crude oil-water systems. Asphaltenes are of basic importance not only in the stabilization of the emulsion, but also in determining its rheological properties. When the oil phase contains only asphaltene besides phase **T**, the flow curve for the emulsion best approaches that for the emulsion prepared from the original crude. The presence of resins definitely reduces the emulsion plasticity (curve **c**), whereas in their absence (curve **e**) it is possible to produce an emulsion having a higher plasticity and viscosity than those of the original emulsion.

References

[1] *Felián, B., Balázs, J. Lakatos, I.:* Acta Phys. et Chem., (Szeged) **29,** 223 (1983).
[2] *Lakatosné-Szabó, J., I. Lakatos:* Magy. Kém. Folyóirat, in press.
[3] *Shinoda, K., H. Arai:* J. Phys. Chem. **68,** 3485 (1964).
[4] *Shinoda, K., H. Sagitani:* J. Coll. and Interface Sci. **255,** 172 (1977).
[5] *Völgyi, L., S. Suba, K. Balla, I. Csalagovits:* Magyarország szénhidrogéntelepei Algyő, OKGT, Budapest (1970).
[6] *Adamson, A. W.:* Physical Chemistry of Surfaces, Interscience Publishers (1963).
[7] *Sherman, P.:* Emulsion Science, Academic Press (1968).
[8] *Marszall, L.:* Coll. and Polymer Sci. **254,** 674 (1976).
[9] *Boyd, J., C. Parkinson, P. Scherman:* J. Coll. and Interface Sci. **41,** 359 (1972).
[10] *Wasan, D. T., S. M. Shah, N. Aderangi, M. S. Chan, J. J. McNamara:* Soc. Pet. Eng. J. **6,** 409 (1979).
[11] *Pasqarelli, C. H., Wasan, D. T.:* The effect of filmforming materials on the dynamic interfacial properties in crude oil-aqueous systems, in Surface Phenomena in Enhanced Oil Recovery Ed. D. O. Shah. Plenum Press, New York (1981).
[12] *Smith, A. L.:* Theory and Practice of Emulsion Technology, Academic Press, London (1976).
[13] *Neumann, A., B. Paczynska-Lehme:* Chem. Ing. Tech. **53,** 911 (1981).

ИССЛЕДОВАНИЕ ЭМУЛЬСИЙ НЕФТИ В ВОДНЫХ РАСТВОРАХ НЕИОНОГЕННЫХ ПОВЕРХНОСТНО—АКТИВНЫХ ВЕЩЕСТВ, II. СВОЙСТВА ЕМУЛЬСИЙ ПРИ ПОВЫШЕННЫХ ТЕМПЕРАТУРАХ И ЭМУЛЬСИФИКАЦИЯ ФРАКЦИЙ НЕФТЫ

Б. Фелиан, Я. Балаж, Й. Лакатош-Сабо и И. Лакатош

Проведено изучение стабильности и реологических свойств эмульсии нефти и ее фракций образованных в воде и растворах поверхносто-активных веществ. Определено влияние температуры на указанные свойства эмульсий. Найдено, что асфальтены содержащиеся в нефти играют роль стабилизатора и важного фактора в определении реологических свойств в эмульсиях, приготовленных без поверхностно-активных веществ. Не найдено корреляции между поверхностным натяжением, поверхностной вязкостью и стабильностью эмульсий различных фракций нефти.

Information for Contributors

1. Manuscripts should be submitted to Prof. Pál Fejes, Institute of Applied Chemistry, József Attila University, Szeged, Rerrich tér 1, Hungary, H-6720.
2. The manuscripts must not exceed in any case 32 pages (Figures, legends, Tables and Summary included). Manuscripts should be submitted in duplicate.
3. The format of the text: A/4, double spaced, 25 lines per page and 50 characters per line. Title: all capital characters; underlined twice. Subtitle(s) should be written in new line(s) in normal writing, underlined also twice, first characters: capital. (See the following example).

STEREOCHEMICAL STUDIES

Studies on Cyclic-2-Hydroxycarboxylic Acids

By

PÁL KISS

Research Institute for Industrial Chemistry, Budapest
(Received.....)

4. After these comes the summary, which is followed by the text proper. If the parts of the paper are separated by secondary titles like: Introduction. Experimental etc., the following rule holds: secondary titles of equal rank are to be written in new lines, the first word with capital letter, otherwise running text underlined once.
   Example:
   Introduction
   Experimental part
5. The names of the authors in the running text are written in capital letters. Exceptions are the names in connection with scientific instruments, etc. where only the first letter should be capital.
6. Citations in the text with reference to selected literature at the end of the paper are to be made with squared brackets, like: [5], [4, 9], [4—9].
7. To make printing easier, mathematical formulas are to be simplified as much as possible. Reference to mathematical equations is made by numbers in parenthesis, like: (16).
8. Tables should be typen on separate pages. Please supply numbers and titles for all tables (Numbering occurs with Roman numerals: Table I).
   Throughout the whole text the IUPAC nomenclature should be used.
   Insert of Tables in the text will be indicated at the appropriate place of the margin, like this: Table I.
9. Figures must be drawn clearly with Chinese ink on oily drawing paper, the thickness of lines as well as size of letters and symbols should be selected with care, the minimum size is nearly 0.3 cm.
   The maximum width of Figures is 24 cm, however, Figures of width equal or less than 12 cm are preferred.
   Please, use upwright on the Figures.
   In the case of real numbers points are used instead of commas.
   The place of Figures in the text is indicated on the margin like this: Figure 13.
   Please supply legends for all figures and compile these on separate sheets. Indicate only the number of the Figures in the original drawing, for this purpose use blue pencil.
10. Literature will be given under the heading References, like this: (on a separate sheet at the end of the manuscript)
    [1] Allinger, N. L., M. T. Tribble: J. Phys. Chem. 33, 1565 (1976).
    [2] Abraham, J. K., H. S. Hoover: Principles of Competitive Oxidation. Mc Graw-Hill, New York, 1977, p. 133.

INDEX

M. G. Benedict and I. Gyémánt: On the Interaction of an Ultrashort Light Pulse with a Thin Resonant Medium 115
G. Papp and F. Beleznay: Special points and Ideal-Vacancy-Induced Deep Level in Si and some III—V Semiconductors 121
J. Hebling, Zs. Bor and B. Rácz: Design of N_2 Laser Pumped Tunable Distributed Feedback Dye Lasers with Extended Tuning Range 127
Z. Konefal: The Influence of Detergents on the Luminescence Properties of Rhodamine B and 6 G in Aqueous Solution 135
F. Koczó, N. Dulić and L. Horváth: The Relative Permittivity Change of $Ce(NO_3)_3 \cdot 6\,H_2O$ and $Y(NO_3)_3 \cdot 5\,H_2O$ between 193—353 K 141
Higaz Nader Ali: Inhibitory Effects of some Heterocyclic Derivatives of Mercaptans, Correlated to their Acidity Expressed as a Proton Level, J 145
Á. Patzkó and F. Szántó: Peptization and Surface Modification of Illit from Füzérradvány (in German) 153
E. Tombácz, I. Dékány and Á. Patzkó: X-Ray Diffraction Examination of Intercalated Alkylammonium Humate Complexes 159
E. Tombácz, M. Gilde and F. Szántó: The Effects of Na-Salicyiate and Na-Fulvate on the Stability and Rheological Properties of Na-Montmorillonite Suspensions 165
J. A. Andor and I. Dreveni: Effect of Hydrodynamic Parameters in the Dispersion Polymerization and Copolymerization of Methylmethacrylate (in Russian) 175
B. Felián, J. Balázs, J. Lakatos-Szabó and I. Lakatos: Investigation of Crude Oil-Water Emulsions in Presence of Non-Ionic Surfactants, II. Behaviour of Emulsions at Elevated Temperatures, and Emulsification of Crude Oil Fractions 183

A kiadásért felelős: Dr. Bartók Mihály
1984
A kézirat nyomdába érkezett 1984. július 5. Megjelenés 1985. január
Példányszám: 425. Ábrák száma: 55. Terjedelem: 7,00 (A/5) ív
Készült monószedéssel, íves magasnyomással, az MNOSZ 5601—50/A szabvány szerint
84-2916 — Szegedi Nyomda — F. v.: Dobó József igazgató